CHAPTER 3 METEOROLOGICAL SURVEY

II-3-1 Outline

II-3-1-1 Objective of meteorological survey

The meteorological survey is conducted for the purpose of obtaining the necessary information and data on the meteorological conditions of the survey areas.

Further for the diffusion calculation of thermal effluent in the process of simulation, the atmospheric temperature, water temperature, mean wind direction and velocity, radiation coefficient and etc. are necessary as the meteorological data.

Also in the current survey, it is necessary to know the influece caused by the drift current which is considered as generated by the wind blowing on the sea surface.

Although it is the exceptional case, the data related to the wind is the most important data for the simulation of oil diffusion which is carried out when the oil leakage occurs.

Also the data of atmospheric pressure is necessary for the pressure correction of tide observation data.

In case of the survey conducted in Japan, such meteorological data are usually obtained from the meteorological observatory located nearby the survey areas and in some cases, the monitoring stations are established for such observation.

II-3-1-2 Meteorological data in this study

In this study, the necessary meteorological data have been supplied by Meteorological Service, Singapore through JTC.

II-3-2 Arrangement of Meteorological Data

II-3-2-1 Wind direction and velocity

Among the data of wind direction and velocity of Changi Air Base and JTC Flatted Factory Jurong, the data obtained for the period of February 23rd to March 17th 1981 have been punched and input to computers, and the vector time series have been produced, which shows in Fig. II-3-1.

II-3-2-2 Statistical data of wind direction and velocity

From the data supplied by Meteorological Service, Singapore, the statistical data of the wind direction and velocity have been extracted and tabulated in Table II-3-1.

II-3-2-3 Temperature

From the data obtained from Meteorological Service, Singapore, the statistical data of temperature have been extracted and tabulated into Table II-3-1.

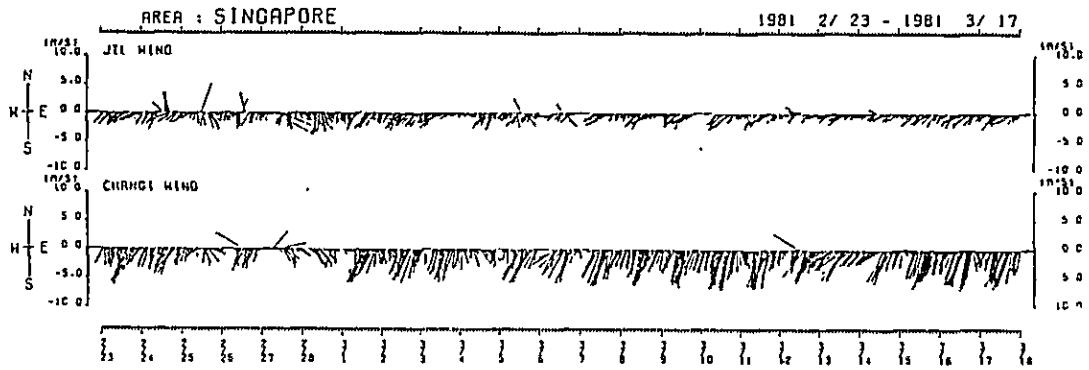

Fig. II-3-1 Vectors time series of wind data

Table II-3-1 Mean temperature, wind velocity and direction

Point	Item		JAN.	FEB.	MAR.	APR.	MAY.	JUN.	JUL.	AUG.	SEP	OCT.	NOV.	DEC.	ANV.	Mean Value of March	Remarks
JTC *1 Jurong Flatted Factory Bldg.	Wind Velocity Appearance Frequency (%)	(kt) 0	6.0	12.6	12.2	17.9	20.0	15.3	12.8	15.5	18.9	22.9	19.6	12.3	15.6		Value of weighted average, obtained multiplying medium value of respective rank with appearance frequency
		1–3	19.7	20.8	33.3	42.0	36.6	30.0	21.1	22.4	29.7	33.2	34.1	22.6	29.2	4.08kt	
		4–6	44.9	41.9	39.2	28.8	27.1	31.3	32.7	28.9	29.3	26.0	32.6	38.7	33.3		
		7–10	25.1	22.9	13.6	10.5	15.0	21.3	30.5	29.2	19.9	15.7	12.2	23.2	19.7		
		11–16	4.3	1.8	1.7	0.8	1.1	1.9	2.9	3.9	2.0	2.1	1.5	3.1	2.2	2.04 m/sec	
		17–21	–	–	–	–	0.2	0.2	–	0.1	0.2	0.1	–	0.1	–		
		22–27	–	–	–	–	–	–	–	–	–	–	–	–	–		
*2 Changi Air Base	Mean Wind Velocity of Respective Directions (kt)	N	(53) 6.7	(51) 6.5	(27) 5.1	(14) 4.9	(5) 3.9	(5) 4.3	(6) 4.2	(1) 4.0	(1) 3.4	(9) 3.4	(27) 3.5	(48) 4.6	(21) 4.5		Value in bracket is appearance frequency
		NE	(13) 8.6	(35) 9.3	(28) 6.7	(13) 6.2	(7) 4.2	(3) 3.7	(4) 4.5	(1) 2.6	(2) 4.3	(5) 4.9	(17) 7.3	(43) 9.3	(14) 6.0		Value of weighted average, obtained multiplying mean velocity of respective directions with appearance frequency
		E	(1) 6.0	(1) 8.3	(5) 7.1	(10) 6.9	(6) 5.6	(4) 4.3	(6) 6.0	(1) 5.0	(1) 3.8	(2) 5.6	(4) 5.1	(1) 7.7	(3) 5.9	4.40kt	
		SE	(1) 7.0	(–) 7.5	(1) 6.5	(6) 7.0	(9) 6.1	(9) 6.7	(9) 7.5	(17) 8.1	(7) 7.1	(5) 6.5	(3) 6.2	(–) 6.3	(5) 6.9		
		S	(–) –	(1) 5.7	(1) 5.2	(6) 6.1	(15) 7.0	(20) 6.1	(27) 7.9	(35) 7.2	(27) 6.7	(16) 6.6	(3) 6.8	(1) 7.2	(13) 6.0		
		SW	(–) 6.0	(–) –	(–) 10.0	(5) 4.0	(8) 5.4	(11) 5.8	(9) 7.1	(14) 5.8	(23) 7.1	(12) 6.2	(2) 5.3	(1) 5.8	(7) 5.7		
		W	(3) 4.0	(–) –	(5) 3.8	(12) 3.6	(9) 3.6	(13) 5.4	(9) 4.9	(11) 5.5	(9) 5.1	(12) 5.2	(7) 5.2	(–) 4.3	(7) 4.2	2.20 m/sec	
		NW	(23) 3.0	(10) 2.2	(16) 2.4	(13) 2.6	(13) 2.9	(8) 4.7	(10) 3.8	(3) 3.2	(11) 6.0	(14) 4.2	(13) 3.8	(3) 4.5	(12) 3.6		
		Calm	(6) –	(2) –	(17) –	(21) –	(28) –	(27) –	(20) –	(17) –	(29) –	(25) –	(19) –	(3) –	(18) –		
	Mean Temperature (°C)		26.2	27.1	27.4	27.7	28.0	27.9	27.4	28.0	27.4	27.3	26.2	26.3	27.2	27.4	24Hr Mean
Singapore total area	Mean Temperature (°C)		25.5	26.1	26.5	26.9	27.3	27.1	27.1	26.9	26.8	26.6	26.1	25.6	26.6	26.5	24Hr Mean

Note: *1 PERIOD 1978 1 year (METEOROLOGICAL SERVICE SINGAPORE)
*2 PERIOD 1975–1979 5 years
*3 PERIOD 1929–1941, 1948–1979 45 years

CHAPTER 4 WATER TEMPERATURE AND SALINITY SURVEY

II-4-1 Outline

Water temperature and salinity survey have been conducted for the purpose of obtaining the data on horizontal and vertical distribution of temperature and salinity of the survey areas. The results of the survey have been used as the basic data for the diffusion calculation of thermal and pollutant effluent of the survey areas. Table II-4-1 shows the outline of the survey.

Table II-4-1 Outline of water temperature and salinity survey

Area	Survey Item	Observation Layer	Survey point	Date, Time
Seraya	Temperature	−0.5m, −2m, −5m −10m, Bottom + 1m	49 points	Mar. 2, 1981 13:00 ~ 16:00
	Salinity	−0.5m	28 points	
		−0.5m, −2m, −5m −10m, Bottom + 1m	21 points	
Tekong	Temperature	−0.5m, −2m, −5m −10m, Bottom + 1m	35 points	Mar. 5, 1981 15:00 ~ 17:00
	Salinity	−0.5m	24 points	
		−0.5m, −2m, −5m −10m, Bottom + 1m	11 points	

* Some modifications made according to the water depth on observation depth.

II-4-2 Specifications of the Field Survey

II-4-2-1 Survey point

Fig. II-4-1 illustrates the survey points. In both areas, the survey points have been scattered so as to surround the proposed sites for power stations and the integrated steel mill.

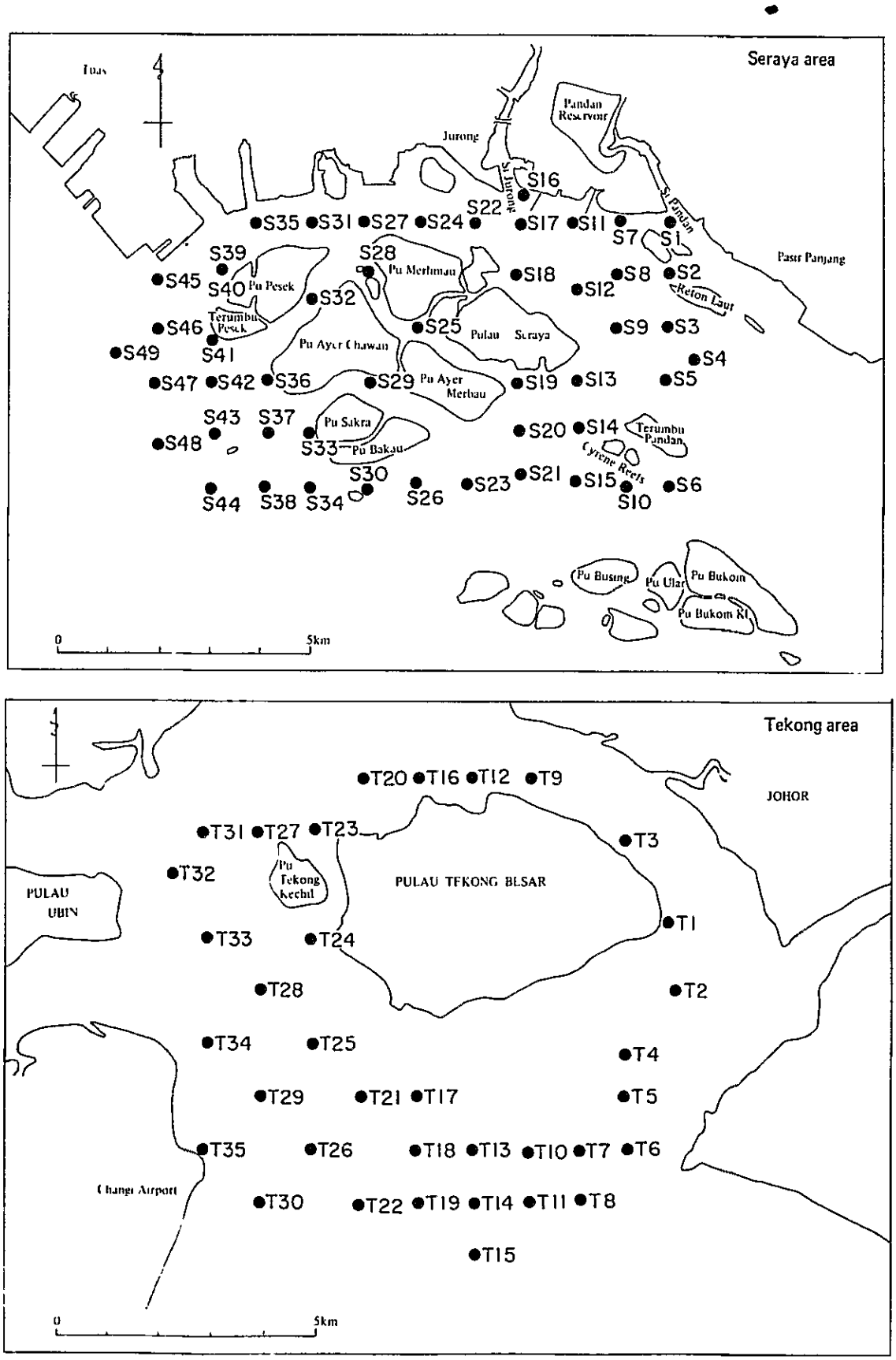

Fig. II-4-1 Survey point of temperature and salinity survey

II-4-2-2 Survey schedule

The surveys have been conducted during 13:00 to 16:00 of March 2nd 1981 at Seraya Area and during 15:00 to 17:00 of March 5th 1981 at Tekong Area.

The survey at Tekong Area was supposed to be conducted on March 4th, but due to the heavy squall, the schedule was extended for one day and on March 5th the survey was conducted.

In view of the fact that the survey should be conducted within the short period during the current velocity being slow, the survey time has been selected from the predicted tide level of Victoria Dock. Both March 2nd and March 5th were favoured with the mild current conditions and the complete data have been obtained.

II-4-2-3 Survey methods

1) Works on board

The survey has been conducted by 5 survey boats as shown in Table II-4-2. The survey boats have been employed as shown in Fig. II-4-2 and those are mostly the bamboats except one launch employed at Seraya as No.4 boat. For the determination of the survey points, the three point fixed method has been sued as shown in Fig. II-4-3.

Table II-4-2 Survey boats

Area	Boat No.	Survey point and observation order
Seraya	No.1 boat	S39 - S35 - S31 - S32 - S28 - S27 - S24 - S22 - S17 - S16
	No.2 boat	S 5 - S 4 - S 3 - S 9 - S12 - S 8 - S 2 - S 1 - S 7 - S11 - S18
	No.3 boat	S 6 - S10 - S15 - S21 - S20 - S14 - S13 - S19 - S25
	No.4 boat	S23 - S26 - S30 - S34 - S38 - S44 - S37 - S33 - S29
	No.5 boat	S48 - S43 - S36 - S42 - S47 - S49 - S46 - S41 - S40 - S45
Tekong	No.1 boat	T12 - T16 - T20 - T23 - T23 - T24 - T27 - T31 - T32
	No.2 boat	T 9 - T 3 - T 1 - T 2 - T 4
	No.3 boat	T 5 - T 6 - T 7 - T 8 - T11 - T10 - T13 - T14
	No.4 boat	T15 - T19 - T18 - T22 - T26 - T30 - T35
	No.5 boat	T17 - T21 - T25 - T29 - T34 - T28 - T33

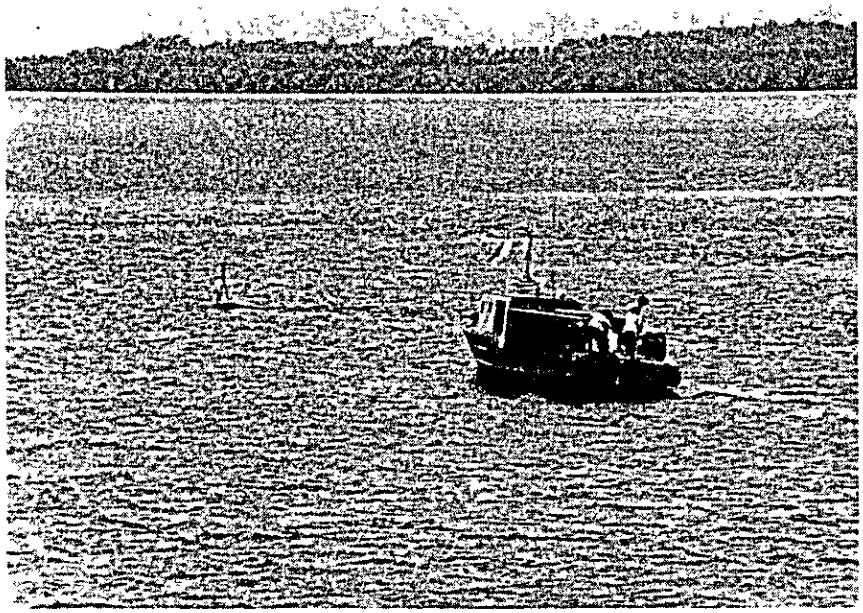

Fig. II-4-2

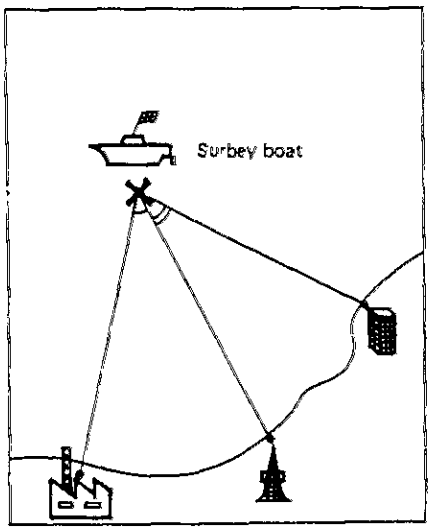

Three point fix method

Decide three making point on the land (for example, tower, building and so on)
Measure left angle and right angle by sextant and fix the point by station pointer.

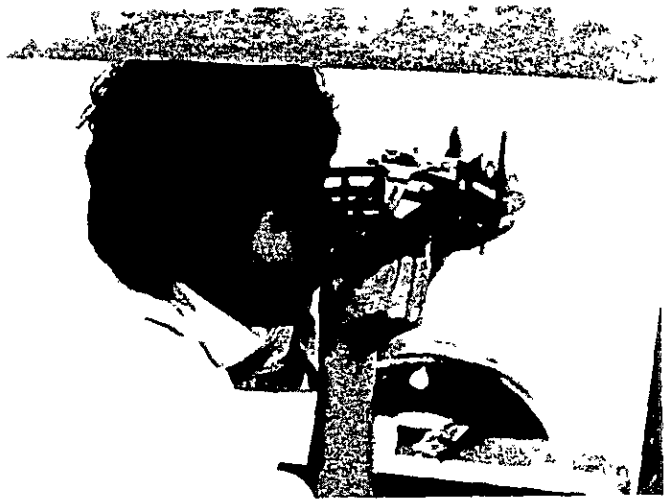

Sextant

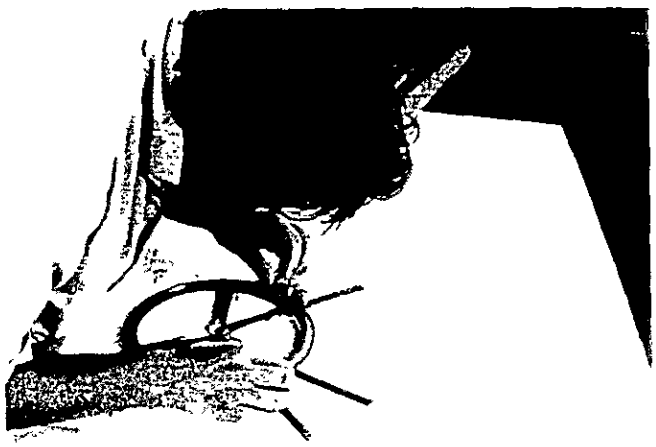

Station pointer

Three point fix method

Fig. II-4-3

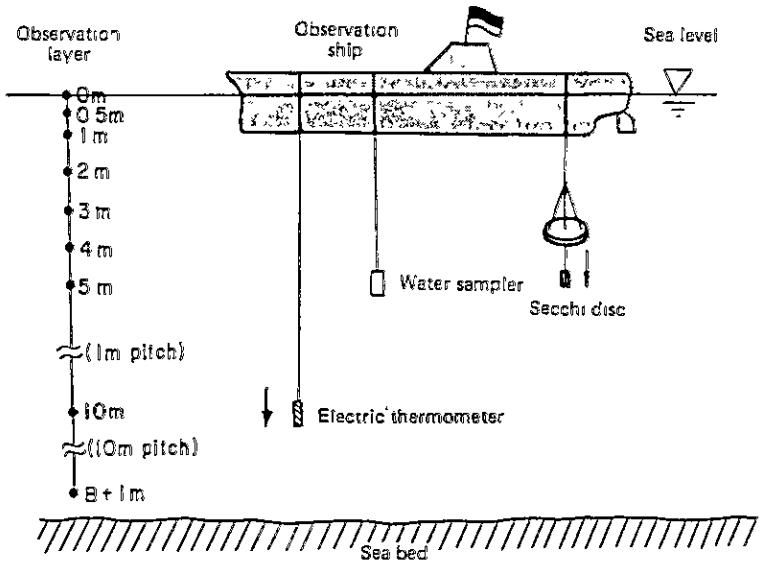

Examples of Observation Layers at Water quality Survey Point

Electric Thermometer ET-II

Electric thermometer on the boat

Water sampler

Water Quality Survey

Fig. II-4-4

Soon after the survey boats reach to the survey points, the depth has been measured by the depth scale and the survey has been conducted as shown in Table II-4-3. For the survey of salinity, the survey has been carried out for 5 depths at the representative points and at the rest of the survey points, the survey has been carried out only for 0.5 m below the sea surface.

Table II-4-3 Observation depth for temperature and salinity survey

Depth (m)	Observation layer (m)				
- 8	-0.5	-1	-2	-3	B+1
8 - 12	-0.5	-1	-2	-5	B+1
12 -	-0.5	-2	-5	-10	B+1

Fig. II-4-4 shows the snaps of the survey. For the temperature, ET-II type Electric Thermometer has been used and for the salinity, the sampling has been made by KITAHARA's Sampling Bottle and collected water sample has been contained in Poly-Ethylene bottles for conveying to the laboratory.

At the representative points, the atmospheric temperature and humidity have been measured by Assmann's Psychrometer and also the wind direction and velocity have been measured by Biran Type wind Vane and Anemometer.

2) Chemical analysis

For the salinity measurement of the sea water, Salinometer method and Mohr's titration method are usually employed.

Salinometer method is to measure the electric conductivity and to convert it into salinity. By this method, the accurate measurement can be carried out within the short time but it is not perferable for the sea water of the coastal areas which is affected by river water and or household effluent.

Mohr's titration method is to measure the chlorinity by silver nitrate titration, and although the accuracy is quite high, the disadvantage of this method is that it takes longer time than salinometer method.

Fig. II-4-5 and II-4-6 show the processes of the two methods. In this study, the Salinometer method has been employed and also for the purpose of checking the measuring results by Samlinometer, the measurement has been conducted at the representative points by titration method.

Table II-4-4 shows the comparison of the results measured by two methods from which it is found the results of the measurement in this study is accurate, the difference between two methods being $\pm$0.2 %.

Table II-4-4 Comparison of Salinometer method and Titration method

Survey point	Observation layer (m)	Salinity (%) (A) Mohr's titration	(B) Salinometer	(B) - (A)
S 5	-0.5	32.77	32.80	0.03
S 16	-0.5	31.00	30.87	-0.13
S 21	-0.5	32.84	32.80	-0.04
S 39	-0.5	32.64	32.73	0.09
S 49	-0.5	32.77	32.90	0.13
T 1	-0.5	30.91	31.02	0.11
T 9	-0.5	30.60	30.64	0.04
T 15	-0.5	31.81	31.92	0.11
T 28	-0.5	31.09	31.19	0.10
T 32	-0.5	30.77	30.92	0.15

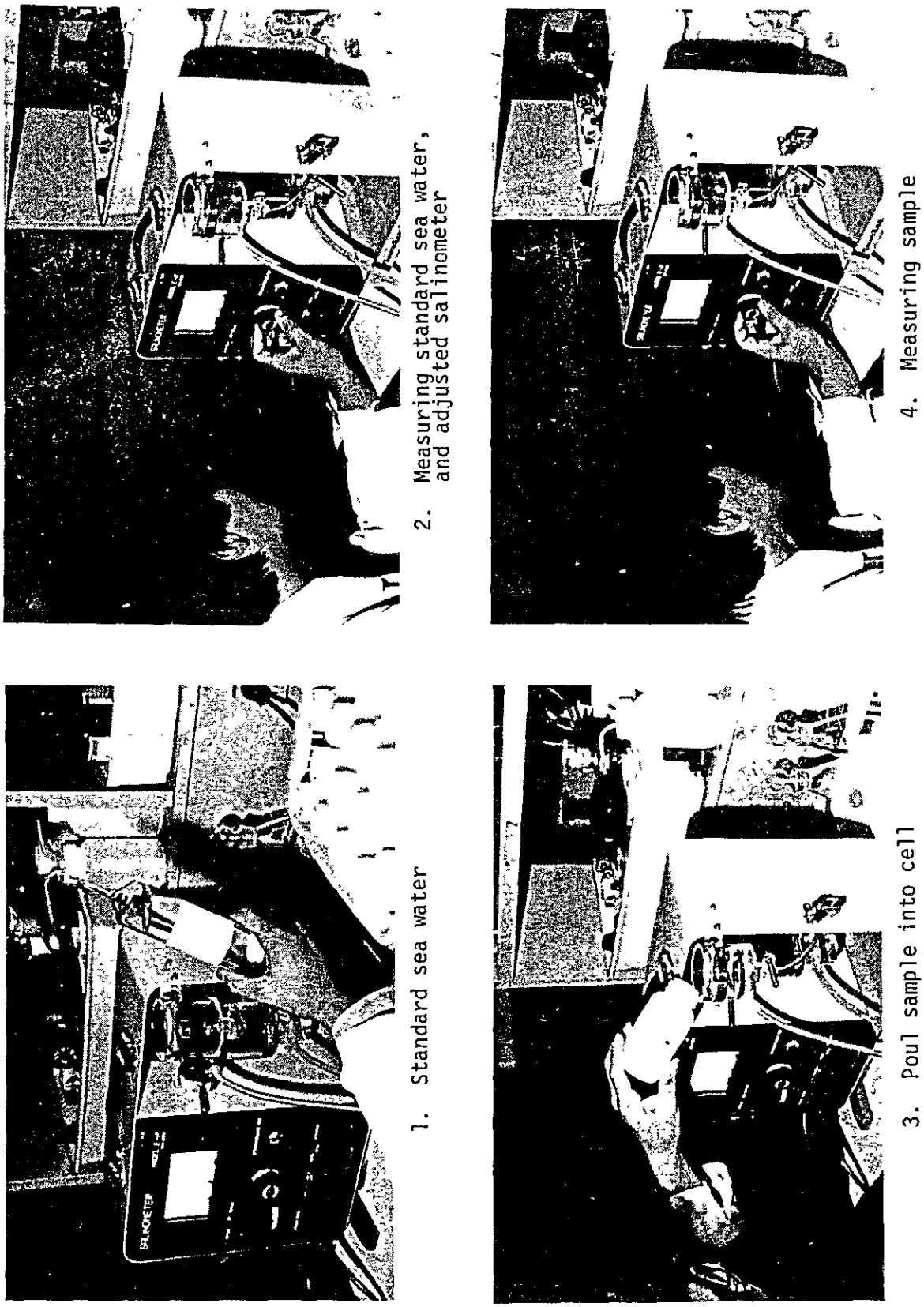

Fig. II-4-5 Processes of Salinometer method

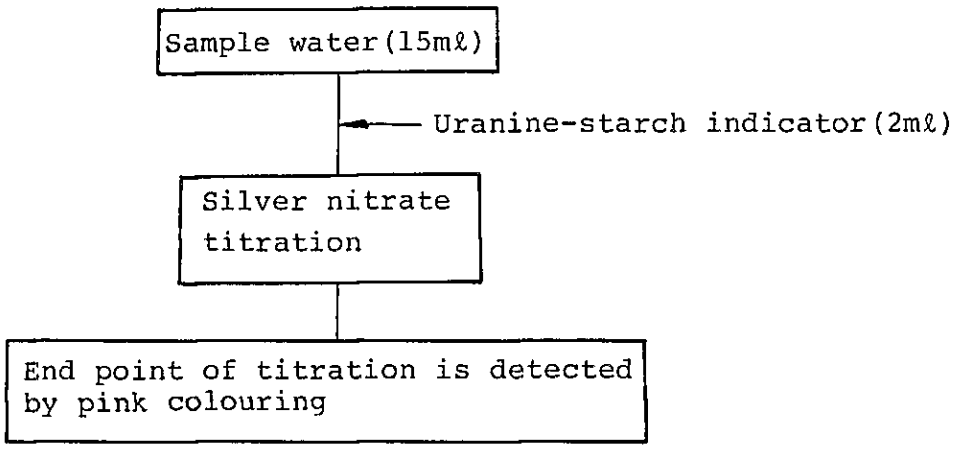

Remarks: 1) to obtain correction value by normal water titration
2) chlorinity is silver nitrate titration value added with above correction value
3) chlorinity is converted by the following equation:

(Salinity) % = 1.80655 x (chlorinity) %.

Fig. II-4-6 Measurement of chlorinity

II-4-2-4 Instruments

The instruments employed in this study are as follows.

1) Surveying sextant and station pointer

The surveying sextant and station pointer are the instruments used for the determination of survey points by three point fix method.

2) Assmann's phychrometer

Assmann's psychrometer is the portable psychrometer as shown in Fig. II-4-7-(1).

3) Biram type wind vane and anemometer

Biram type wind vane and anemometer is the portable instrument for the measuremnt of wind direction and velocity as shown in Fig. II-4-7-(1).

4) Electric thermometer (ET-II)

Electric thermometer (ET-II) is also the portable thermometer and it measures the water temperature as shown in Fig. II-4-7-(2).

5) KITAHARA's SAMPLING BOTTLE

KITAHARA's SAMPLING BOTTLE is widely used for water sampling as shown in Fig. II-4-7-(2).

6) Salinometer

Salinometer is the instrument for measuring the salinity by electric conductivity as previously described. Refer to Fig. II-4-7-(2).

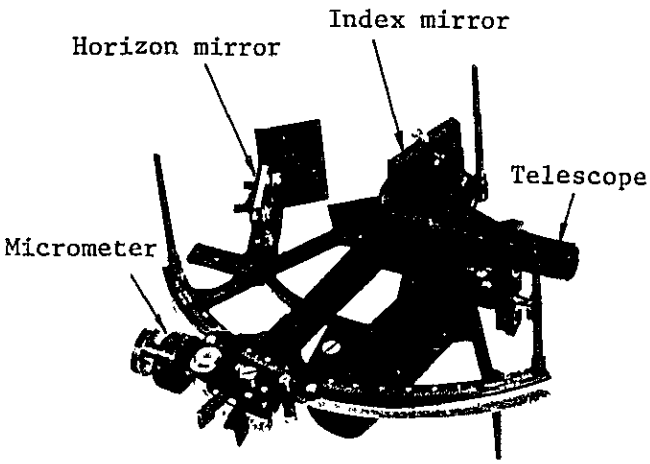

SURVEYING SEXTANT

Specifications

Light alloy casting:	
Radius:	162 mm
Graduation:	–5°C to 125°C
Reading:	
Micrometer reading:	1 min
Telescope:	4 x 40 mm
Horizon mirror: Circular:	50 mm dia.
Index mirror: Rectanguar	33 x 49 mm

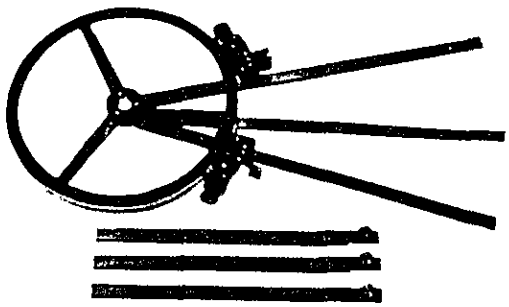

STATION POINTER

Specification:

Out side diam. of circle:	24.5 cm
Graduation:	1°
Micrometer reading:	1 min
Length of arm:	40 cm
With adjustable arm:	65 cm

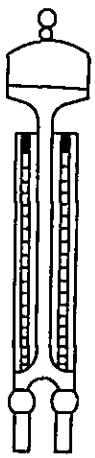

ASSMANN'S PSYCHROMETER

Range: –30 ~ 50°C
Minimum Scale: 0.2°C

WIND VANE and ANEMOMETER (Biram type)

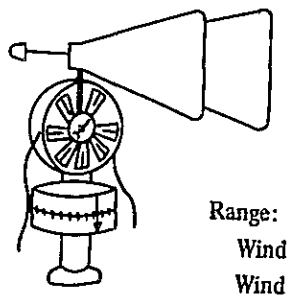

Range:
Wind Speed 0.5 ~ 15m/S
Wind Direction

Fig. II-4-7-(1) Instruments for temperature and salinity survey

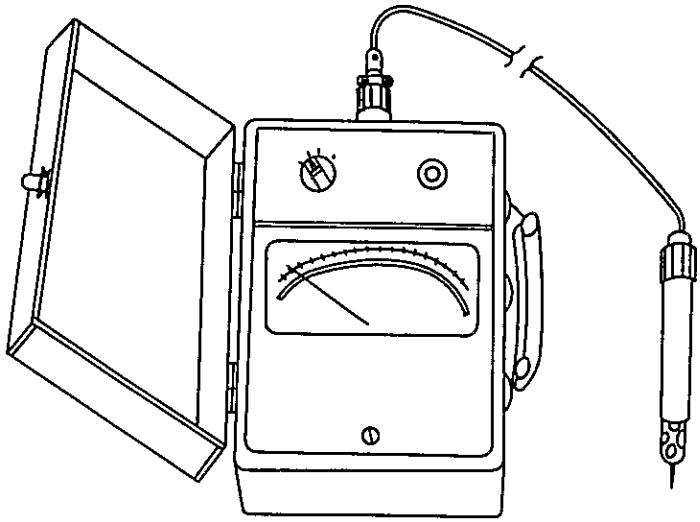

Sensor Type: Thermistor

Range: -5 ~ 10°C
10 ~ 25°C
25 ~ 40°C

Power Source: 2 pcs. of SUM-2

KITAHARA'S
SAMPLING BOTTLE

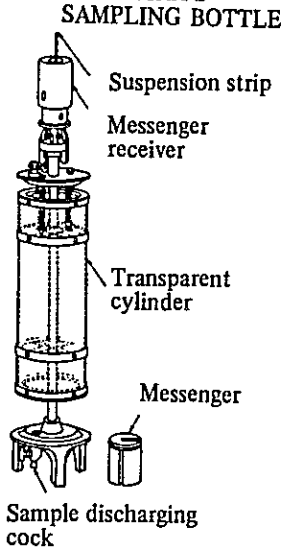

SALINOMETER
(T.S-E2)

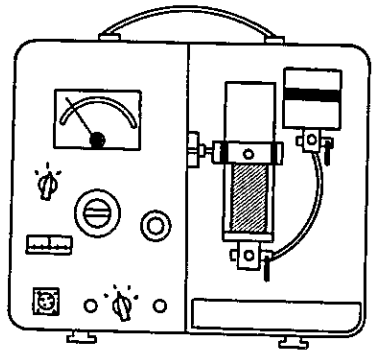

Range: 0 ~ 40‰ S
30 ~ 40‰ S

Accuracy:
0 ~ 40‰ Range 0.04‰ S
30 ~ 40‰ Range 0.01‰ S

Power Source: AC 100V or
DC 12V

Fig. II-4-7-(2) Electric thermometer (ET-II)

II-4-3 Survey Results of Seraya Area

II-4-3-1 Meteorological and oceanographic conditions at survey time

Table II-4-5 shows the meteorological conditions of the survey time which were measured on the survey boat.

The atmospheric temperature and humidity have been measured by Assmann's Phychrometer and the wind direction and velocity have been measured by Biram type Wind Vane and Anemometer. The meteorological conditions of the survey day was so mild under calm wind.

Table II-4-5 Meteorological conditions of survey data for temperature, salinity and water quality survey

Survey point	Time	Air temperature (°C)	Humidity (%)	Wind direction	Wind speed (m/sec)
S 5	13:00	29.5	86	N	2.9
S 18	15:25	29.5	89	SE	6.6
S 16	15:30	30.5	93	S	0.7

Fig. II-4-8 shows the tides and current conditions of the time when the survey is conducted.

From the figure, it is shown that the survey was conducted at during 13:00 to 16:00 which corresponds the time range of low water at 15:04. The current conditions as a whole express the eastward flow. The turn of tide from the slack water at the time of low water is beginning from about 16:00 and because of the time difference with the tides being about 1 hour, the survey could not be conducted during the slow current as expected.

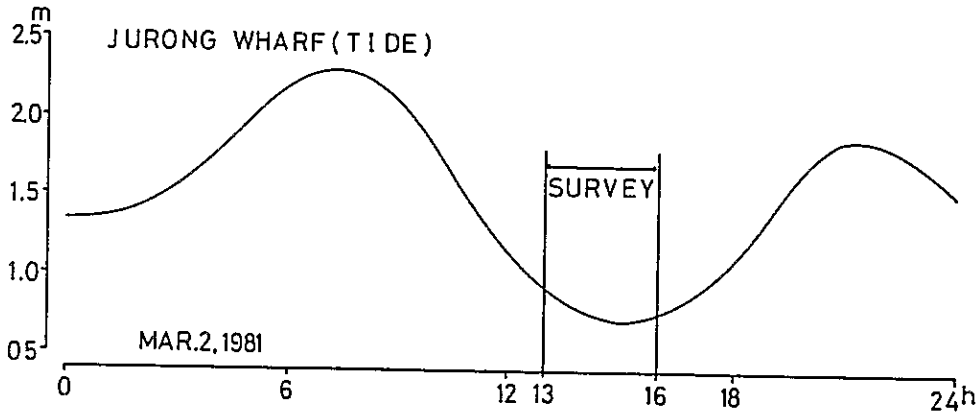

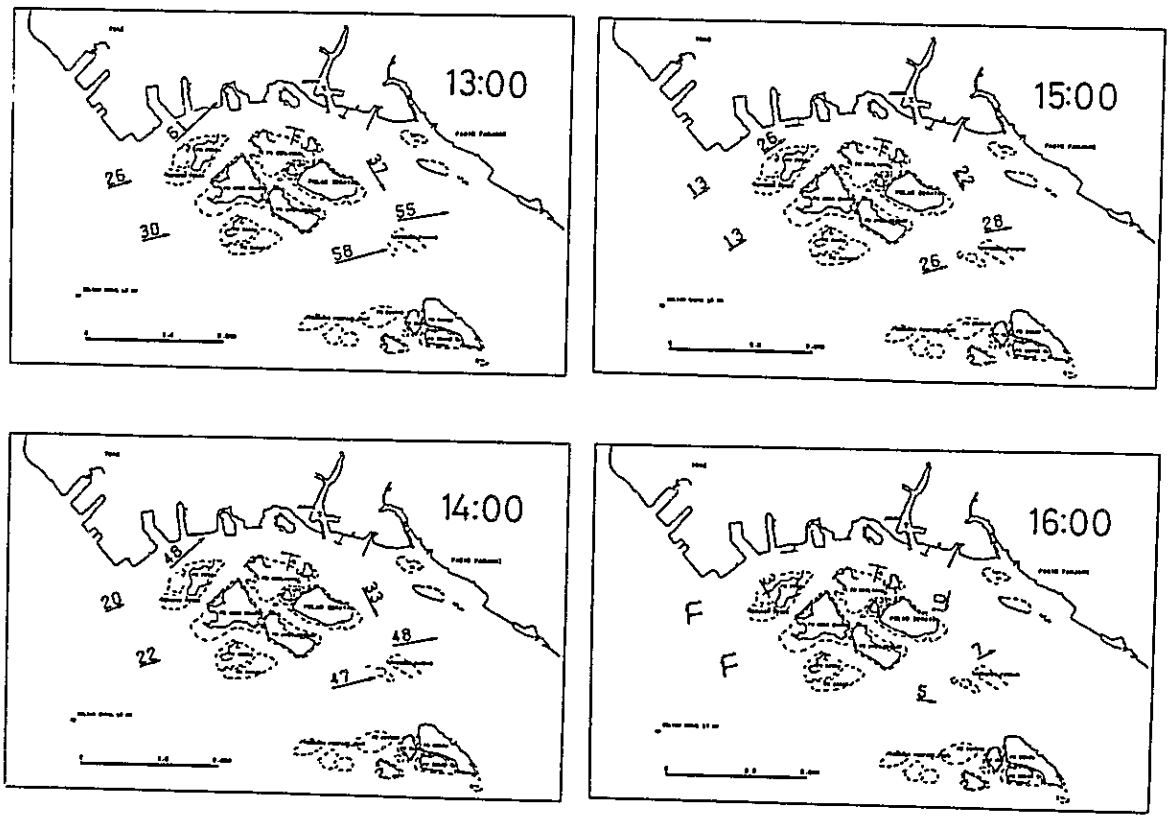

Fig. II-4-8 Tide and current conditions of survey time

II-4-3-2 Distribution of temperature and salinity

Table II-4-6 shows the observed values of temperature and salinity of the each depth, and Table II-4-7 shows the results of analysis and also Fig. II-4-9 shows ST diagram.

At S16 located in the mouth of Jurong River, the temperature is high and salinity is low compared with other points but generally the temperature is slightly lower in the deeper layer and deviation of the data is so small. For the salinity, the difference between depths could not be observed.

Table II-4-6 Temperature and salinity of each layer

Layer	Temperature (°C)					Salinity (‰)				
	Min.		Max.	$\bar{x}$	σ	Min.		Max.	$\bar{x}$	σ
-0.5 m	28.1	~	29.8	28.4	0.30	30.87	~	32.91	32.78	0.28
-2 m	28.0	~	28.9	28.3	0.19	31.81	~	32.88	32.74	0.23
-5 m	27.9	~	28.5	28.1	0.10	32.73	~	32.88	32.83	0.04
-10 m	27.9	~	28.3	28.1	0.09	32.73	~	32.89	32.83	0.04
B+1 m	27.9	~	28.3	28.1	0.09	32.68	~	32.90	32.81	0.09

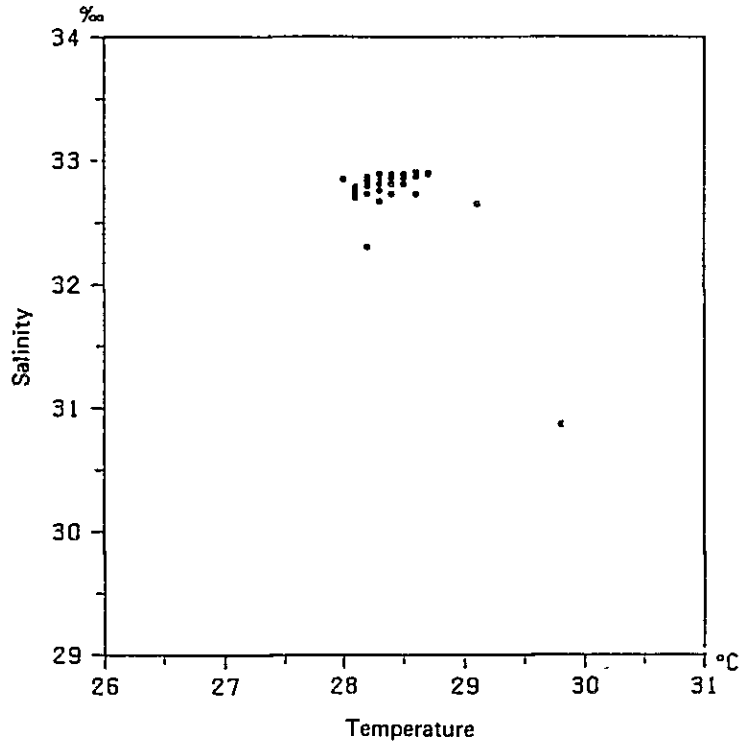

Fig. II-4-9 ST diagram

1) Horizontal distribution of temperature

Fig. II-4-10 shows the horizontal distribution of temperature of each depth.

As for the depths of -0.5 m and -2 m, the higher values were obtained at S1 and S16 which are located in the mouth of River Pandan and Jurong River respectively compared with other points. The west side area of Pulau Merlibau shows a little higher value than the east side of the same island.

As for the depts of -5 m, -10 m and B+1 m, the averaged temperature shows 28.1°C and shows small deviation.

2) Horizontal distribution of salinity

Fig. II-4-11 shows the horizontal distribution of salinity of each depth.

Taking the particular points, S1 and S16, where the temperature values showed higher, the salinity of S16 is lower about 2% at -0.5 m depth compared with other points and about 1% lower at -2 m depth. The salinity of S1 does not show any remarkable difference with other points which means the River Pandon is not flowing the fresh water so much.

The salinity of each depth of the remaining points shows about 32.8% and deviation of the values are so small.

3) Vertical distribution of temperature and salinity

Fig. II-4-12 shows the vertical distribution of temperature and salinity of the representative points.

The temperature of S16 shows the difference of 1.6°C between -0.5 m and B+1 m but in other points, the difference between each depth is small having the tendency that the temperature of deeper depth is slightly low.

The salinity of S16 shows the difference of about 2% between -0.5 m and B+1 m, but in other points there are almost no differences between depths.

Table II-4-7 Results of Analysis of Temperature and Salinity survey

Seraya (1)

Station No	Time	Depth (m)	Temperature (°C)							Salinity (‰)						
			-0.5 m	-1 m	-2 m	-3 m	-5 m	-10 m	B+1 m	-0.5 m	-1 m	-2 m	-3 m	-5 m	-10 m	B+1 m
S 1	14.50 ~ 14 56	9.5	29 1	29 0	28 9	28.6	–	–	28 0	32 65	32.62	32.65	32 63	–	–	32.68
S 2	14 30 ~ 14 34	11 7	28 2	–	28.0	–	28 0	28.0	28 0	32 73	–	–	–	–	–	–
S 3	13 37 ~ 13 45	13 2	28.4	–	28.4	–	28.3	28.3	28.3	32.73	–	32.73	–	32 73	32.73	32.74
S 4	13 20 ~ 13 28	27 0	28 2	–	28 2	–	28 1	28.1	28 0	32.82	–	–	–	–	–	–
S 5	13 00 ~ 13 10	25 0	28 2	–	28 2	–	28 1	28 1	28.1	32 80	–	32.62	–	32.77	32.78	32 79
S 6	13 00 ~ 13 30	26 0	28 1	–	28 1	–	28 1	28 1	28 1	32.77	–	32.75	–	32.77	32.76	32.57
S 7	15 03 ~ 15 06	12.3	28.6	–	28 5	–	28.1	28 1	28 1	32.73	–	–	–	–	–	–
S 8	14 23 ~ 14 26	8 7	28 2	–	28 1	–	28.0	28.0	28.0	32 79	–	–	–	–	–	–
S 9	13 55 ~ 14 01	16 8	28 1	–	28 1	–	28.0	28.0	28.0	32 76	–	–	–	–	–	–
S10	13 36 ~ 13 45	27.0	28.3	–	28 2	–	28.2	28.1	28 1	32.81	–	–	–	–	–	–
S11	15 12 ~ 15 15	11.5	28.3	28.3	28.2	–	28 1	–	28 0	32 76	–	–	–	–	–	–
S12	14 10 ~ 14 17	13 9	28 1	–	28.0	–	28.0	28.0	28 0	32.79	–	32.53	–	32 80	32.81	32.81
S13	14 52 ~ 15 00	19.0	28.3	–	28.3	–	28 1	28 1	28 1	32.84	–	32.82	–	32.82	32 82	32 84
S14	14 40 ~ 14 44	18.0	28 2	–	28.3	–	28 2	28 1	28.1	32 82	–	–	–	–	–	–
S15	13 51 ~ 13 58	18 0	28 1	–	28 1	–	28 2	28 1	28 1	32.70	–	–	–	–	–	–
S16	15 25 ~ 15 37	6 2	29 2	29 8	28.5	28 2	–	–	27 9	30 87	31.32	31.81	31 75	–	–	32.75
S17	15 15 ~ 15 19	18 0	28.3	–	28 2	–	28 1	28 0	28 0	32.67	–	–	–	–	–	–
S18	15 23 ~ 15 26	13 2	28.3	–	28.3	–	28 1	28.1	28 1	32.89	–	–	–	–	–	–
S19	15 11 ~ 15 15	17 0	28 5	–	28.3	–	28.3	28.2	28.1	32.81	–	–	–	–	–	–
S20	14 30 ~ 14.35	18 0	28.3	–	28.3	–	28 2	28.1	28 1	32.81	–	–	–	–	–	–
S21	14 07 ~ 14 23	20 0	28 2	–	28.2	–	28.2	28 2	28 1	32.80	–	32.84	–	32.82	32 82	32.83
S22	14 57 ~ 15 03	25.3	28 2	–	28 2	–	28 1	28 1	28.0	32.83	–	–	–	–	–	–
S23	12.57 ~ 13 05	23.0	28 2	–	28.2	–	28 2	28.2	28.2	32.86	–	–	–	–	–	–
S24	14 37 ~ 14 50	18 4	28 2	–	28.2	–	28 2	28 1	28 1	32.85	–	32.60	–	32.81	32.81	32 74
S25	15 33 ~ 15 32	11 5	28 4	28 4	28.3	–	28.3	–	28.1	32 86	32.84	32.84	–	32.84	–	32.82
S26	13 16 ~ 13 19	19 0	28 2	–	28 2	–	28.2	28 2	28 2	32.86	–	–	–	–	–	–
S27	14 23 ~ 14 30	25 1	28 2	–	28 2	–	28 1	28 0	28.0	32.83	–	–	–	–	–	–
S28	14 08 ~ 14 15	12 0	28 4	–	28.2	–	28 2	28.1	28 1	32.81	–	32.83	–	32.80	32 81	32 83
S29	14 43 ~ 14 51	11 6	28 2	28.2	28 2	–	28 1	–	28.1	32.87	32.87	32.86	–	32.86	–	32.86
S30	13 28 ~ 13 39	18.5	28 2	–	28 2	–	28 2	28 2	28.2	32.86	–	32 86	–	32.86	32 86	32.65
S31	13.31 ~ 13 44	24 2	28 1	–	28.1	–	28 1	28 0	28 0	32.73	–	32.84	–	32 84	32 84	32.86
S32	13 58 ~ 14 03	14 5	28.2	–	28 2	–	28 1	28 1	28 1	32.86	–	–	–	–	–	–
S33	14 35 ~ 14.38	9 7	28.5	28.5	28 4	–	28 2	–	28 1	32.89	–	–	–	–	–	–
S34	13 49 ~ 13 53	15.4	28 4	–	28.3	–	28 2	28 2	28 2	32.89	–	–	–	–	–	–
S35	13 20 ~ 13 24	15.7	28 0	–	28.0	–	28 0	28 0	28 0	32 85	–	–	–	–	–	–
S36	13 45 ~ 13 59	12.0	28 5	–	28.3	–	28 2	28 0	28 0	32.86	–	32.86	–	32.88	32.89	32.89
S37	14 26 ~ 14 29	12.0	28.6	28.6	28.5	–	28 1	–	28.1	32.90	–	–	–	–	–	–
S38	14 00 ~ 14 08	19 0	28 7	–	28.6	–	28 2	28 2	28 2	32.89	–	32.84	–	32 87	32.87	32 87
S39	13 00 ~ 13 12	13 4	28 1	–	28 1	–	28 1	28 1	28 1	32.73	–	32 82	–	32 83	32.83	32.84
S40	15 29 ~ 15 32	16 0	28 6	–	28.6	–	28.5	28 2	28 2	32 88	–	–	–	–	–	–
S41	15 21 ~ 15 24	8 5	28.6	28.6	28.6	–	28 1	–	28.1	32 87	–	–	–	–	–	–
S42	14 11 ~ 14 15	14 0	28.6	–	28 4	–	28 1	28 0	27.9	32.89	–	–	–	–	–	–
S43	13 28 ~ 13 34	13.0	28 7	–	28 4	–	28 2	28.0	28 0	32.89	–	–	–	–	–	–
S44	14 16 ~ 14 20	14 5	28.6	–	28 5	–	28 1	28 0	28 0	32.91	–	–	–	–	–	–
S45	15 36 ~ 15 45	12.0	28 2	–	28 2	–	27.9	27.9	27 8	32 60	–	32.61	–	32 83	32.86	32 87
S46	15 08 ~ 15 12	11 0	28 6	28.6	28 6	–	28 1	–	28 0	32.90	–	–	–	–	–	–
S47	14 22 ~ 14.35	16.0	28 7	–	28 7	–	28 1	28 0	27 9	32 90	–	32.88	–	32 88	32 88	32 88
S48	13 00 ~ 13 20	14 0	28 7	–	28 4	–	28 1	28 0	28 0	32 90	–	32 88	–	32 87	32.87	32 89
S49	14 47 ~ 15 02	11 0	28 5	28 5	28 4	–	28 0	–	27 9	32.89	32 89	32.88	–	32 88	–	32.90

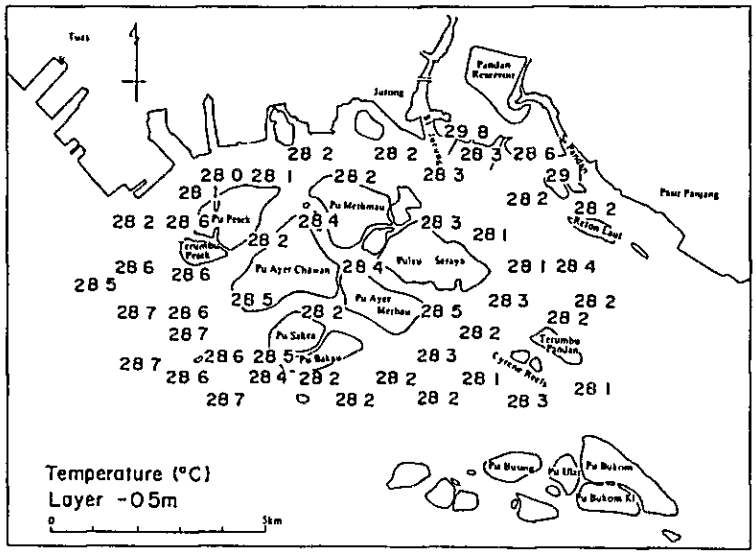

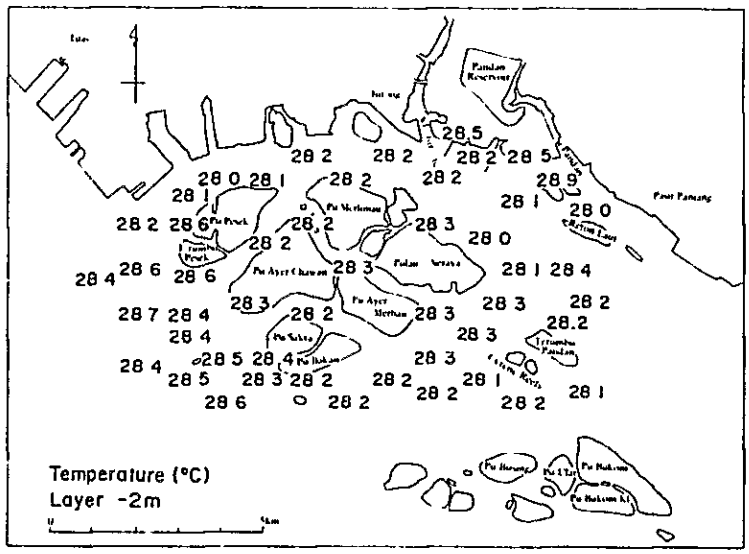

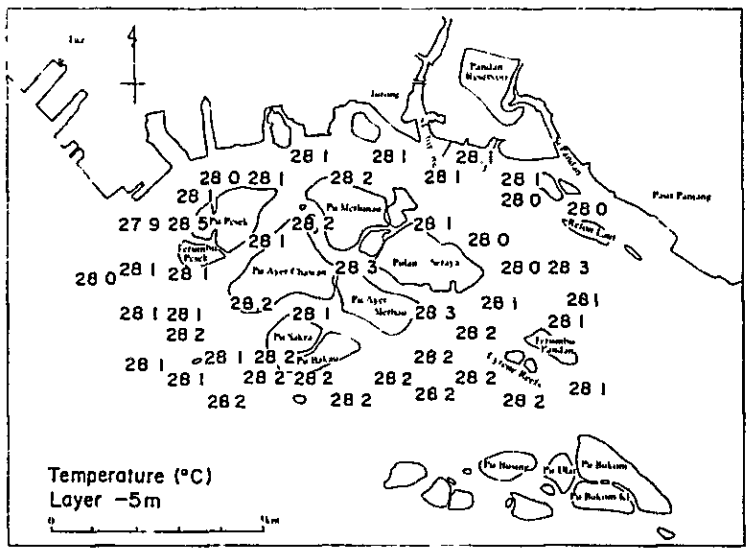

Fig. II-4-10 Horizontal distribution of temperature (1)

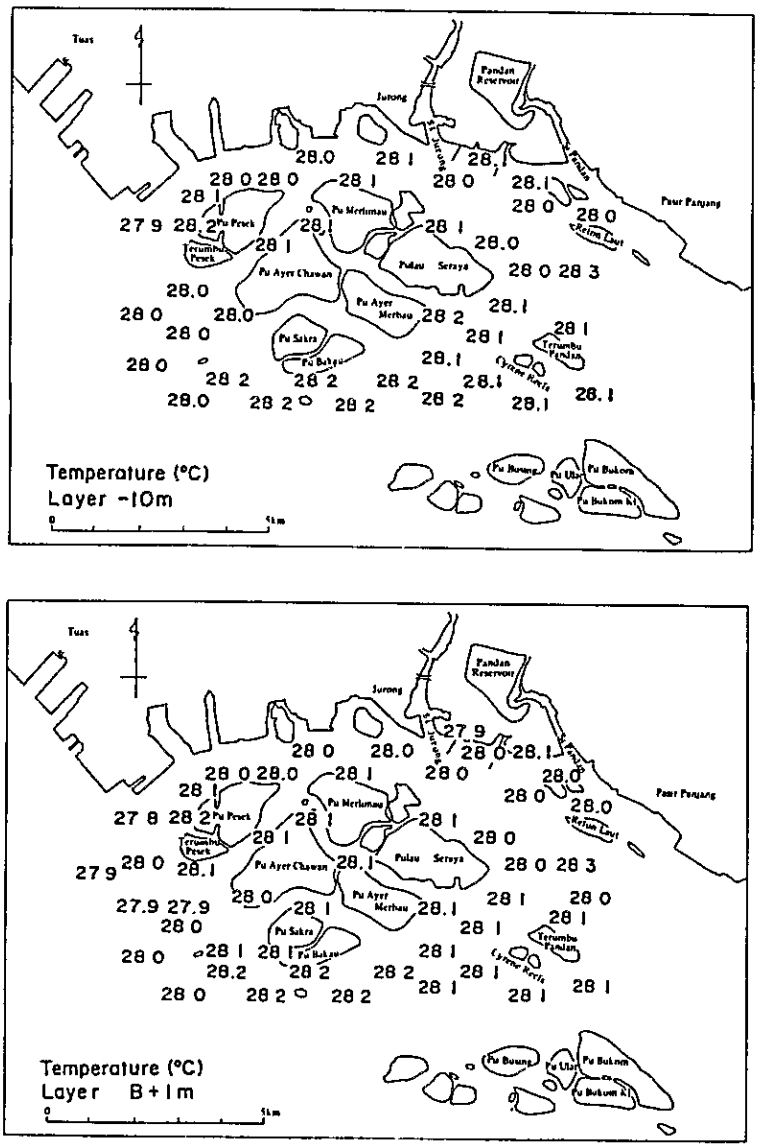

Fig. II-4-10 Horizontal distribution of temperature (2)

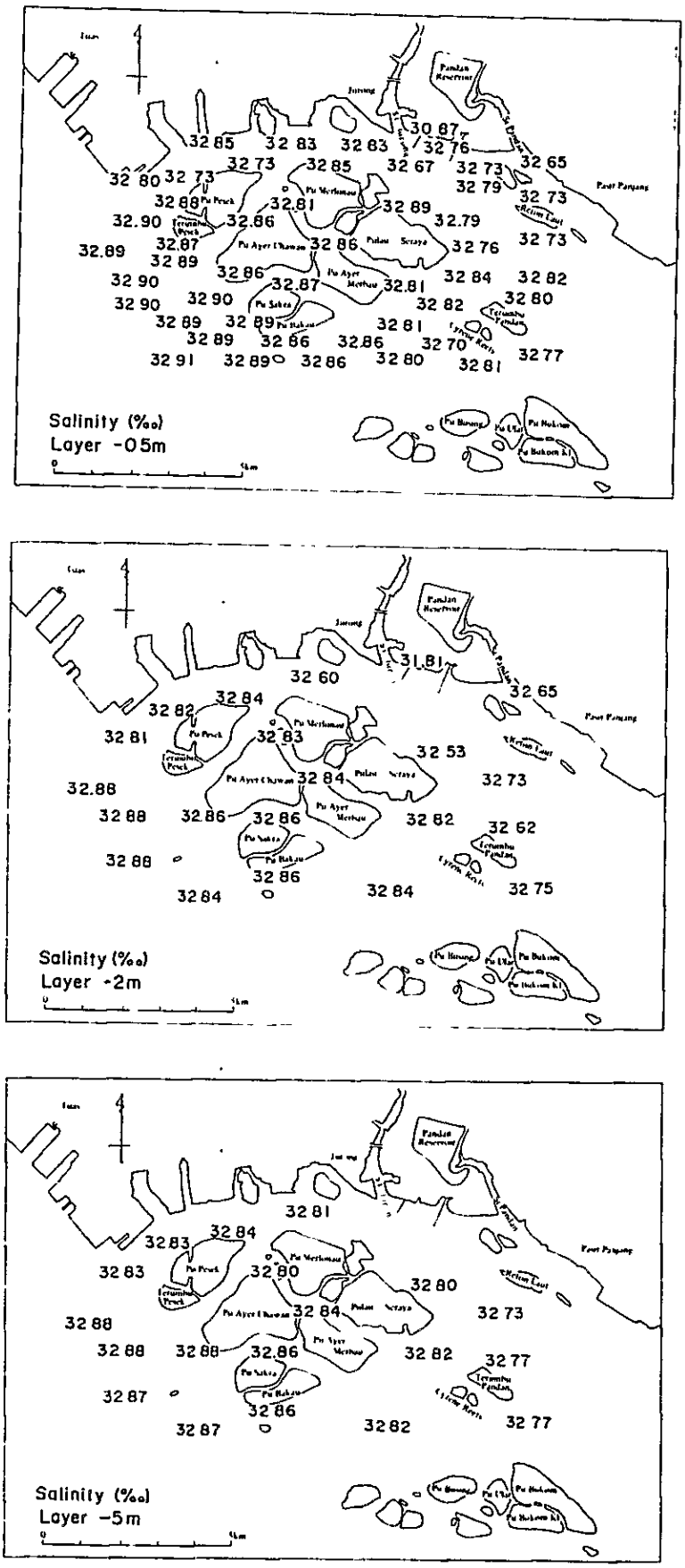

Fig. II-4-11 Horizontal distribution of salinity (1)

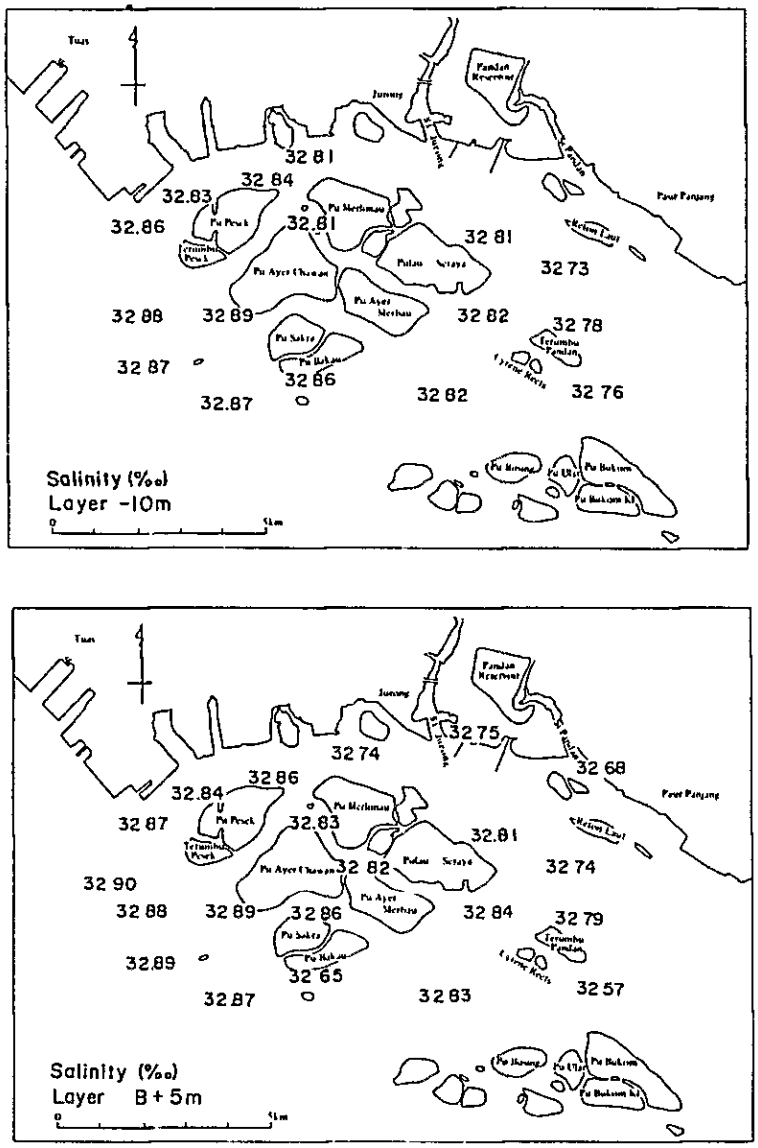

Fig. II-4-11 Horizontal distribution of salinity (2)

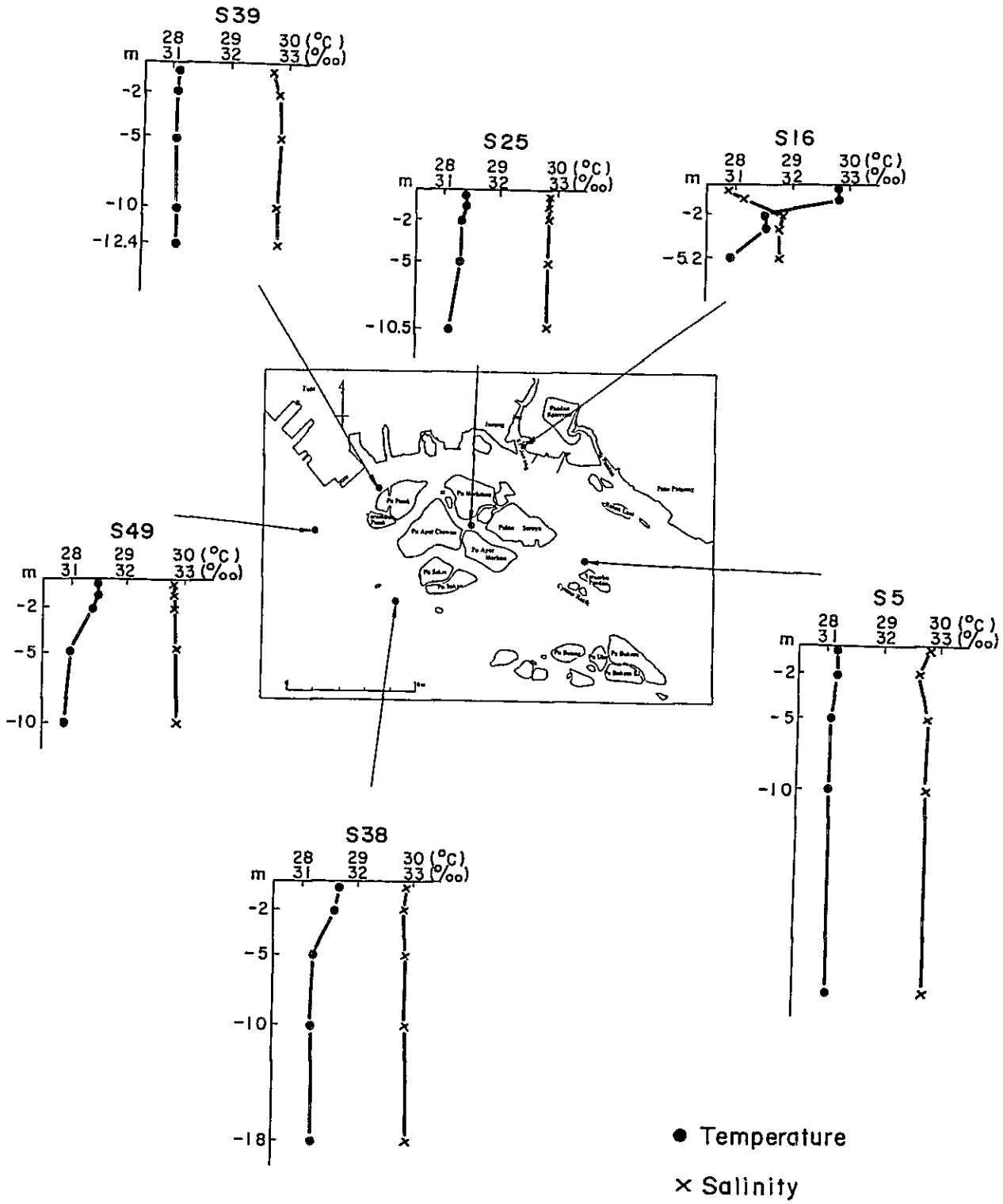

Fig. II-4-12 Vertical distribution of temperature and salinity

II-4-4 Survey Results of Tekong Area

II-4-4-1 Meteorological and Oceanographic conditions of survey day

As Table II-4-8 shows, the meteorological conditions of the survey day was mild under calm wind.

Table II-4-8 Meteorological conditions of survey day for temperature, salinity and water quality survey

Survey point	Time	Air temperature (°C)	Humidity (%)	Wind direction	Wind speed (m/sec)
T 12	15:00	30.5	70	NW	2.6
T 15	15:00	29.1	80	N	5.5

Fig. II-4-13 shows the tides and current conditions of the time when the survey was conducted.

From the figure, the survey time between 15:00 to 17:00 coincides with the neap tides, lowest tide level being at 15:50. As for the current conditions, the turn of the tides is at around 16:00 in the survey area and so the survey could be conducted under slow current as expected. Generally the current direction was southward before the turn of the tide and it was the northward after the turn of the tide.

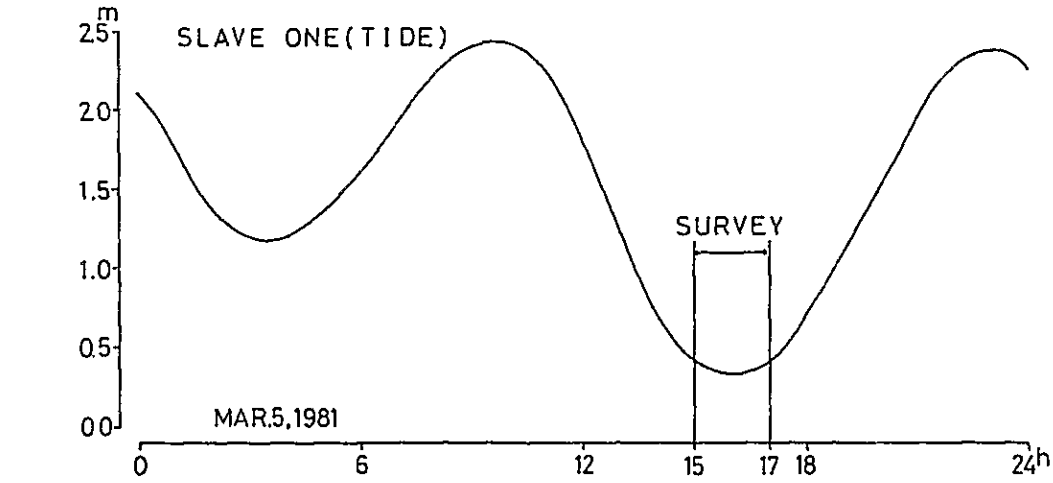

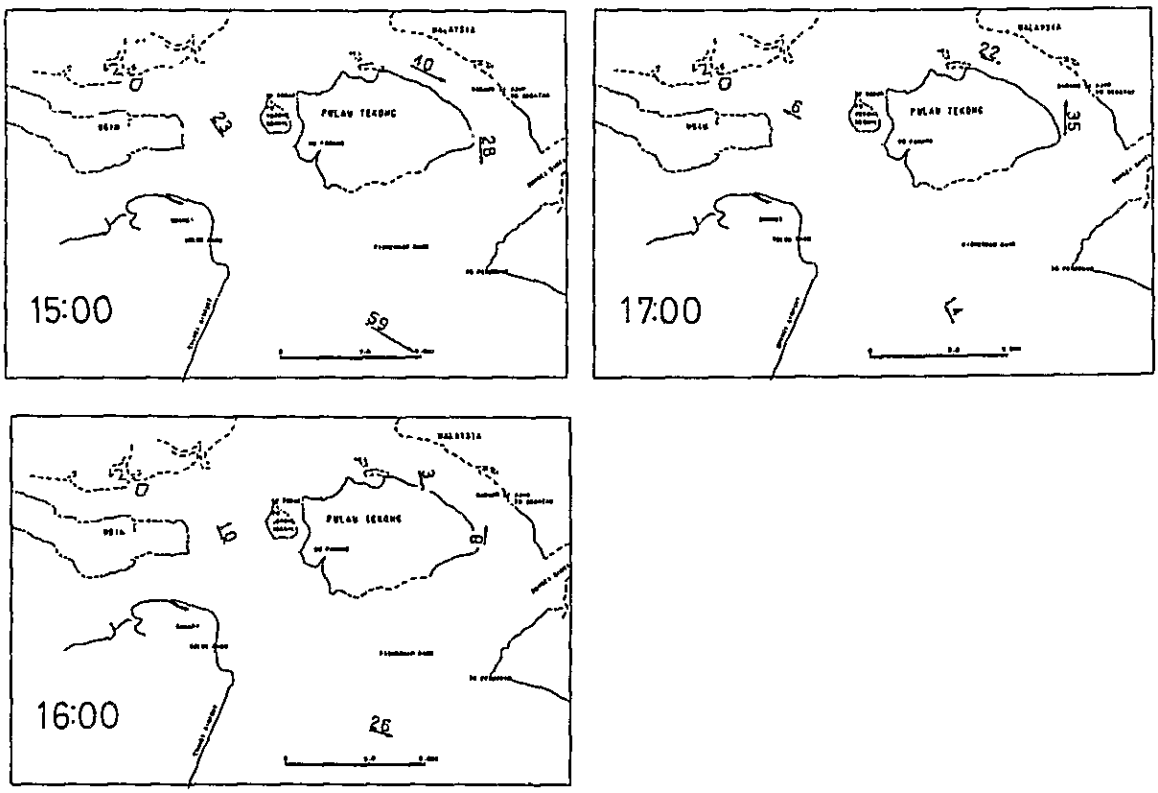

Fig. II-4-13 Tide and current conditions of survey time

II-4-4-2 Distribution of temperature and salinity

Table II-4-9 shows the observed data of temperature and salinity of each depth, Table II-4-10 shows the results of analysis and Fig. II-4-14 shows ST diagram.

As for the temperature, the difference among depths could not be found at all the points, and the observed values concentrated around 28°C.

As for the salinity, the difference among depths could not be also found and the values of all the points showed 30.50% to 32.39%. Thus the deviation of the values is rather larger than Seraya Area.

Table II-4-9 Temperature and salinity of each depth

Layer	Temperature (°C)					Salinity (‰)				
	Min.		Max.	$\bar{x}$	σ	Min.		Max.	$\bar{x}$	σ
-0.5 m	28.2	~	28.9	28.5	0.14	30.64	~	32.38	31.43	0.50
-2 m	28.2	~	28.9	28.5	0.14	30.59	~	31.93	31.16	0.47
-5 m	28.2	~	28.7	28.4	0.13	30.58	~	31.95	31.20	0.46
-10 m	28.2	~	28.5	28.4	0.09	30.60	~	31.99	31.34	0.49
B+1 m	28.2	~	28.9	28.4	0.15	30.59	~	32.39	31.51	0.60

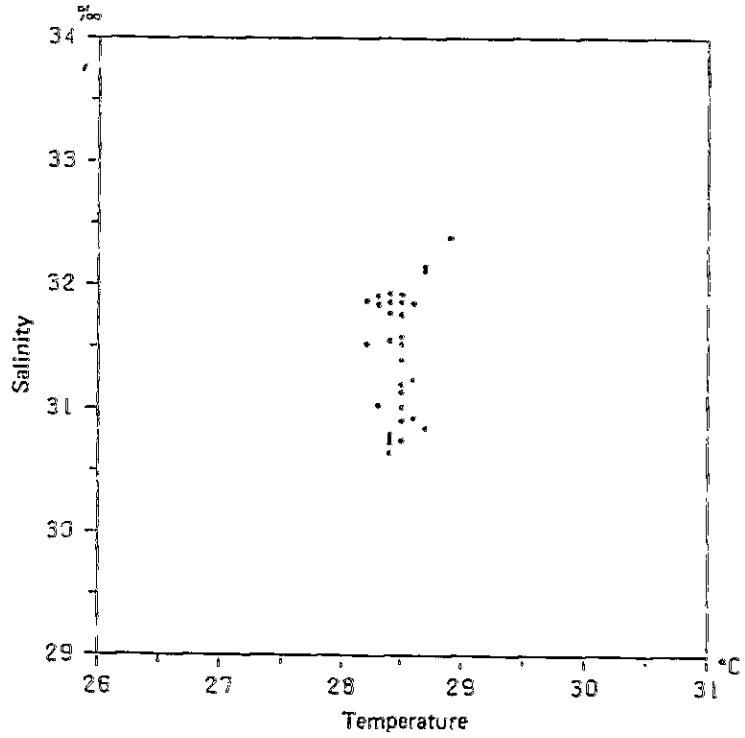

Fig. II-4-14 ST diagram

1) Horizontal distribution of temperature

Fig. II-4-15 shows the horizontal distribution of temperature. At T4 where the depth is shallow as 2.4 m, the temperature at -0.5 m and -2 m indicated rather high value as 28.9°C. But in other depths and points, any remarkable differences could not be found and the deviation of the values is smaller than Seraya Area.

2) Horizontal distribution of salinity

Fig. II-4-16 shows the horizontal distribution of salinity. At T4 the salinity of -5 m depth indicated 32.38% which was rather high value than other points, same as the case of temperature.

Generally the north side of Pulau Tekong indicated about 1% lower values than the south side of the island which considered as caused by the effect of Johor River.

As for the depths of -2 m, -5 m, -10 m and B+1 m, the survey have been conducted only for the representative points and these results also show the same tendency that the values of the north side of Pulau Tekong were lower than the south side, same as the case of -0.5 m.

3) Vertical distribution of temperature and salinity

Fig. II-4-17 shows the vertical distribution of temperature and salinity. Any remarkable difference in the vertical distribution could not be found.

Table II-4-10 Results of analysis of temperature and salinity survey (Tekong Area)

Tekong (-)

Station No	Time	Depth (m)	Temperature (°C)							Salinity (‰)						
			-0.5 m	-1 m	-2 m	-3 m	-5 m	-10 m	B+1 m	-0.5 m	-1 m	-2 m	-3 m	-5 m	-10 m	B+1 m
T 1	15 45 ~ 15 55	12.7	28.3	-	28.3	-	28.2	28.2	28.2	31.02	-	30.95	-	30.96	31.17	31.21
T 2	16 15 ~ 16 25	12.7	28.2	-	28.2	-	28.2	28.2	28.2	31.52	-	-	-			-
T 3	15 25 ~ 15 38	10.0	28.5	28.5	28.5	-	28.3	-	28.3	30.90	30.89	30.89	-	30.90	-	30.90
T 4	16 35 ~ 16 45	2.4	28.9	28.9	28.9	-		-	28.9	32.38	32.39	-	-	-	-	32.39
T 5	15 00 ~ 15 10	6.0	28.7	28.7	28.7	28.7	28.7	-	28.7	32.11	-	-	-	-	-	
T 6	15 20 ~ 15 27	12.5	28.2	-	28.2	-	28.2	28.4	28.4	31.87	-	-	-	-		-
T 7	15 40 ~ 15 45	4.0	28.5	28.5	28.5	28.5	-	-	28.5	32.05	-		-		-	-
T 8	15 51 ~ 15 55	7.0	28.3	28.3	28.3	28.3	-	-	28.2	31.91	-	-	-	-	-	
T 9	15 00 ~ 15 15	13.7	28.4	-	28.4	-	28.4	28.4	28.4	30.64	-	30.59	-	30.58	30.60	30.59
T10	16 12 ~ 16 17	4.5	28.4	28.4	28.4	28.4	-	-	28.4	31.93	-	-	-	-		-
T11	16 00 ~ 16 06	11.2	28.3	28.3	28.3	-	28.3	-	28.2	31.85		-		-		
T12	15 00 ~ 15 06	7.7	28.7	28.7	28.7	28.6		-	28.6	30.84	-	-	-			
T13	16 21 ~ 16 36	6.9	28.3	28.3	28.3	28.3	-	-	28.2	31.64	31.80	31.80	31.72			32.17
T14	16 42 ~ 16 50	15.0	28.4	-	28.4	-	28.4	28.3	28.2	31.77		-	-			-
T15	14 58 ~ 15 10	18.2	28.5	-	28.5	-	28.5	28.4	28.4	31.92	-	31.93		31.95	31.99	32.01
T16	15 17 ~ 15 21	4.3	28.5	28.5	28.5	28.5	-	-	28.5	30.74	30.74	30.74	30.74	-		30.75
T17	15 00 ~ 15 05	7.0	28.5	28.5	28.4	28.4		-	28.3	31.13			-	-	-	-
T18	15 32 ~ 15 36	17.8	28.5	-	28.5	-	28.5	28.4	28.4	31.58	-		-	-	-	-
T19	15 21 ~ 15 26	23.4	28.4	-	28.4	-	28.4	28.4	28.3	31.86	-	-		-	-	
T20	15 32 ~ 15 35	2.4	28.4	28.4	28.4	-		-	28.4	30.74	-	-	-			-
T21	15 21 ~ 15 38	16.0	28.5		28.5	-	28.5	28.5	28.5	31.75		31.75	-	31.77	31.89	32.00
T22	15 41 ~ 15 46	19.8	28.5	-	28.5	-	28.5	28.4	28.4	31.76	-		-			
T23	15 45 ~ 15 50	3.0	28.4	28.4	28.4	-		-	28.4	30.77	-					
T24	15 55 ~ 16 00	7.2	28.3	28.3	28.3	28.3			28.4	31.03	-					
T25	16 00 ~ 16 06	17.0	28.4		28.4	-	28.4	28.4	28.3	31.55	-	-				
T26	15 57 ~ 16 02	23.5	28.5		28.5	-	28.5	28.4	28.4	31.52			-			
T27	16 12 ~ 16 18	3.2	28.4	28.4	28.4	28.4	-			30.72	30.82	30.81	30.84			
T28	16 41 ~ 16 52	17.0	28.5	-	28.5	-	28.4	28.4	28.4	31.19		31.25	-	31.32	31.46	31.52
T29	16 12 ~ 16 17	19.0	28.5	-	28.5	-	28.5	28.5	28.5	31.39						
T30	16 11 ~ 16 14	7.8	28.6	28.6	28.6	-	28.6		28.6	31.85	-		-			
T31	16 25 ~ 16 30	16.0	28.4		28.3	-	28.3	28.3	28.3	30.79			-			-
T32	16 37 ~ 16 45	20.7	28.6		28.6	-	28.6	28.5	28.5	30.92		30.90		30.95	30.95	31.58
T33	16 57 ~ 16 59	15.0	28.5		28.5		28.5	28.5	28.4	31.01						
T34	16 27 ~ 16 31	25.0	28.6		28.6		28.6	28.5	28.4	31.23						
T35	16 22 ~ 16 26	8.2	28.5	28.5	28.5		28.5		28.5	31.87						

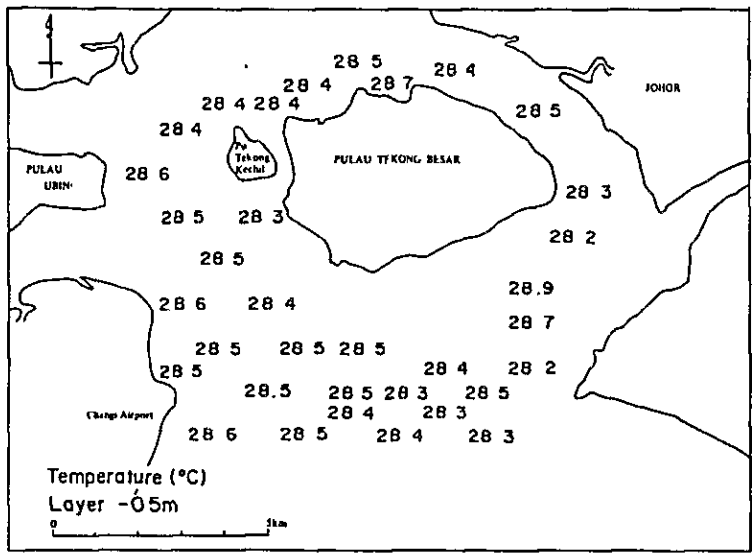

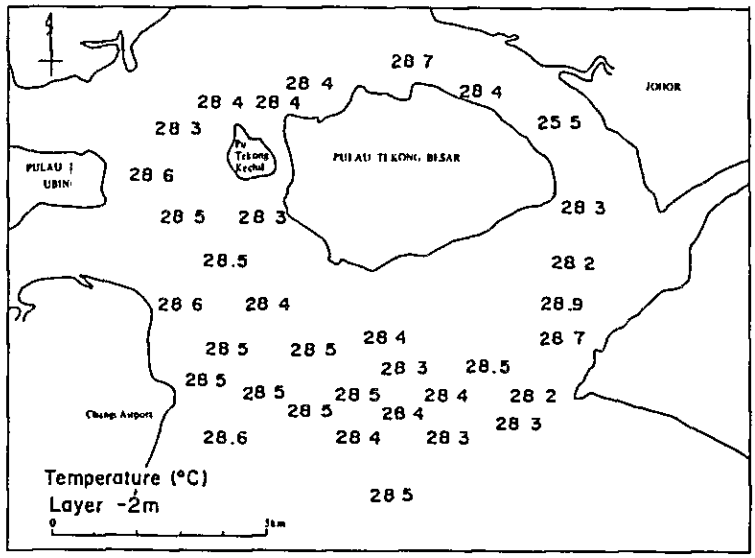

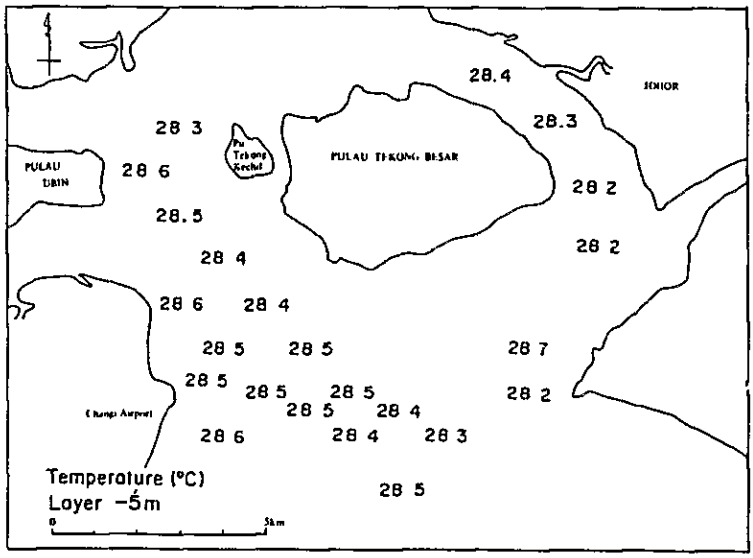

Fig. II-4-15 Horizontal distribution of temperature (1/3)

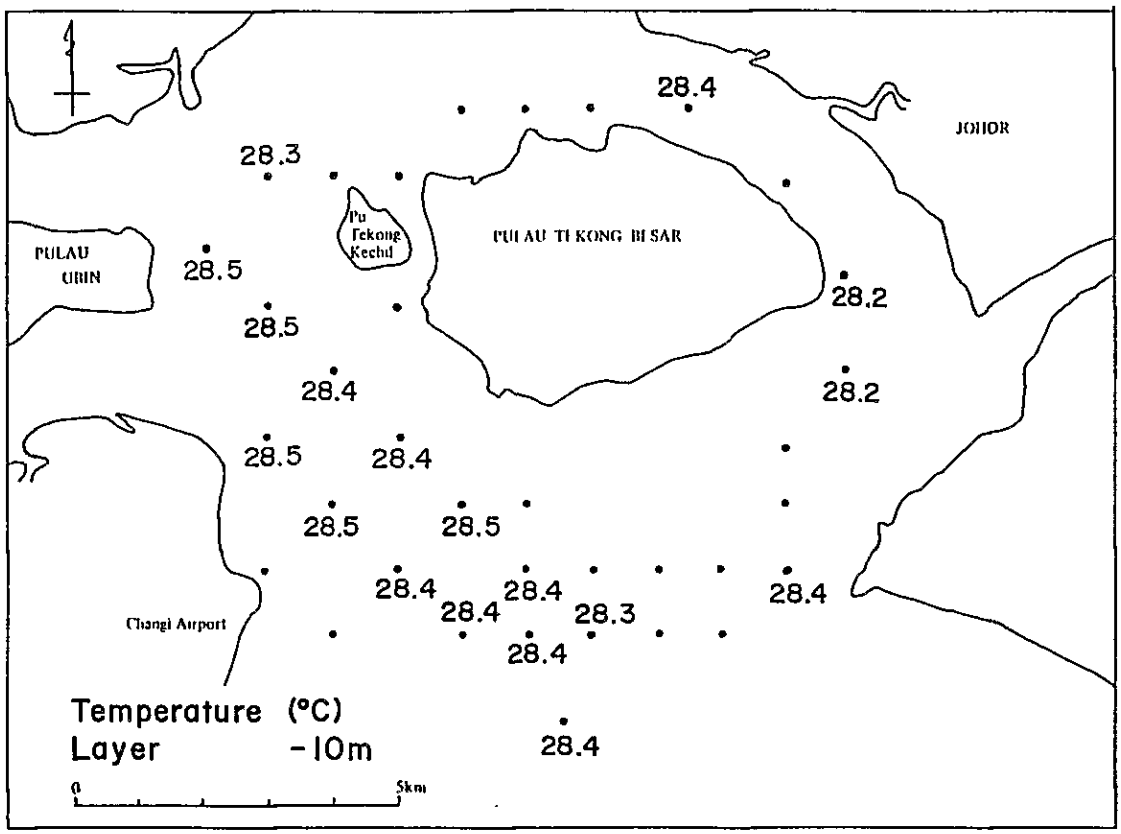

Fig. II-4-15 Horizontal distribution of temperature (2/3)

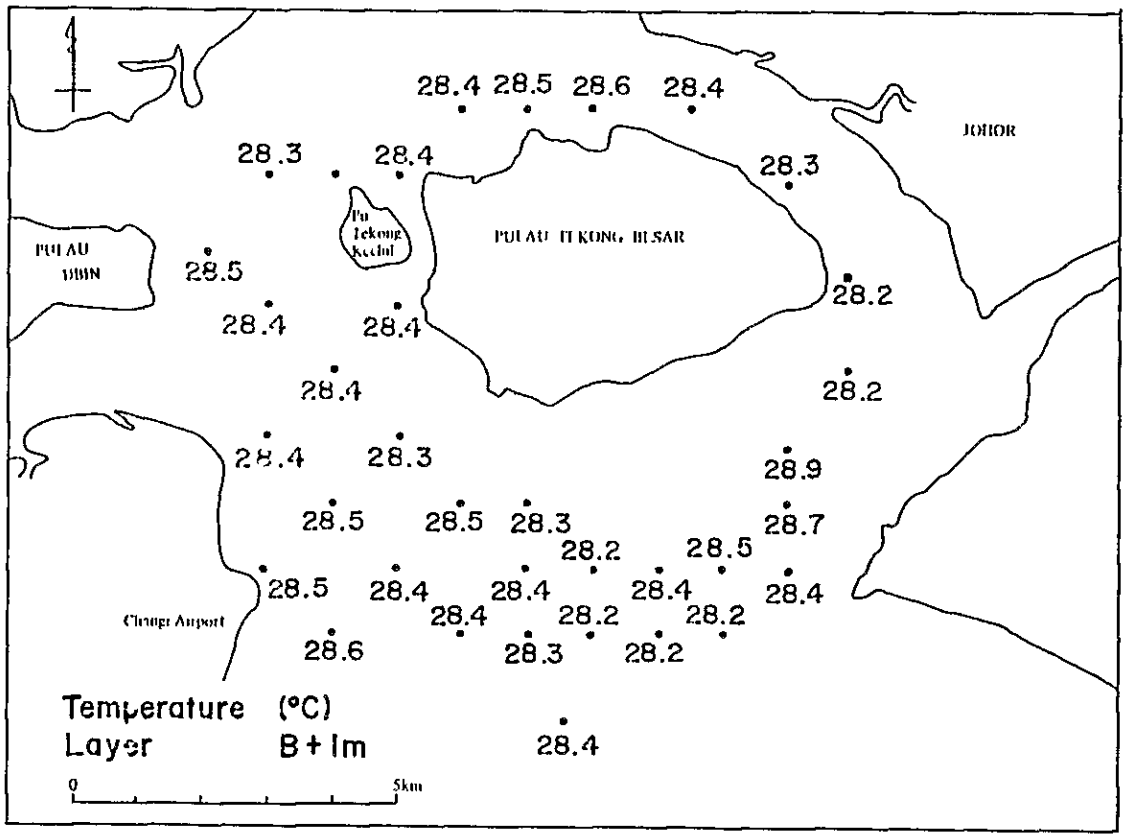

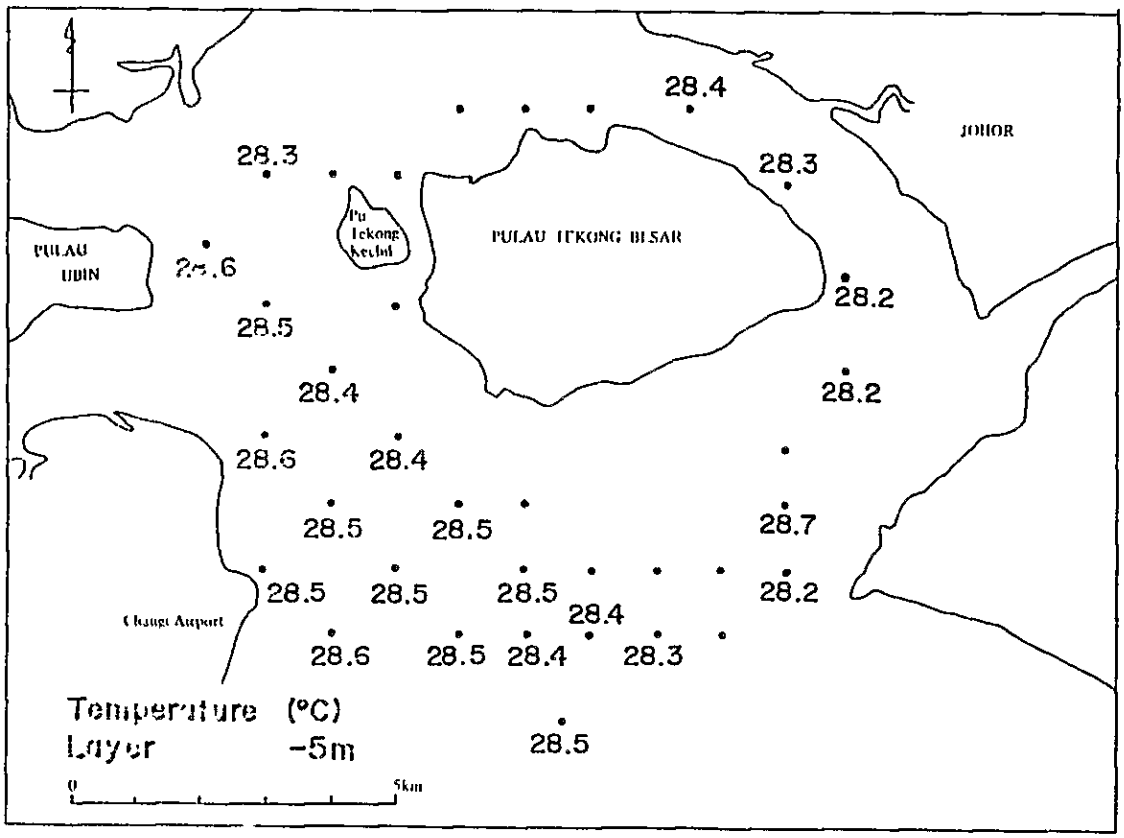

Fig. II-4-15 Horizontal distribution of temperature (3/3)

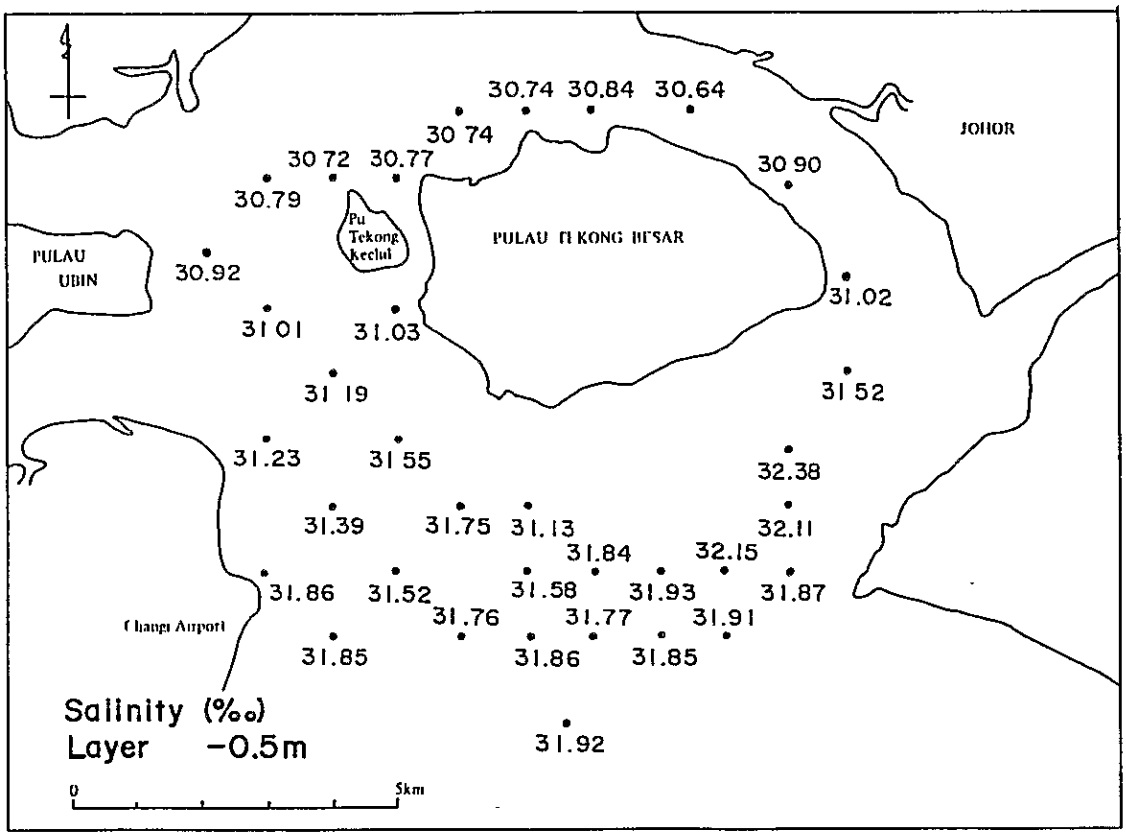

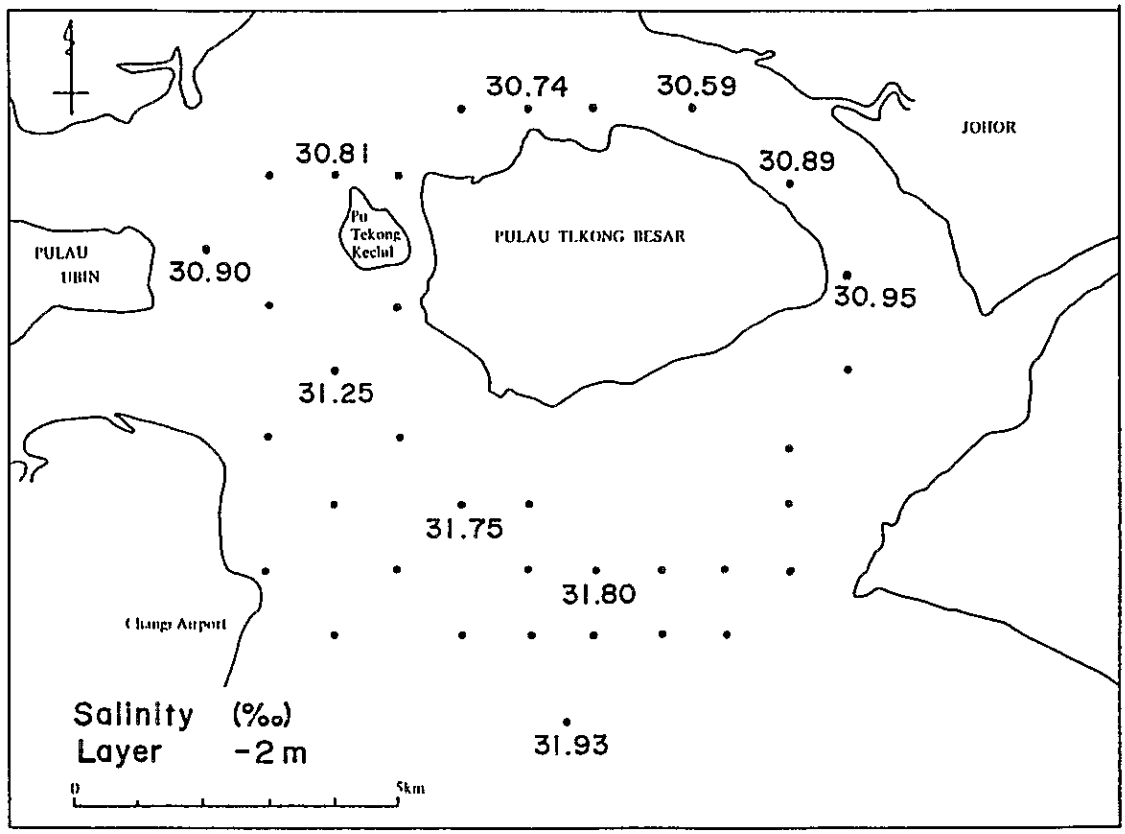

Fig. II-4-16 Horizontal distribution of salinity (1/3)

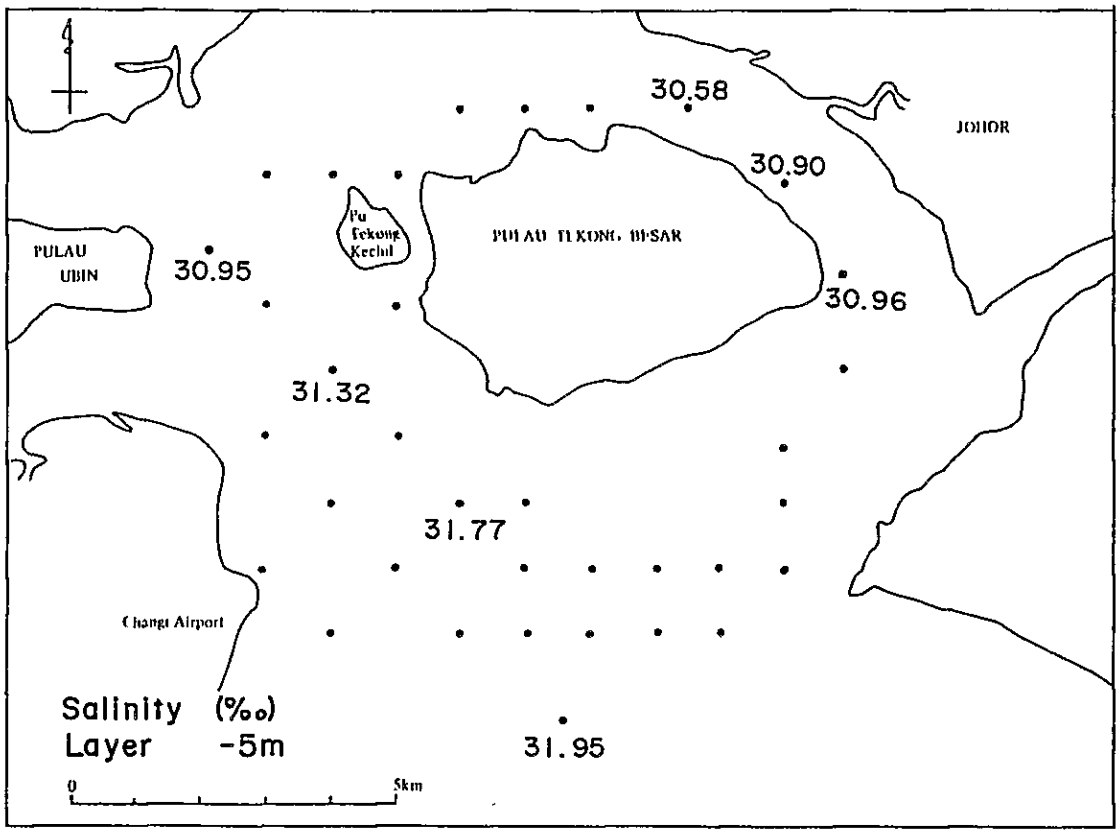

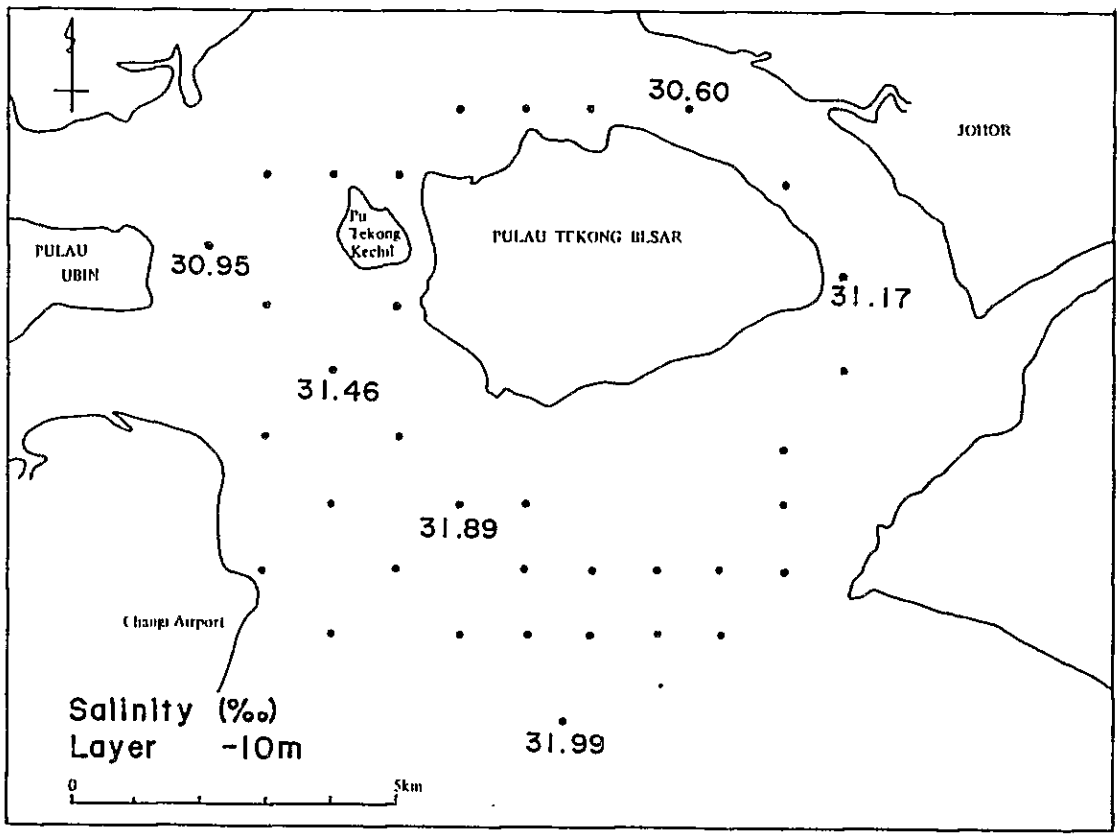

Fig. II-4-16 Horizontal distribution of salinity (2/3)

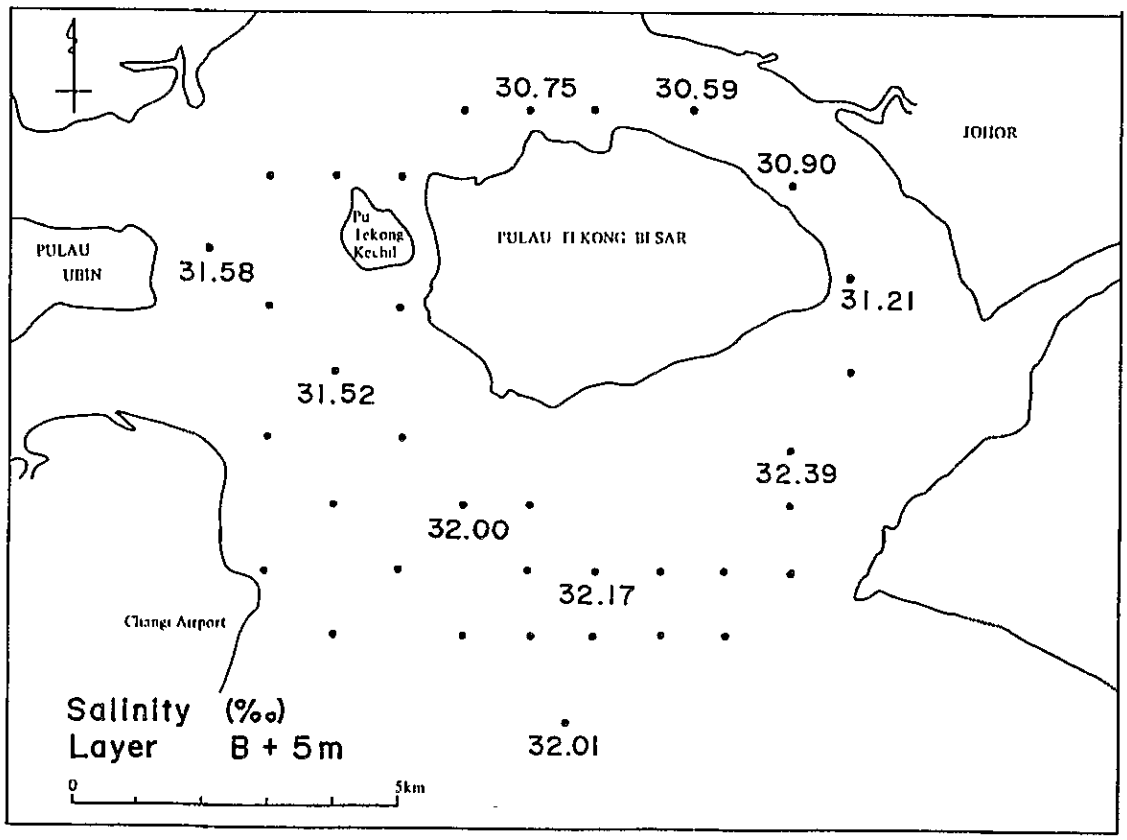

Fig. II-4-16 Horizontal distribution of salinity (3/3)

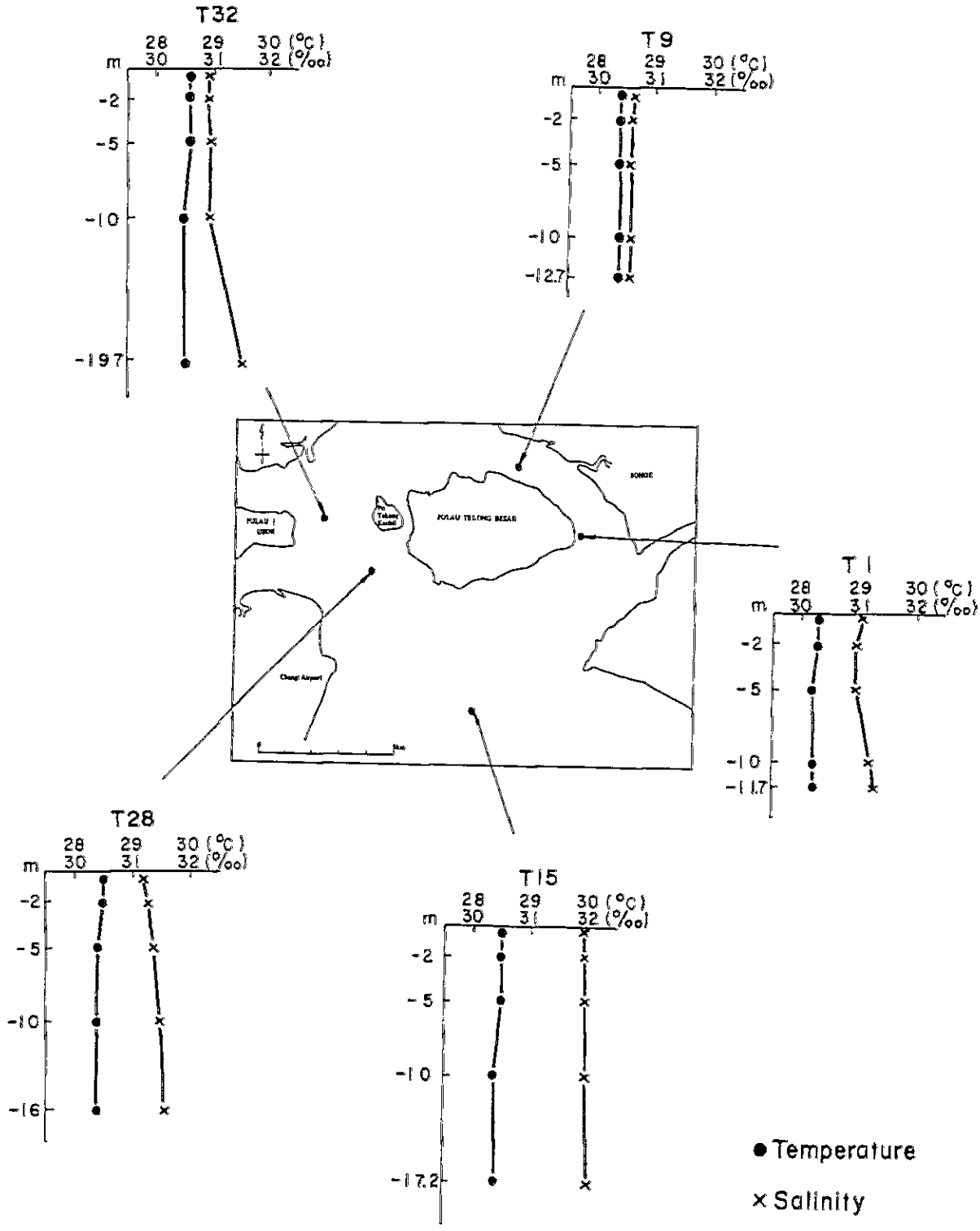

Fig. II-4-17 Vertical distribution of temperature and salinity

CHAPTER 5 WATER QUALITY SURVEY

II-5-1 Outline

The water quality survey has been conducted for the purpose of obtaining the necessary data on water quality distribution in the survey areas (sea areas surrounding Pulau Seraya and Tekong).

Further, the results of the survey have been used as the baisc data for water quality diffusion calculation in the processes of simulation. Table II-5-1 shows the outline of the survey.

Table II-5-1 Outline of water quality survey

Area	Survey Item	Observation Layer	Survey Point	Data, Time
Seraya	COD	−0.5m	21 points	Mar. 2, 1981 13:00 ~ 16:00
	Transparency	—	49 points	
	Color of sea	—	49 points	
	Chlorophyll-a	−0.5m	5 points	
Tekong	COD	−0.5m	11 points	Mar. 5, 1981 15:00 ~ 17:00
	Transparency	—	35 points	
	Color of Sea	—	35 points	
	Chlorophyll-a	−0.5m	5 points	

II-5-2 Specifications of Field Survey

II-5-2-1 Survey point

Fig. II-5-1 is the survey points chart. The survey points for COD and chlorophyll-a have been selected as the representative points from the survey points for temperature and salinity survey, and the survey points for transparency and water colour have been measured at the same points as the temperature and salinity survey.

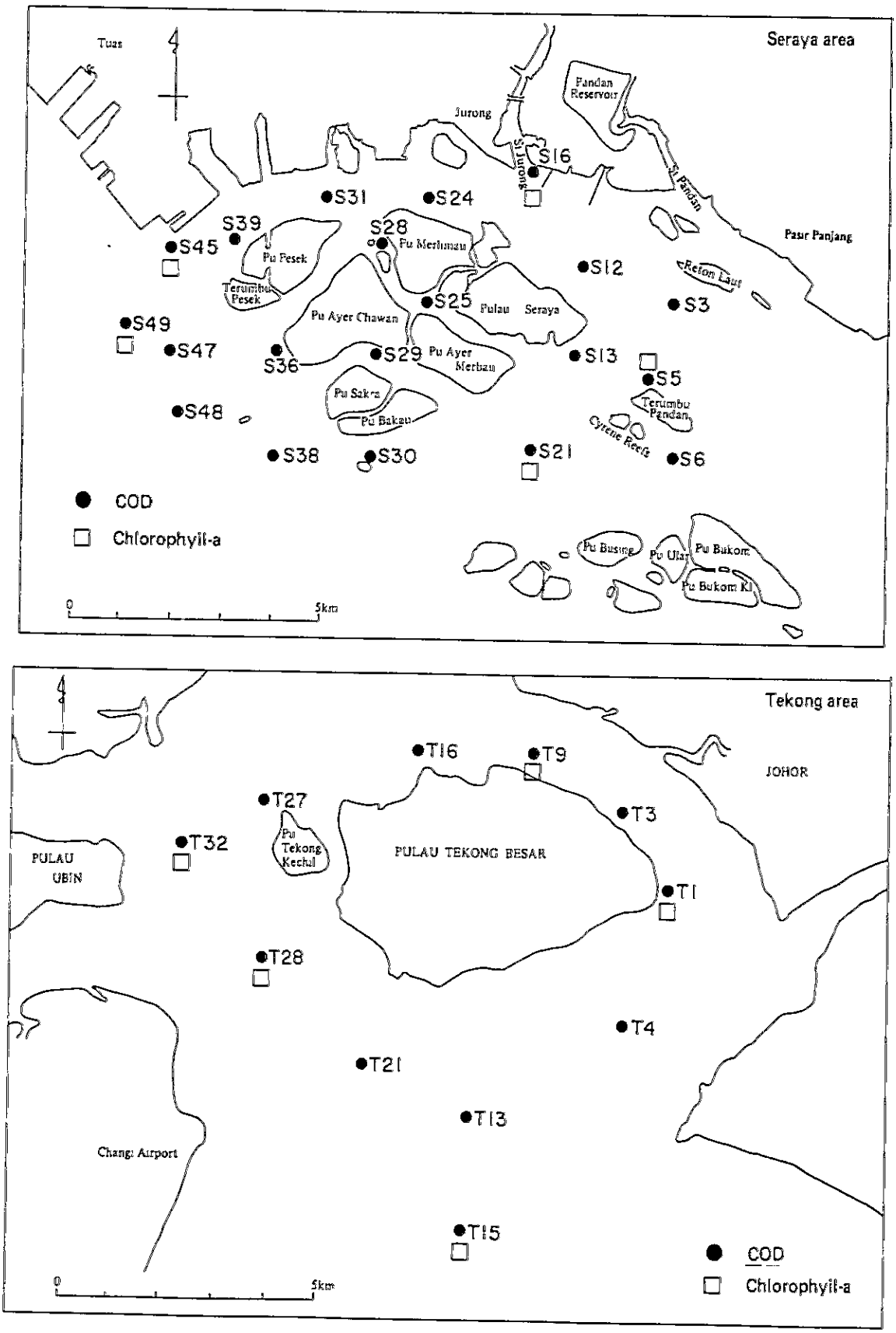

Fig. II-5-1 Survey point of water quality survey

II-5-2-2 Survey schedule

The water quality survey has been conducted simultaneously with the temperature and salinity survey, and so the survey day was March 2nd 1981 at Seraya Area and March 5th 1981 at Tekong Area.

II-5-2-3 Survey method

1) Works on board

The survey has been conducted on board. Transparency and water colour have been measured, and water smapling for the analysis of COD and chlorophyll-a has been conducted by KITAHARA's sampling bottles. The water samples collected have been kept in the poly-ethylene bottles and transported to the laboratory by the poly-urethane container filled with ice blocks.

The transparency is one of the indicators to determine the turbidity of water, and the white round board of diameter about 30 cm which is called as SECCHI DISC has been thrown into sea water until the board came invisible, and it is indicated by the depth of such moment in terms of "meter".

Water colour is the colour of sea water seen from the right above under the broad daylight, and the colour is compared with the standard colour index.

2) Chemical analysis

COD is one of the indicators to determine the pollution level by the organic substances, and it is expressed by the oxygen demand necessary to oxidize the organic substances by oxidizing agents.

There are several analysing methods by the kinds of oxidizing agents, concentration, oxidizing conditions & etc., but in this study, Japanese Industiral Standard method (JIS K0102) has been employed which applies the oxidation reaction with Potassium Permanganate at $100^{\circ}C$.

The principle of analysing method is (1) Potassium Permanganate has the strong oxidation power in acid solution as equation (1) and oxidize the organic substances contained in the sample water, (ii) and add Sodium Oxalate (NaC_2O_4) for resolving Permanganate Ion (MnO_4^-)as equation (2). And (iii) obtains COD by back titrating surplus Oxalate Ion ($C_2O_4^{2-}$) with Potassium Permanganate.

$$MnO_4^- + 8H^+ + 5e \rightleftharpoons Mn^{2+} + 4H_2O \quad \text{--- (1)}$$

$$2MnO_4^- + C_2O_4^{2-} + 16H \rightleftharpoons 2Mn^{2+} + 10CO_2 + 8H_2O \quad \text{--- (2)}$$

Further by the above method, COD values indicate higher when the water sample contains much Chloride Ion as a part of Chloride Ion is oxidized and comes to free Chloride.

In this analysis, Silver Nitrate (Ag_2SO_4) has been added in order to avoid the interference of Chloride Ion.

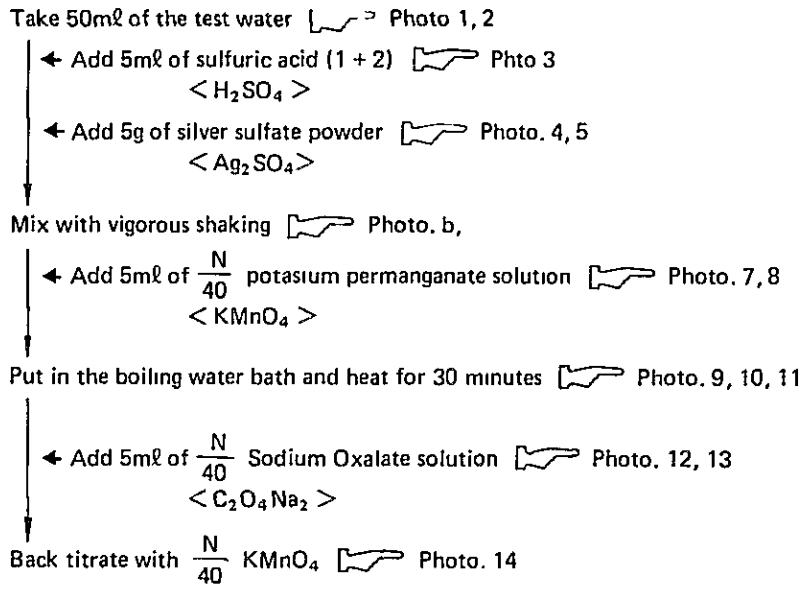

Fig. II-5-2 Determination of COD (Chemical Oxygen Demand) at 100°C by Potasium Permangaate Method (1/4)

Photo. 1

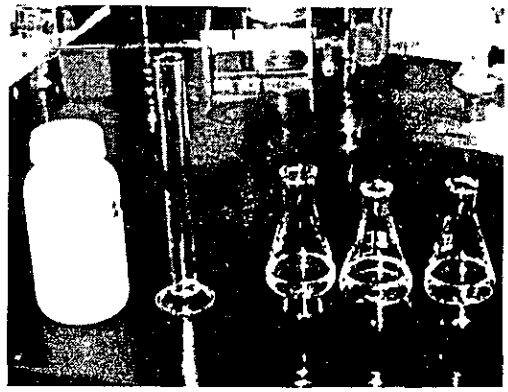

Photo. 2

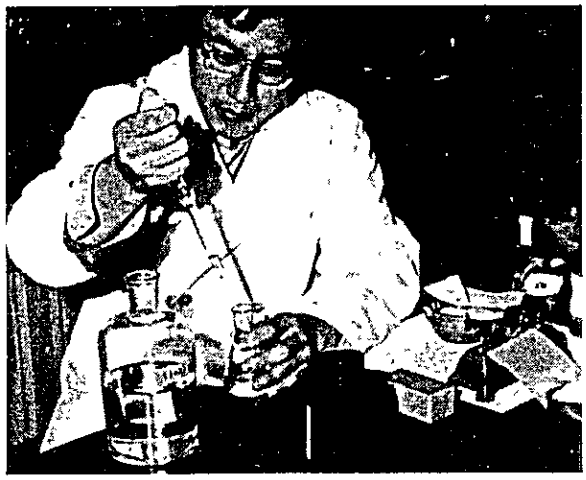

Photo. 3

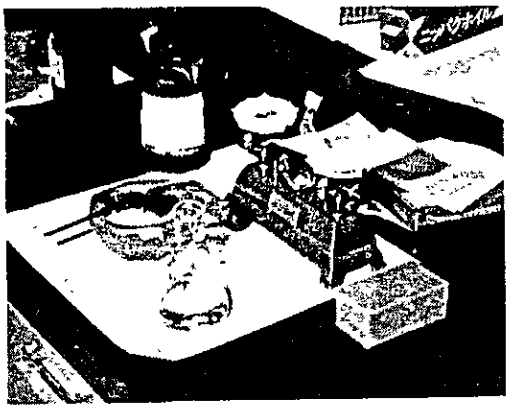

Photo. 4

Photo. 5

Fig. II-5-2 Determination of COD (Chemical Oxygen Demand) at 100°C by Potasium Permangaate Method (2/4)

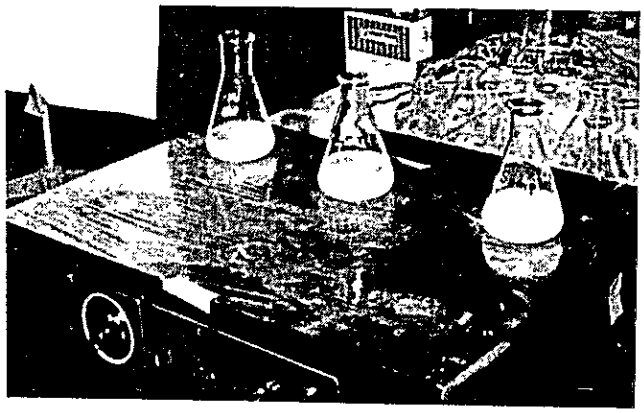

Photo. 6

Photo. 7

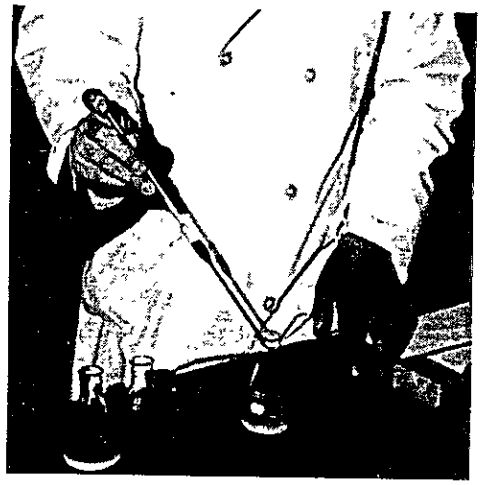

Photo. 8

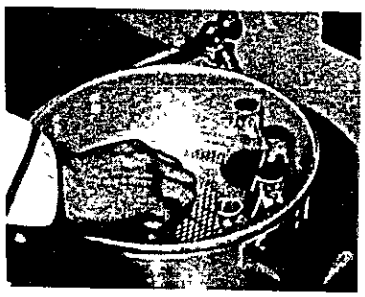

Photo. 9

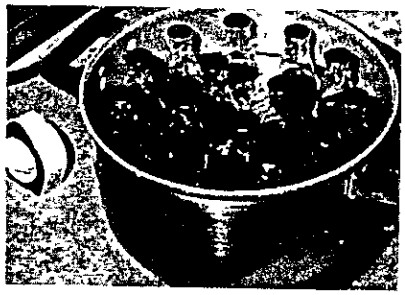

Photo. 10

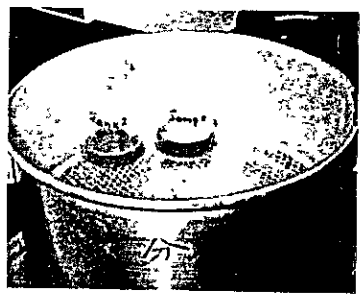

Photo. 11

Fig. II-5-2 Determination of COD (Chemical Oxygen Demand) at 100°C by Potasium Permangaate Method (3/4)

Photo. 12

Photo. 13

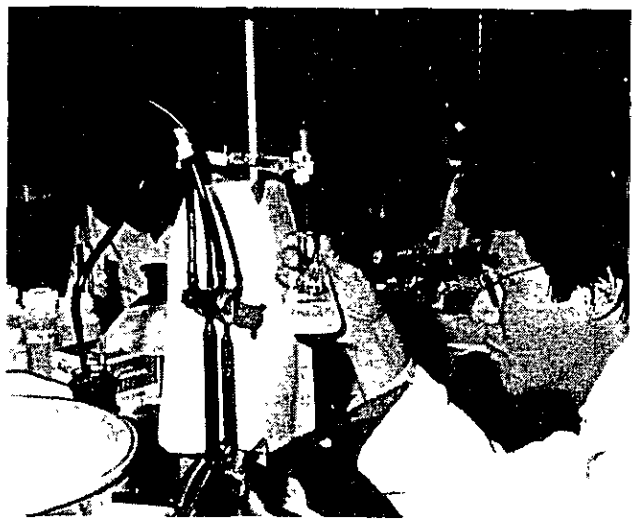

Photo. 14

Fig. II-5-2 Determination of COD (Chemical Oxygen Demand) at 100°C by Potasium Permangaate Method (4/4)

Chlorophyll-a is one of the indicators to show the degree of activity of Phytoplankton in the sea water, and extract the chlorophyll from the filter by acetone and measure the absorbance by the spectrophotometer in the wave range of 750, 663, 645 and 630nm. Fig. II-5-3 shows the analysing methods of Chlorophyll-a.

Filter a dosage of sea water	add 3-4ml of 92% acetone
Extract chlorophyll	treat filter for 5-10 minutes by supersonic generator
Centrifugal separation	treat about 10 minutes by 10.000G
Measure absorbance	Measure absorbance of upper layer of sample after centrifugal separation by various range of waves

Calculation equation

$$\text{Chlorophyll-a} = \frac{(11.64D_{663} - 2.16D_{645} + 0.10D_{630}) \times U}{V \times L}$$

where;

$D_{663}, D_{645}, D_{630}$: Amended absorbance of each wave after deducting absorbance of 750nm

U : Sample volume (ml) used for absorbance measurement

V : Filtered volume of sea water (liter)

L : Length of absorbance cell (cm)

Fig. II-5-3 Analysing method of Chlorophyll-a

II-5-2-4 Instruments

1) SECCHI DISC

SECCHI DISC is composed by white, flat, round board of having about 30 cm diameter and about 5 kgs weight by which SECCHI DISC is having down into the sea water, as shown in Fig. II-5-4.

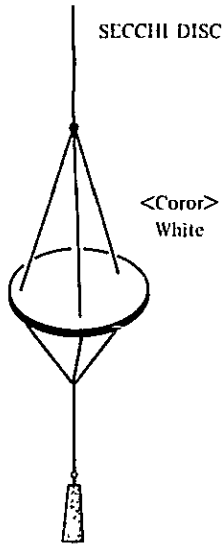

Fig. II-5-4 SECCHI DISC

2) Forel & Ule standard water colour

Forel & Ule standard water colour are contained in colourless small tubes, having 8 mm inner diameter and 10 mm outside diameter, after mixing the three kinds of basic liquids as shown in Table II-5-2. These small tubes are contained in the wooden box carpetted by white cloth and set in order from standard No. 1.

Table II-5-2 Forel & Ule standard water colour

Standard solution No.	1	2	3	4	5	6	7	8	9	10	11	12	13	14	15	16	17	18	19	20	21
Solution No. 1 (%)	100	98	95	91	86	80	73	65	56	46	35	35	35	35	35	35	35	35	35	35	35
Solution No. 2 (%)	0	2	5	9	14	20	27	35	44	54	65	60	55	50	45	40	35	30	25	20	15
Solution No. 3 (%)	0	0	0	0	0	0	0	0	0	0	0	5	10	15	20	25	30	35	40	45	50

Solution No. 1 (deep blue)		Solution No. 2 (yellow)		Solution No. 3 (brown)	
Copper sulfate	1 g	Potassium chromate	1 g	Primary cobalt sulfate	1 g
Aqueous ammonia (25%)	10 cc	Distilled water	200 cc	Aqueous ammonia (25%)	10 cc
Distilled water	190 cc			Distilled water	1990 cc

II-5-3 Survey Results of Seraya Area

Table II-5-3 shows the results of the survey and Fig. II-5-8 to Fig. II-5-8 show the distribution of COD and others.

II-5-3-1 COD

The COD concentrations have been in the ragne of 0.1 to 3.9 ppm, and as a whole the concentrations show lower values. The survey points exceeding 1 ppm were only 3 of S1, S3 and S16. Ther average values of 18 points except the above 3 points was 0.3 ppm and the standard deviation was 0.2 ppm. S1 and S16 are located in the mouth of River Pandan and River Jurong respectively, and it is considered these two points shows higher values due to the influence of sewage effluent.

In general, the COD concentration has the tendency of being higher in the coastal waters by the flow of sewage effluent and lower in the offshore.

In this study, the COD concentration in the survey areas indicated very low and so the exact comparison is difficult taking the analysis error into consideration, but the offshore area, south side of Pulau Seraya indicated a little higher values than the coastal area, north side of the same island. Further, the west side of Pulau Merlibau showed the higher values than the east side. This is considered as influenced by the ocean water which is very low in COD, because the survey had been conducted in the time of eastward flow.

II-5-3-2 Transparency

Transparency indicated the values in the range of 0.9 m to 8.2 m. The average value was 3.9 m and the standard deviation was 2.0 m. Generally, the values in the coastal waters indicated lower than offshore area and the values in the coastal waters area showed lower than 3.5 m.

In general, the transparency in the sea has the tendency of being low at the coastal waters and being high at the offshore area.

In this survey areas, the influence from the River Pandan and River Jurong can be considered but both of these two rivers are not so big as to give the influence to lower the transparency of the coastal waters. As the current velocity is fast in this area, the mud and sand of the sea bed might have rolled up at the shallow region and this might be the reason why the transparency is low.

Further, the east side area shows higher values than the west side. This is considered as influenced by the offshore water which has the high transparency.

Transparency and COD have generally negative correlation. In this study the obtained coefficient was -0.44 and correlation has not been found.

II-5-3-3 Water colour

The colour of sea water have been in the range of 7 to 12, and generally it was bluish green.

As for the colour of sea water, as the standard number increases from 1 to 21, the colours change from blue to bluish green to brown.

At the coastal waters, particularly in the mouth of rivers, the colour number showed the bigger number and the offshore area, such numbers were smaller.

In general, the water colour of the high transparent sea water shows the small number and the obtained coefficient between water colour and transparency in this study was -0.77 which means two factors have the high correlation.

II-5-3-4 Chlorophyll-a

Chlorophyll-a has been measured and found in the range of 1.0 to 2.6 g/liter, and at S39, the high value of 2.6 g/liter has been measured although the accurate comment is difficult because of the number of survey points were only limited.

Table II-5-3 Results of water quality survey (Seraya Area)

Seraya

Station No	Time	Depth (m)	COD (ppm)	Transparency (m)	Colour of Sea Water	Chlorophyll a (μg/ℓ)	Station No	Time	Depth (m)	COD (ppm)	Transparency (m)	Colour of Sea Water	Chlorophyll a (μg/ℓ)
S 1	14 50 ~ 14 56	6 5	1.3	1.5	12	-	S26	13 16 ~ 13 19	19 0	-	7 2	8	
S 2	14 30 ~ 14 34	11 7	–	1 5	12	–	S27	14 23 ~ 14 30	25 1		2 0	9	–
S 3	13 37 ~ 13 45	13 2	2 4	2 9	9	–	S28	14 08 ~ 14 15	12 0	0 2	2.5	9	-
S 4	13 20 ~ 13 28	27 0	–	3 1	9		S29	14 43 ~ 14 51	11 6	0 1	7 7	7	
S 5	13 00 ~ 13 10	25 0	0 7	3.5	7	1 2	S30	13 28 ~ 13 39	18 5	0 6	6 9	8	
S 6	13 00 ~ 13 30	26 0	0 7	3 6	9	-	S31	13 31 ~ 13 44	24 2	0 5	2 0	10	-
S 7	15 03 ~ 15 06	12.3	–	2.3	10	-	S32	13 58 ~ 14 03	14 5		3 0	9	-
S 8	14 23 ~ 14 26	11 7	–	1 9	11	–	S33	14 35 ~ 14 38	9 7	–	7 8	7	-
S 9	13 55 ~ 14 01	16 8	–	2 5	9	–	S34	13 49 ~ 13 53	15 4		8 0	8	
S10	13 36 ~ 13 45	27 0	–	3 8	9	–	S35	13 20 ~ 13 24	15 7	-	1 8	10	-
S11	15 12 ~ 15 15	11.5	–	2 1	10	–	S36	13 45 ~ 13 59	12.0	0 1	4 1	9	–
S12	14 10 ~ 14 17	13 9	0 7	2 1	9	–	S37	14 26 ~ 14 29	12 0	-	8 2	7	-
S13	14 52 ~ 15 00	19.0	0.3	2 8	9	–	S38	14 00 ~ 14 08	19 0	0 2	7 9	7	-
S14	14 40 ~ 14 44	18 0	–	3 7	10	–	S39	13 00 ~ 13 12	13 4	0 1	2 0	11	2 6
S15	13 51 ~ 13 58	18 0	–	4 2	10	–	S40	15 29 ~ 15 32	16 0		3 0	9	–
S16	15 25 ~ 15 37	6 2	3 9	0 9	12	1 7	S41	15 21 ~ 15 24	8 5	–	3 2	9	–
S17	15 15 ~ 15 19	18 0	–	2.0	9	–	S42	14 11 ~ 14 15	14 0	–	5 0	9	–
S18	15 23 ~ 15 26	13 2	–	3 2	8	–	S43	13 28 ~ 13 34	13 0	-	4 8	9	–
S19	15 11 ~ 15 15	17 0	–	2 2	11	–	S44	14 16 ~ 14 20	14 5	-	7 8	7	–
S20	14 30 ~ 14 35	18 0	–	4 1	10	–	S45	15 36 ~ 15 45	12.0	0 6	2 5	9	-
S21	14 07 ~ 14 23	20 0	0 1	4 7	10	1.0	S46	15 08 ~ 15 12	11 0	-	3 5	9	–
S22	14 57 ~ 15 03	25.3	–	3.5	9	–	S47	14 22 ~ 14 35	16 0	0 1	4 9	9	–
S23	12 57 ~ 13 05	23.0	–	7 1	7	–	S48	13 00 ~ 13 20	14 0	0 1	4 8	9	-
S24	14.37 ~ 14 50	18 4	0 4	3 0	9	–	S49	14 47 ~ 15 02	11 0	0 1	3.3	9	1 4
S25	15 23 ~ 15 32	11.5	0 4	2 6	10	–							

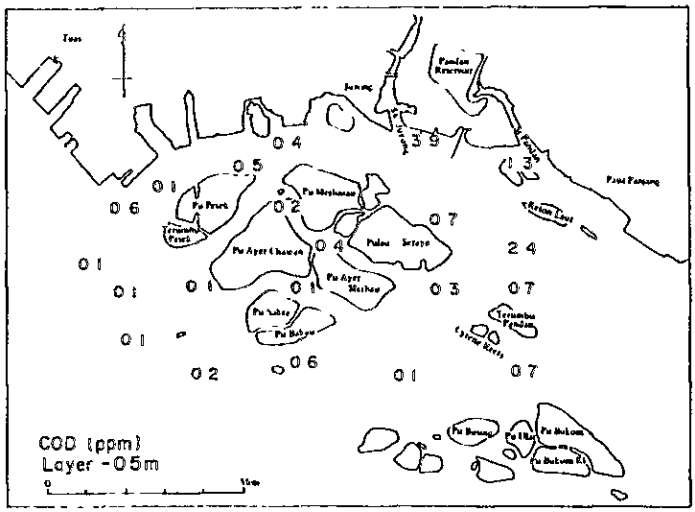

Fig. II-5-5 COD concentration distribution chart

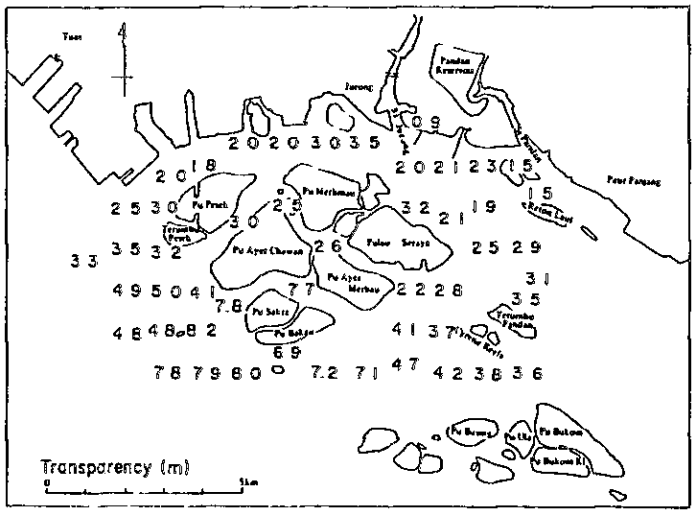

Fig. II-5-6 Transparency distribution chart

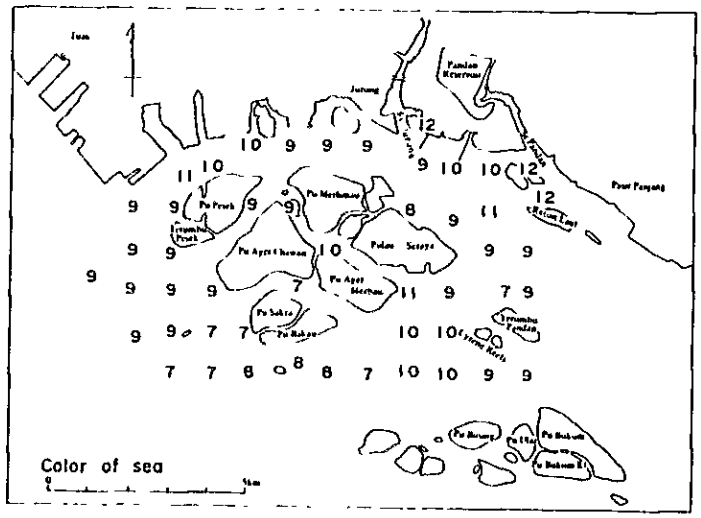

Fig. II-5-7 Water colour distribution chart

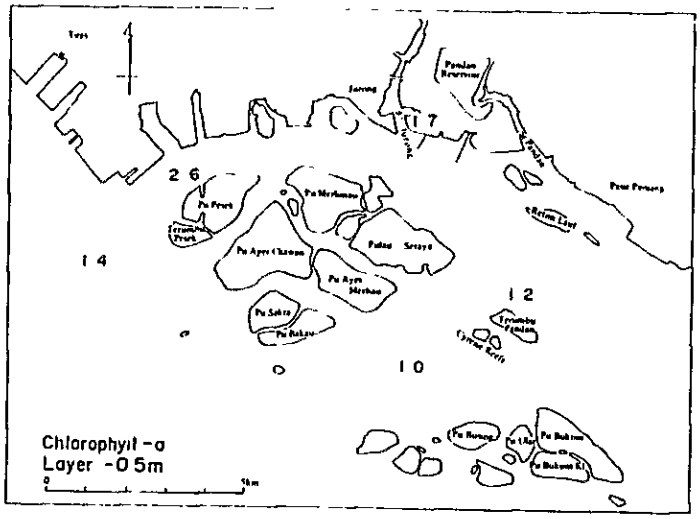

Fig. II-5-8 Chlorophyll-a concentration distribution chart

II-5-4 Survey Results of Tekong Area

Table II-5-4 shows the survey results of Tekong Area, and Fig. II-5-9 to Fig. II-5-12 show the distribution chart of COD concentration and other items.

II-5-4-1 COD

The COD concentration of this area were in the range of 0.7 to 2.5 ppm, and the average value was 1.5 ppm, having the standard deviation of 0.6 ppm.

COD values of Tekong Area are generally higher by about 1 ppm than Seraya Area, and the north side of Tekong shows the higher values than the south side which is considered as the influence from the Straits of Johor and Johor River.

II-5-4-2 Transparency

The transparency showed the values in the range of 0.5 to 2.5 m, and the average value was 1.3 m having the standard deviation of 0.4 m. The values of transparency in this area indicates lower than Seraya Area and the scattering of the values are also small. The transparency of the north side of Tekong shows the lower value than the south side which is considered to be the effect from Johor River.

Coefficient between COD and transparency is -0.46 and found no correlation.

II-5-4-3 Water colour

The water colour has been in the range of 11 to 15 and it is brownish and the scattering is small.

The north side of Tekong indicates the bigger number and the degree of brown is large which is considered as the influence from the Straits of Johor and Johor River.

Coefficient between water colour and transparency was -0.59 and correlation was not so high as Seraya Area.

II-5-4-4 Chlorphyll-a

The values of chlorophyll-a indicate in the range of 3.4 to 9.7 g/l, and rather higher than Seraya Area.

As the number of survey points are only limited, it cannot be possible to obtain the most accurate values but at T32 the highest value has been obtained.

Table II-5-4 Results of water quality survey

Tekong

Station No	Time		Depth (m)	COD (ppm)	Transparency (m)	Colour of Sea Water	Chlorophyll a (μg/l)	Station No	Time		Depth (m)	COD (ppm)	Transparency (m)	Colour of Sea Water	Chlorophyll a (μg/l)
T 1	15 45	15 55	13 7	1 1	1 0	14	3 4	T19	15 21	15 26	23 4		1 8	12	–
T 2	16 15	16 25	12 7		1 0	12		T20	15 32	15 35	2 4	-	1 0	14	-
T 3	15 25	15 38	10 0	1 5	1 0	13		T21	15 21	15 38	16 0	0 9	1 5	12	-
T 4	16 35	16 45	2 4	1 6	0 5	14	-	T22	15 41	15 46	19 2	-	1 4	13	–
T 5	15 00	15 10	6.0	–	0 8	14	-	T23	15 45	15 50	3 0	–	1.0	14	–
T 6	15 20	15 27	12 5		1 0	13	–	T24	15 55	16 00	7 2	–	1 2	14	–
T 7	15 40	15 45	4 0	–	0 9	13		T25	16 00	16 06	17 0		2 5	12	–
T 8	15 51	15 55	7.0	-	1.0	12		T26	15 57	16 02	23 5	-	1 3	12	–
T 9	15 08	15 15	13 7	2.3	1 0	14	3 8	T27	16 12	16 18	3 2	2 1	1 0	14	–
T10	16 12	16 17	4 5	–	1.0	13		T28	16 42	16 52	17 0	1 2	1 7	11	4 9
T11	16 02	16 06	11.2	–	1.2	13	–	T29	16 12	16 17	19 0	–	2 5	12	–
T12	15 00	15 06	7 7	–	1.3	14	–	T30	16 11	16 14	7 8	-	1.3	12	–
T13	16 28	16 36	6 9	0 7	1 1	13		T31	16 25	16 30	16 0	-	1 1	14	–
T14	16 43	16 50	15 0	-	1.2	12	-	T32	16 37	16 45	20 7	2 5	1 0	15	9 7
T15	15 58	15 10	18.2	1 1	1 7	12	3 6	T33	16 57	16 59	15 0		1 6	11	–
T16	15 17	15 21	4.3	1.9	1.0	14	–	T34	16 27	16 31	25.0		2.0	11	–
T17	15 00	15 08	7 0		1 2	12	-	T35	16 22	16 26	8 2		0 9	12	-
T18	15 32	15 36	17 8		1 5	13									

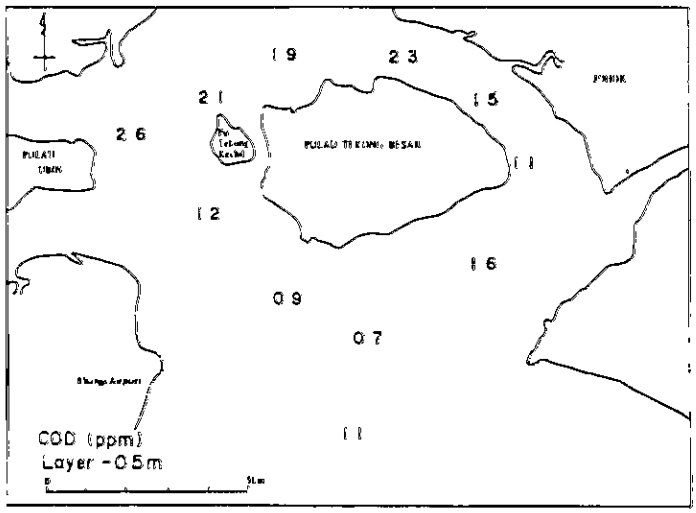

Fig. II-5-9 COD concentration distribution chart

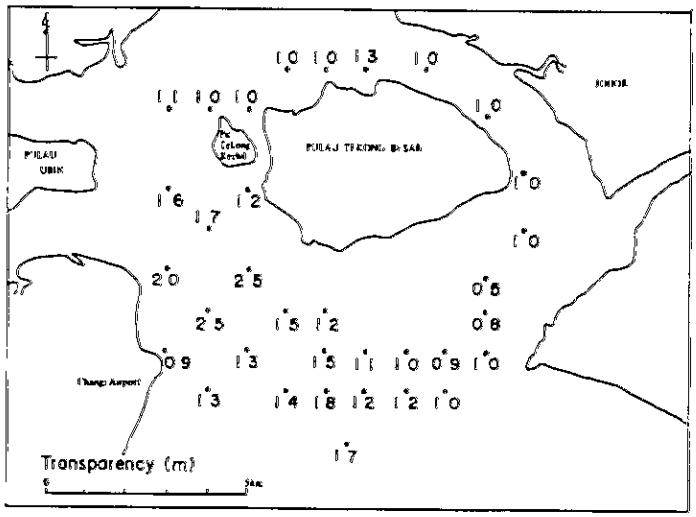

Fig. II-5-10 Transparency distribution chart

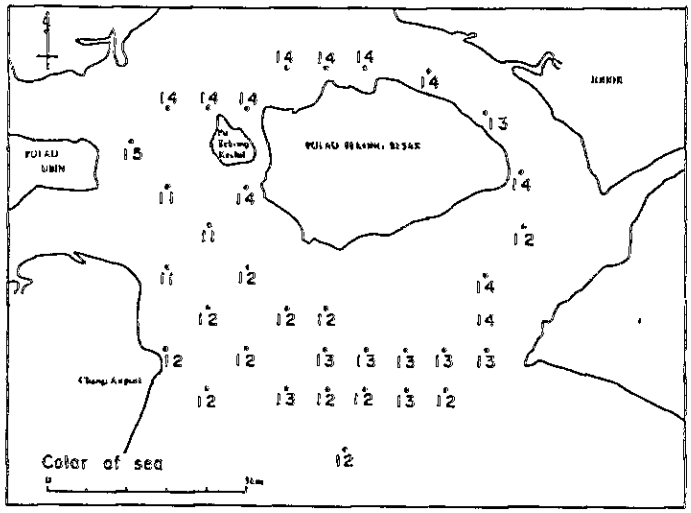

Fig. II-5-11 Water colour distribution chart

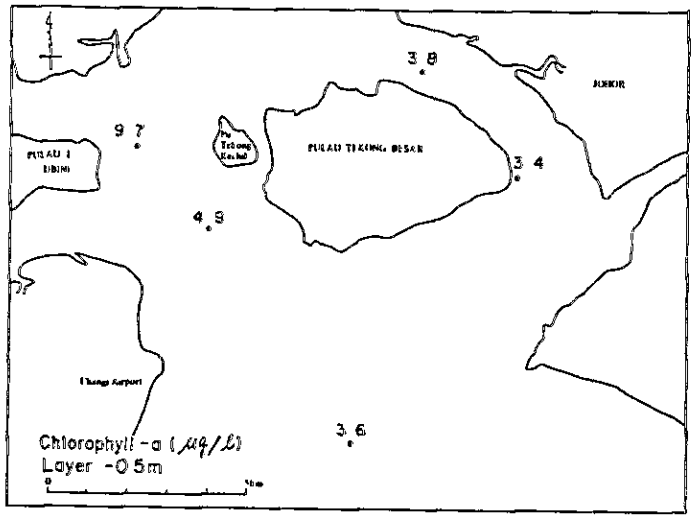

Fig. II-5-12 Chlorophyll-a concentration distribution chart

PART III SIMULATION

CHAPTER 1 NUMERICAL SIMULATION APPROACH ON POLLUTION PREDICTION

In this chapter the numerical simulation approach on pollution prediction applied in this report is summarized. The process of numerical simulation is illustrated in Fig. III-3-1.

Concerned with several key points on the simulation process, the explanations are given as follows:

a) Analysis of the averaged physical processes

The current and the water quality in coastal sea area are varying unsteadily. The main factors of the unsteadiness in flow depend on the tidal force and the current fluctuations with long time scale etc. In case of water quality, the unsteadiness arises mainly from tidal current, the pollutant flux, the internal production and consumption.

It is impossible to carry out the numerical simulation completely including all these factors, because unsteady physical processes are too complicated. So we must simplify the actual process to adjust the model as much as possible to make a model. The current can be assumed as the combination of various periodic flows, and these periods have the orders from half day to a day sometimes a month or a year. The data analysis show that the observed current can be classified into tidal current, lower frequency component current than tidal period and turbulence as a first approximation.

As for water quality, the water quality prediction model is often evaluated as the distribution of averaged concentrations which derived from the long term observation.

From this point of view, the model is accomplished.

b) Establishment of the numerical simulation model

The numerical simulation model has to be established so as to be compatible with the above mentioned observed data. If the observed data show the baroclinic nature such as internal mode wave, or if the current velocity profile has the large vertical shear or the vertical density profiles show the remarkable stratification, the three dimensional model should be adopted. If the motion shows the barotropic nature or if the vertical profile of density shows uniform distribution, the barotropic model (horizontally two dimensional model) is appropriate.

As for the water quality, we only consider the physical diffusion process of pollution in general. However, sometimes it is necessary to consider the pollutant to be non-conservative materials.

c) Establishment of the boundary conditions

Numerical model can be solved approximately by computer based on some kind of boundary conditions. We adopted the finite element method as approximation technique which can represent the shoreline topography accurately and boundary conditions reasonably.

d) Model adjustments

The numerical results must be justified that the results have well agreement with observed data. In order to make it possible, the boundary conditions are adjusted by trial and error until the agreement is obtained.

e) Numerical simulation

After the simulation model verification, the adjusted boundary conditions concerning with the topography, the inflow rates and the pollutant fluxes are changed according to the future plan, and the prediction is made out. Comparing the result of the future prediction with the present stage, the influence on the tidal current and water quality caused by the developing plan in the future can be examined.

STEP 1 Model setup and boundary specification

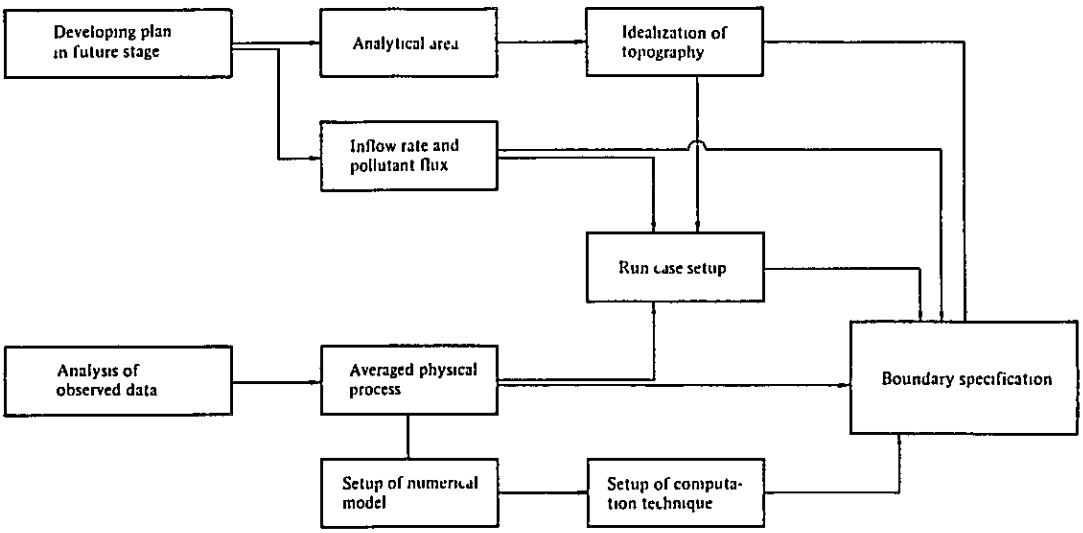

STEP 2 Computation

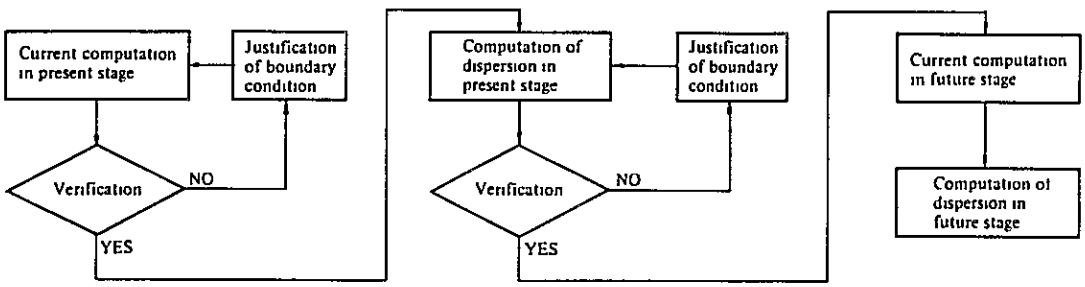

STEP 3 Verification and prediction

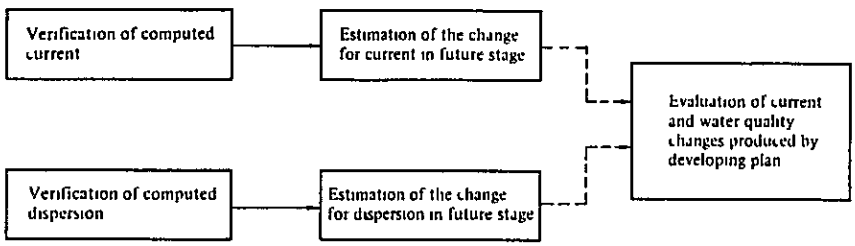

Fig. III-1-1 Process of numerical simulation

CHAPTER 2 PHYSICAL PROCESSES IN SERAYA AND TEKONG AREAS

The brief summary is performed about the typical current and water quality in both areas.

III-2-1 Tide

Based on the harmonic constant of tide at Victoria Dock and Jurong Wharf near Seraya island and at Slave One near Tekong island (v.Table III-2-1), following features of tide are shown in both areas.

At Victoria Dock and Jurong Wharf, M2 component of semidiurnal tides is dominant. The phase lag of every constituents indicate that the tidal wave propagates from the side of Victoria Dock to the side of Jurong Wharf, from east to west.

Between Victoria Dock and Jurong Wharf (about 15km far), semidiurnal tide is also dominant.

Between Victoria Dock and Slave One (about 30km far), semidiurnal tide has the 10^{o} to 20^{o} (20 to 40 minutes) phase lag and, as diurnal tides it reaches to 40^{o} to 50^{o} (160 to 240 minutes).

It is shown that the tidal wave propagates from east to west as same with Seraya area.

In the area of Johore channel, the tide and its phase are not elucidated, but according to the relations of tide and phase between Victoria Dock and Slave One it is estimated that the tidal wave propagates from Slave One to Johore channel, open sea to narrow channel and the amplitudes increases accordingly.

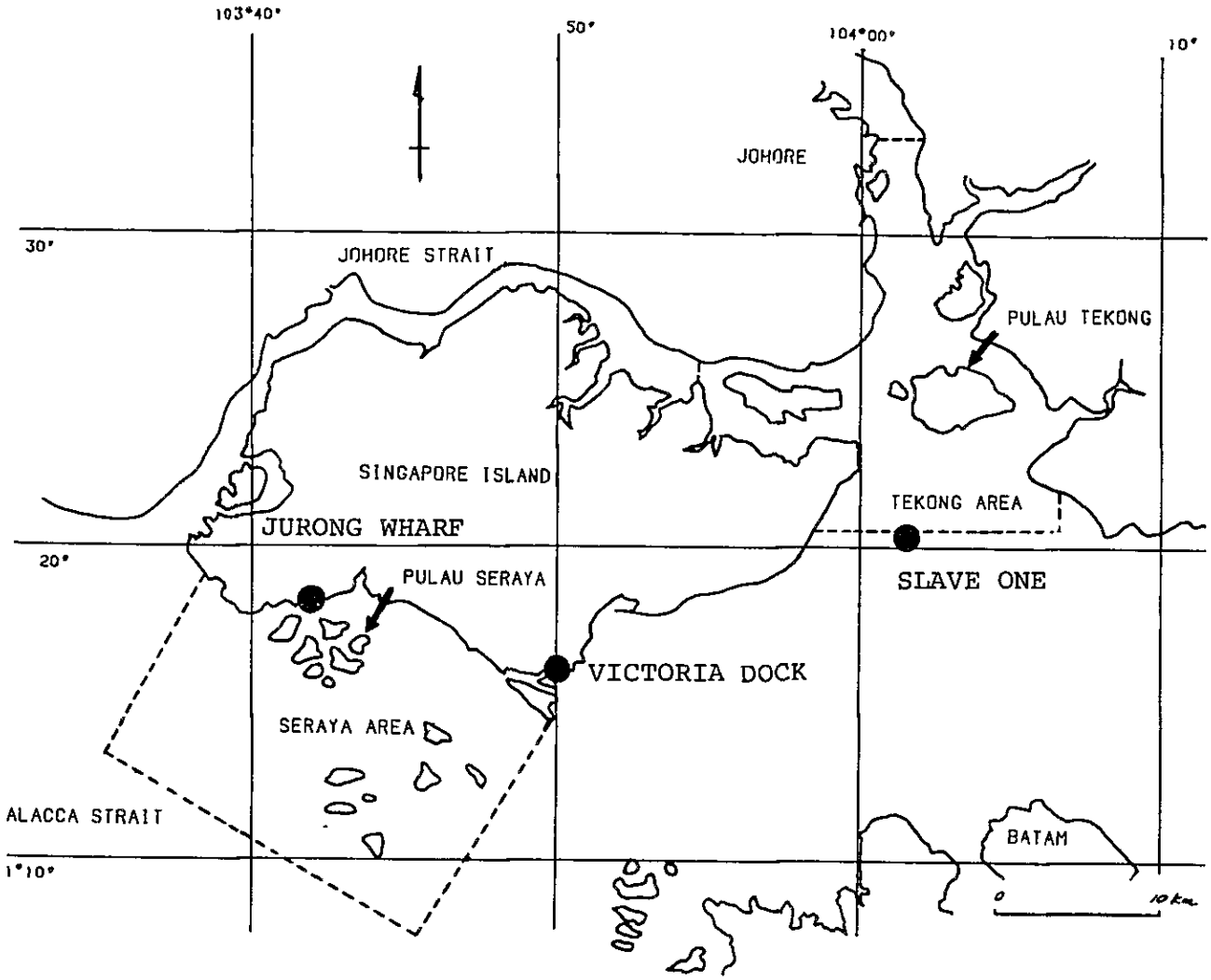

Table III-2-1 Harmonic constants of tide

Point	Jurong Wharf		Victoria Dock		Slave One	
Component	amplitude (m)	phase (°)	amplitude (m)	phase (°)	amplitude (m)	phase (°)
K_1	0.262	123	0.289	99	0.299	76
O_1	0.266	82	0.296	57	0.270	41
M_2	0.811	303	0.773	302	0.689	293
S_2	0.361	356	0.349	351	0.250	338

III-2-2 Currents

According to the current observation performed in 1979 and 1981, the current in Seraya and Tekong areas are summarized as follows:

--- Seraya area

The predominant currents consist of diurnal tidal currents as K_1 and O_1 component, and the velocity reaches to 20-50 cm/sec. This maximum velocity is over two times larger than the velocity of semi diurnal tidal currents as M_2 and S_2 components which reach to 7-14 cm/sec. M_2 component is predominant on the tidal level as referred but the diurnal current is predominant on the tidal current.

Judging from the long axis direction of current ellipse, the oscillating currents along the shore line are observed at every observation stations.

As for the constant current, the observed data in 1981 are different from one in 1979. In 1979 the eastward current is observed whose velocity is from 1 cm/sec to 20 cm/sec, on the other hand in 1981 the westward current is observed whose velocity is from 7 cm/sec to 20 cm/sec. It is supposed that the seasonal difference of water surface gradient direction produces such different current patterns in the straits of Malacca.

--- Tekong area

The predominant current consists of semidurnal tidal current as M_2 component, and the maximum velocity reaches to 30 cm/sec to 40 cm/sec which value is two or six times larger than that of diurnal current.

Judging from the long axis direction of current ellipse, the current is oscillating between open sea and Johore channel.

As for the constant current, observed data show the current from open sea to Johore channel at st.TC.1, TC.3 and TC.4, on contrary at st.TC2 the current direction is for open sea.

Those constant currents have the velocity as from 3 cm/sec to 7 cm/sec and such magnitudes are considerably smaller than maximum velocity of tidal current.

III-2-3 Water Quality

According to the observation of water quality performed in 1981, the summary of water quality in Seraya and Tekong areas are as follows (v.chapt.2-5):

— Seraya area

As for COD concentrations, their values are equal to 0.1-0.7ppm at almost all observed points except the areas around Jurong and Pasir Panjung, which show the rapid mixing of pollutant flux. The observed data show that in the west to Seraya island COD concentration is low (0.1-0.6ppm) and in the east to the island it is higher (0.3-2.4ppm). This distribution of COD concentration is supposed to be produced by the eastward current.

As for salinity concentrations, at almost all observed points the vertical distribution of concentration is ranged within 32.5-33.0% except st.S16 where the inflow from river has the influence on salinity concentration and the vertical change of it as 1% is shown.

As for water temperature, the same characteristic is shown with salinity distribution, and the vertical distribution of water temperature is ranged within 28°C to 29°C except st.S16.

— Tekong area

As for COD concentrations, in northern part of Tekong area, they are rather high concentrations ranged 1.2-2.6ppm and in southern part of Tekong area considerably low concentrations ranged 0.9-1.6ppm are shown. It is considered that the current from open sea to Johore channel as already referred produces such a distribution of COD concentrations.

As for salinity concentrations, the vertically averaged concentrations are ranged 31% in northern part of Tekong area, and ranged from 31% to 32% in southern part of this area. The vertical changes of salinity concentrations remains within 1%.

As for the water temperature, the vertically averaged water temperatures have almost uniform distributions and their values are ranged from 28.2°C to 28.9°C, and the vertical changes of water temperatures remain within 1°C.

CHAPTER 3 AVERAGED PHYSICAL PROCESSES

Based on the field data in Seraya area and Tekong area, the averaged tidal current pattern and corresponding water quality pattern are obtained. The model is applied to the averaged pattern to adjust the boundary conditions to verify the simulation model. Then the model is establlished. In 1979, the tidal current observation was also carried out in Seraya area, and those data are supplemented to the model verification.

III-3-1 Tidal Currents

In Seraya and Tekong area, according to the vertical distributions of the salinity and the temperature, no stratification is observed, since the tidal motion seems to be barotropic.

a) Seraya area

In Seraya area the predominant currents consist of the diurnal tidal currents and the constant current. The diurnal tidal currents prevail over the many tidal components, and the constant current means the slow varying unsteady flow whose time scale is longer than a day.

Comparing the velocities between the diurnal tidal currents and the constant current, the former is about two times larger than the latter, and it means that the diurnal currents are mainly governing the sea current in Seraya area.

The tidal current consists of various components whose phases and periods are different each other, so that, the spring tide, the neap tide, the diurnal inequality and any other phenomena come out.

As for the model for tidal current, it is possible to combine the four principal component currents (K_1, O_1, M_2 and S_2 component currents).

Although on the dispersion process, the constant current has more effect than the tidal currents which have the oscillating motion, and the quasi steady state water quality distribution has to be simulated, consequently, it is not important to combine the principal component currents.

According with this sense, the prediction model for the numerical simulation is represented by superposing the K_1 component current and constant current as Fig. III-3-1.

b) Tekong area

In Tekong area, the M_2 component current and the constant current are predominant from the field data. The prediction model for the numerical simulation is represented by superposing the M_2 component current and the constant current in the same way as Seraya area (Fig. III-3-2).

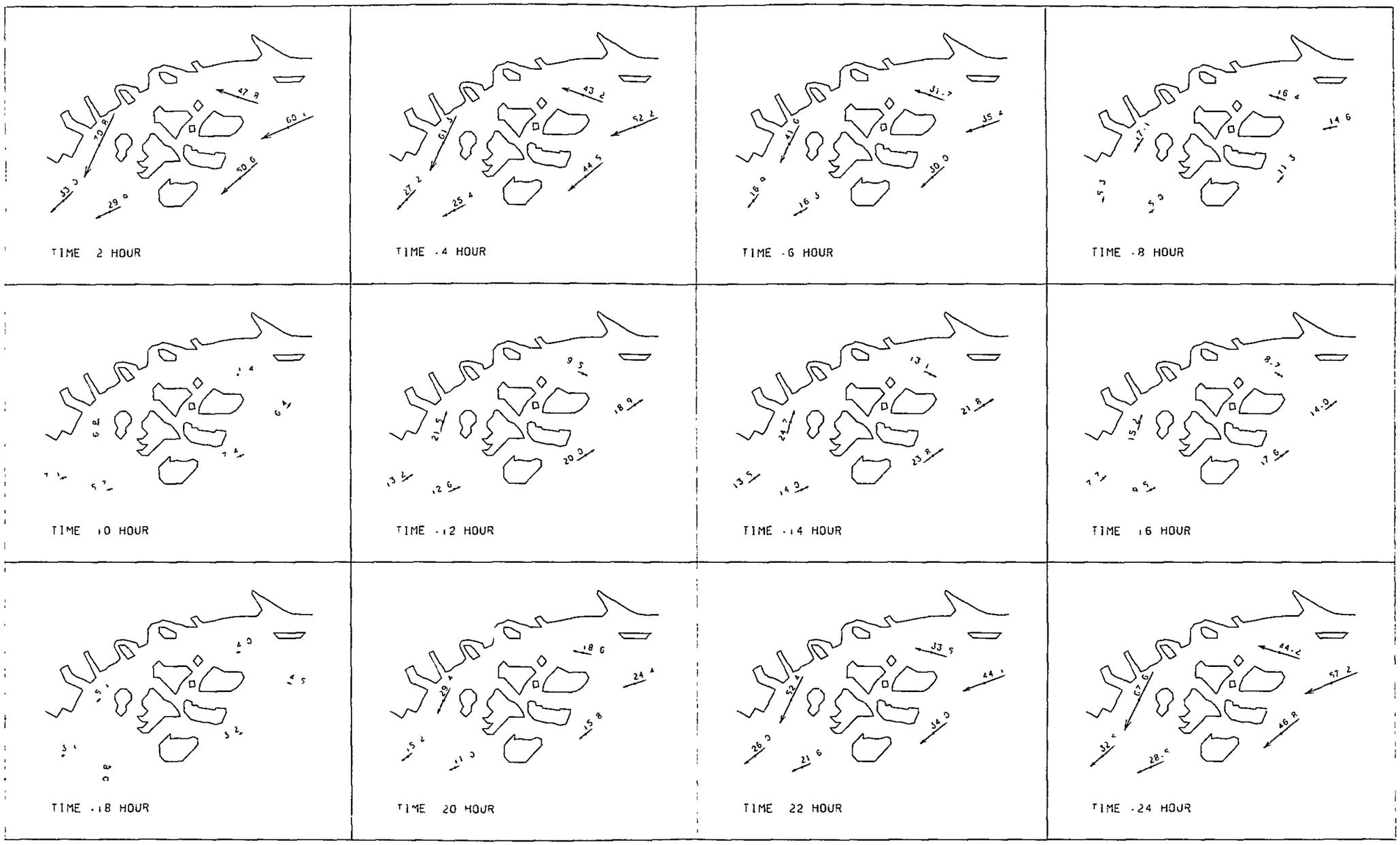

Fig. III-3-1 Averaged current pattern in Seraya area (constant current + K_1, component)

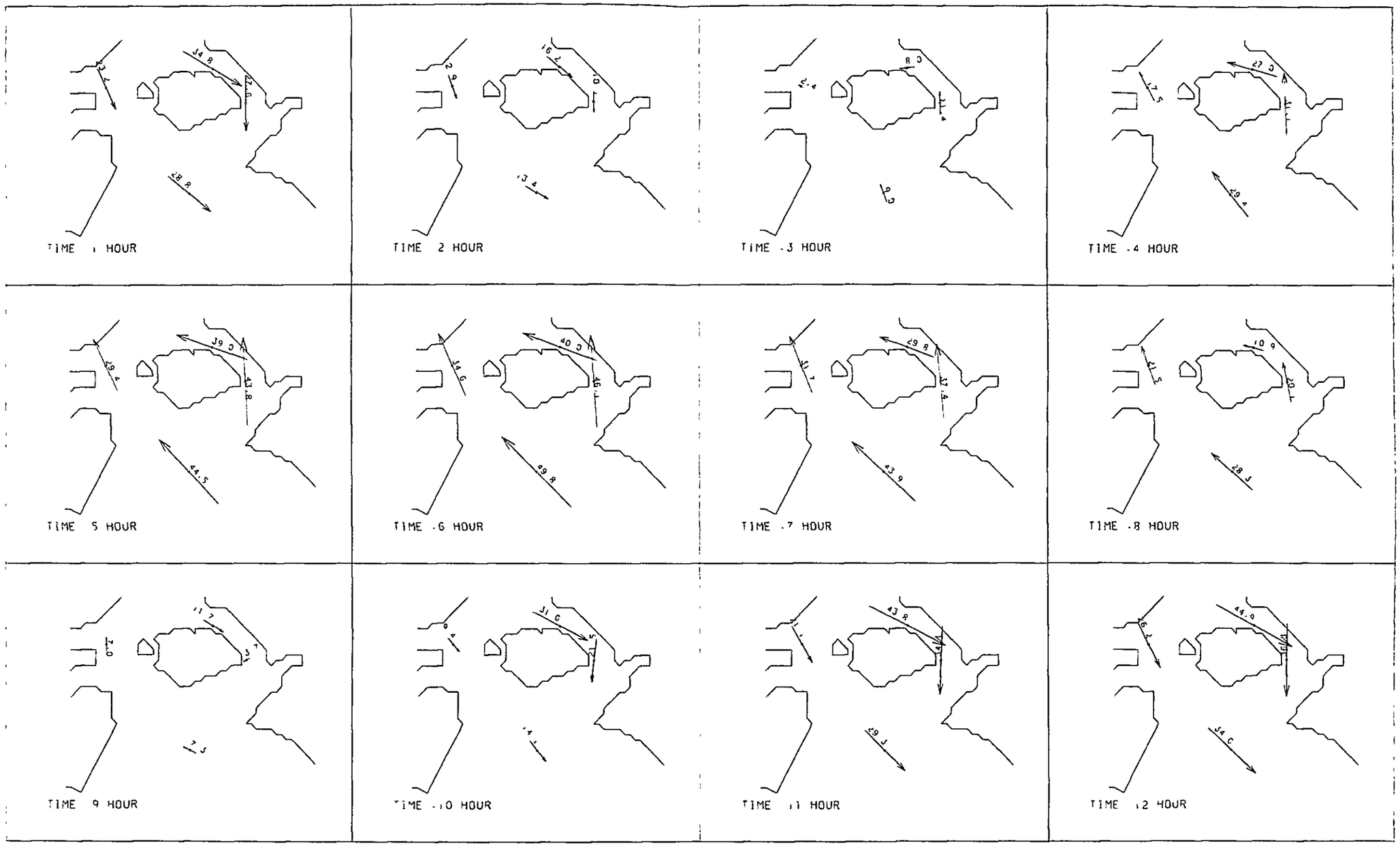

Fig. III-3-2 Averaged current pattern in Tekong area (constant current + M_2 component)

III-3-2 Water Quality

In order to establish the prediction model for water quality, it is important to continue the observation for long term. But in this research only one time observation has carried out. Consequently, the observed data on the water quality does not represent the averaged phenomena sufficiently, but this data is applied in the numerical simulation for adjustment. As the water quality indicators, the COD (Chemical Oxgen Demand) and the water temperature are used.

In Figs. III-3-3 and, III-3-4 vertically averaged horizontal distributions of the COD and the water temperature are illustrated.

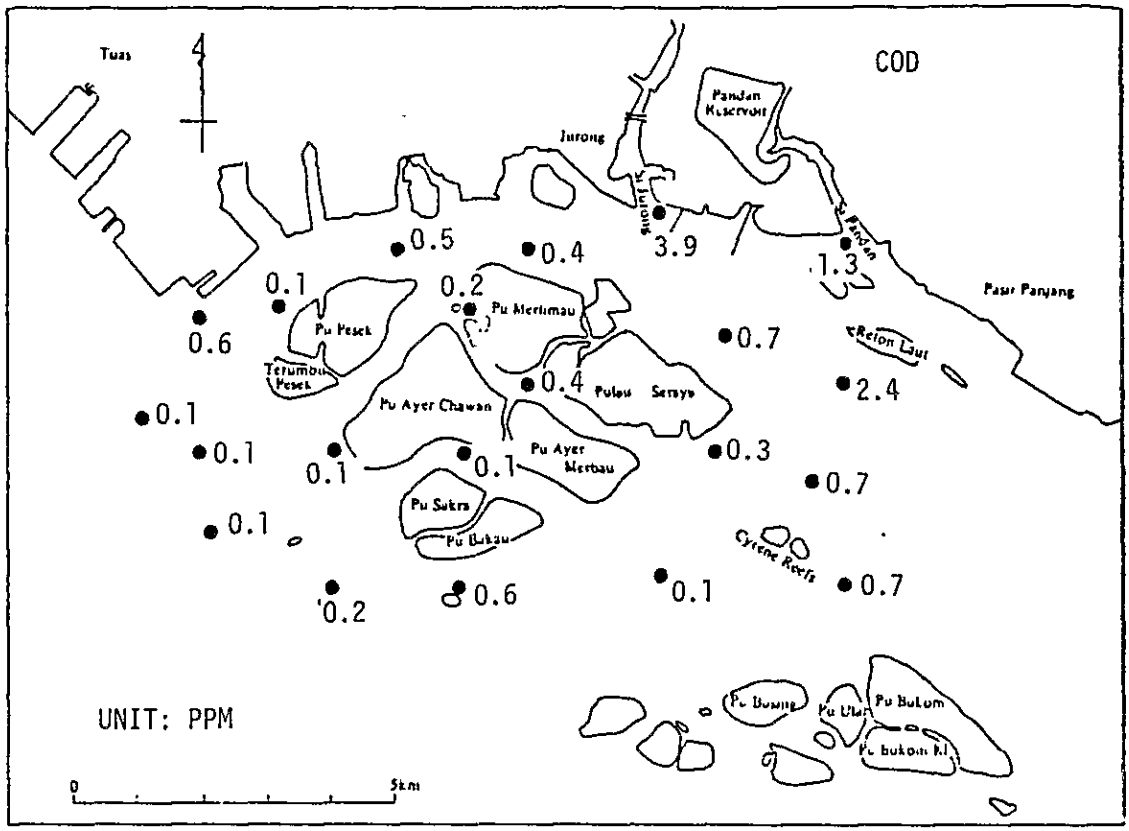

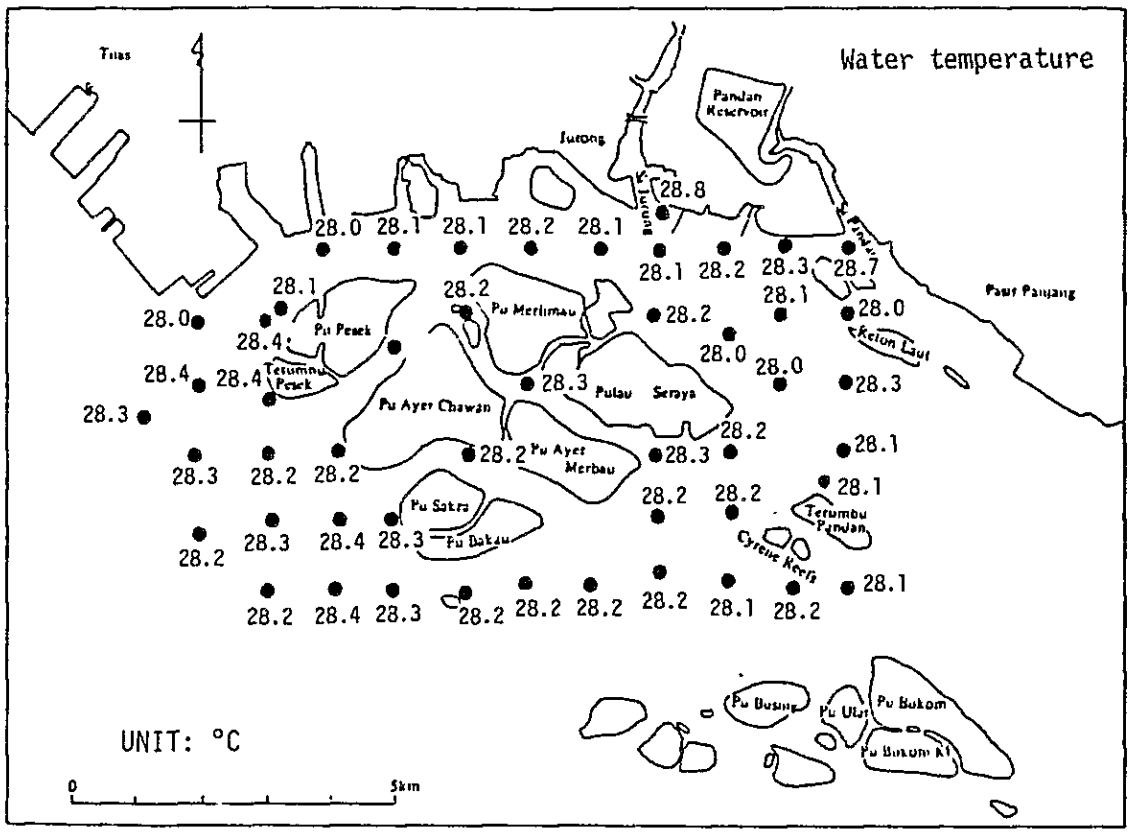

Fig. III-3-3 Observation results of water quality in Seraya Area

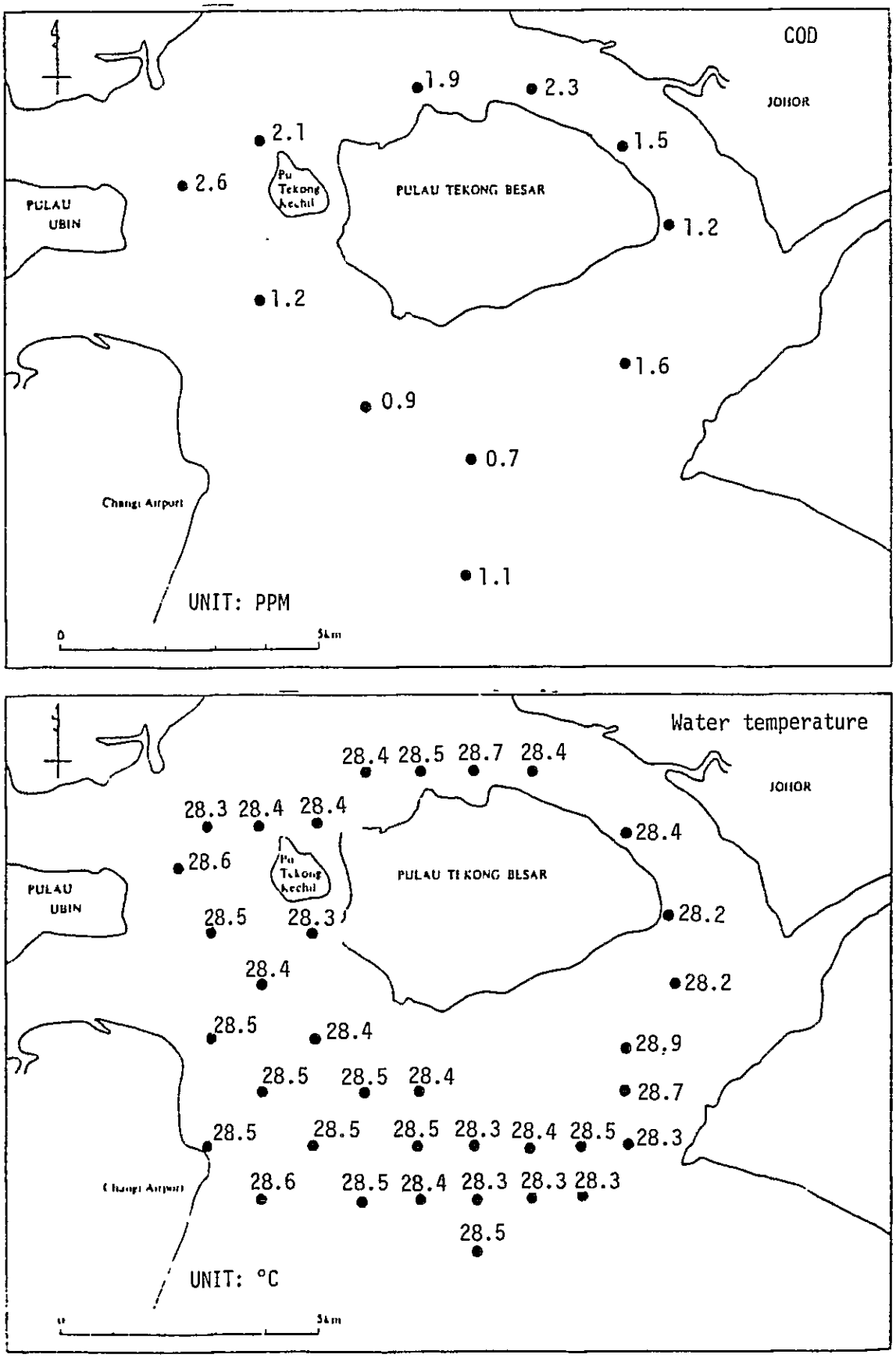

Fig. III-3-4 Observation results of water quality in Tekong Area

CHAPTER 4 FINITE ELEMENT APPROXIMATIONS FOR SHALLOW WATER WAVE AND DISPERSION

III-4-1 Shallow Water Wave

III-4-1-1 Basic equations

A set of equations appropriate for areal modeling of vertically well-mixed water bodies is obtained by averaging the three-dimensional equations over the depth. It is further assumed that the fluid density is a constant. In the subsequent development of the equations, the following notation will be used: ρ is the density, u,v, and w are the velocity components in the x,y, and z directions, respectively, x is positive eastward, y positive northward, z positive upward, and t is time.

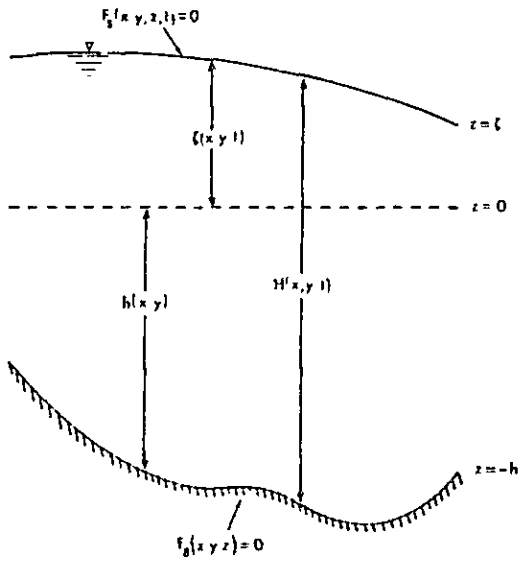

Fig. III-4-1 Cross section of a typical estuary

(1) Boundary conditions on velocity

When the three-dimensional flow equations are integrated over the depth, the need arises for conditions on the flow at the surface and bottom of the estuary. If the equation of a boundary is $F(x,y,z,t) = 0$, then at every point on the boundary we must have

$$\frac{DF}{Dt} = \frac{\partial F}{\partial t} + u\frac{\partial F}{\partial x} + v\frac{\partial F}{\partial y} + w\frac{\partial F}{\partial z} = 0 \qquad (1)$$

which indicates that F remains the equation for the boundary through time. At the surface of the estuary,

$$F_S(x,y,z,t) = z - \zeta(x,y,t) \qquad (2)$$

so Eq. (1) becomes

$$w_S - \frac{\partial \zeta}{\partial t} - u_S\frac{\partial \zeta}{\partial x} - v_S\frac{\partial \zeta}{\partial y} = 0 \qquad (3)$$

where the subscript S refers to a velocity at the surface. At the bottom of the estuary,

$$F_B(x,y,z) = z + h(x,y) \qquad (4)$$

and is independent of time. Substitution into (1) yields

$$w_B + u_B\frac{\partial h}{\partial x} + v_B\frac{\partial h}{\partial y} = 0 \qquad (5)$$

where the subscript B refers to a velocity at the bottom of the estuary.

Equations (3) and (5) are the conditions at the boundary needed for the integration of the flow equations to obtain their two-dimensional form.

(2) Continuity equation

The general equation for the conservation of mass is

$$\frac{\partial \rho}{\partial t} + \frac{\partial(\rho u)}{\partial x} + \frac{\partial(\rho v)}{\partial y} + \frac{\partial(\rho w)}{\partial z} = 0 \qquad (6)$$

For an incompressible fluid, $D\rho/Dt=0$ and (6) reduces to

$$\frac{\partial u}{\partial x}+\frac{\partial v}{\partial y}+\frac{\partial w}{\partial z}=0 \tag{7}$$

This equation may be integrated over the depth to obtain

$$\int_{-h}^{\zeta}\frac{\partial u}{\partial x}\,dz+\int_{-h}^{\zeta}\frac{\partial v}{\partial y}\,dz+\int_{-h}^{\zeta}\frac{\partial w}{\partial z}\,dz=0 \tag{8}$$

Application of Leibnitz' rule for interchanging the order of differentiation and integration in the first two integrals and direct evaluation of the third integral yield

$$\begin{aligned}&\frac{\partial}{\partial x}\int_{h}^{\eta}u\,dz-u_S\frac{\partial\eta}{\partial x}-u_B\frac{\partial h}{\partial x}+\frac{\partial}{\partial y}\int_{-h}^{\eta}v\,dz-v_S\frac{\partial\eta}{\partial y}\\&\quad+u_B\frac{\partial h}{\partial y}+w_S-w_S\\&=\frac{\partial}{\partial x}\int_{-h}^{\zeta}u\,dz+\frac{\partial}{\partial y}\int_{-h}^{\zeta}v\,dz+\left(w_S-u_S\frac{\partial\zeta}{\partial x}-v_S\frac{\partial\zeta}{\partial y}\right)\\&\quad-\left(w_B+u_B\frac{\partial h}{\partial x}+v_B\frac{\partial h}{\partial y}\right)=0\end{aligned} \tag{9}$$

Boundary conditions (3) and (5) can be applied to this equation to reduce it to the form

$$\frac{\partial\zeta}{\partial t}+\frac{\partial}{\partial x}\int_{-h}^{\zeta}u\,dz+\frac{\partial}{\partial y}\int_{-h}^{\zeta}v\,dz=0 \tag{10}$$

If average values of u and v are defined by

$$U=(\zeta+h)^{-1}\int_{-h}^{\zeta}u\,dz \tag{11a}$$

$$V=(\zeta+h)^{-1}\int_{-h}^{\zeta}v\,dz \tag{11b}$$

Eq. (10) becomes

$$\frac{\partial \zeta}{\partial t} + \frac{\partial (HU)}{\partial x} + \frac{\partial (HV)}{\partial y} = 0 \tag{12}$$

where use has been made of the face that $H = \zeta + h$. Because h is independent of time, this equation can alternatively be expressed as

$$\frac{\partial H}{\partial t} + \frac{\partial (HU)}{\partial x} + \frac{\partial (HV)}{\partial y} = 0 \tag{13}$$

Either one of these last two forms of the continuity equation is appropriate for use in an areal estuary model.

3 Momentun equations

For a constant density fluid, the equations of motion in the x, y, and z directions are

$$\frac{\partial u}{\partial t} + \frac{\partial (uu)}{\partial x} + \frac{\partial (uv)}{\partial y} + \frac{\partial (uw)}{\partial z} - fv + \frac{1}{\rho}\frac{\partial p}{\partial x} - \frac{1}{\rho}\left(\frac{\partial \tau_{xx}}{\partial x} + \frac{\partial \tau_{xy}}{\partial y} + \frac{\partial \tau_{xz}}{\partial z}\right) = 0 \tag{14}$$

$$\frac{\partial v}{\partial t} + \frac{\partial (uv)}{\partial x} + \frac{\partial (vv)}{\partial y} + \frac{\partial (vw)}{\partial z} + fu + \frac{1}{\rho}\frac{\partial p}{\partial y} - \frac{1}{\rho}\left(\frac{\partial \tau_{yx}}{\partial x} + \frac{\partial \tau_{yy}}{\partial y} + \frac{\partial \tau_{yz}}{\partial z}\right) = 0 \tag{15}$$

$$\frac{\partial w}{\partial t} + \frac{\partial (uw)}{\partial x} + \frac{\partial (vw)}{\partial y} + \frac{\partial (ww)}{\partial z} + \frac{1}{\rho}\frac{\partial p}{\partial z} + g - \frac{1}{\rho}\left(\frac{\partial \tau_{zx}}{\partial x} + \frac{\partial \tau_{zy}}{\partial y} + \frac{\partial \tau_{zz}}{\partial z}\right) = 0 \tag{16}$$

where p is pressure, f the Coriolis parameter, g gravity, and τ_{xx}, τ_{xy}, etc., are shear stresses.

These equations are unnecessarily general for use in modeling a vertically well-mixed estuary. Equation (16) can be simplified by assuming that the vertical accellerations are negligible and that the shear stresses are negligible compared to gravity and the vertical pressure gradient. These assumptions are equivalent to stating that the pressure in the z direction is hydrostatic, so (16) becomes

$$\frac{1}{\rho}\frac{\partial p}{\partial z} + g = 0 \tag{17}$$

If the pressure is assumed to be atmospheric at the surface, the solution to this equation is

$$p - p_A = \rho g(\zeta - z) \tag{18}$$

where p_A is the atmospheric pressure. Substitution for p into Eqs. (14) and (15) with p_A assumed constant yields

$$\begin{aligned}\frac{\partial u}{\partial t} + \frac{\partial (uu)}{\partial x} + \frac{\partial (uv)}{\partial y} + \frac{\partial (uw)}{\partial z} - fv + g\frac{\partial \zeta}{\partial x} \\ -\frac{1}{\rho}\left(\frac{\partial \tau_{xx}}{\partial x} + \frac{\partial \tau_{xy}}{\partial y} + \frac{\partial \tau_{xz}}{\partial z}\right) = 0\end{aligned} \tag{19}$$

and

$$\begin{aligned}\frac{\partial v}{\partial t} + \frac{\partial (uv)}{\partial x} + \frac{\partial (vv)}{\partial y} + \frac{\partial (vw)}{\partial z} + fu + g\frac{\partial \zeta}{\partial y} \\ -\frac{1}{\rho}\left(\frac{\partial \tau_{yx}}{\partial x} + \frac{\partial \tau_{yy}}{\partial y} + \frac{\partial \tau_{yz}}{\partial z}\right) = 0\end{aligned} \tag{20}$$

The vertically averaged forms of these equations are obtained by a series of virtually identical steps. For the sake of brevity, the specific arguments will be applied only to Eq. (19) with the integrated form of (20) deduced by analogy. Integration of (19) over z yields

$$\begin{aligned}\int_{-h}^{\zeta} \frac{\partial u}{\partial t}\,dz + \int_{-h}^{\zeta} \frac{\partial (uu)}{\partial x}\,dz + \int_{-h}^{\zeta} \frac{\partial (uv)}{\partial y}\,dz + \int_{-h}^{\zeta} \frac{\partial (uw)}{\partial z}\,dz - \int_{-h}^{\zeta} fv\,dz \\ + g\int_{-h}^{\zeta} \frac{\partial \zeta}{\partial x}\,dz - \int_{-h}^{\zeta} \frac{1}{\rho}\frac{\partial \tau_{xx}}{\partial x}\,dz - \int_{-h}^{\zeta} \frac{1}{\rho}\frac{\partial \tau_{xy}}{\partial y}\,dz - \frac{1}{\rho}\int_{-h}^{\zeta} \frac{\partial \tau_{xz}}{\partial z}\,dz = 0\end{aligned} \tag{21}$$

With ρ assumed constant, application of Leibnitz' rule to the first three and the seventh and eighth integrals, and integration of the derivatives with respect to z directly, yields

$$\frac{\partial}{\partial t}\int_{-h}^{\zeta} u\,dz + \frac{\partial}{\partial x}\int_{-h}^{\zeta} uu\,dz + \frac{\partial}{\partial y}\int_{-h}^{\zeta} uv\,dz - \int_{-h}^{\zeta} fv\,dz$$
$$+ gH\frac{\partial \zeta}{\partial x} - \frac{1}{\rho}\tau_{xz}\Big|_{\zeta} + \frac{1}{\rho}\tau_{xz}\Big|_{-h} - \frac{1}{\rho}\frac{\partial}{\partial x}\int_{-h}^{\zeta}\tau_{xx}\,dz$$
$$-\frac{1}{\rho}\frac{\partial}{\partial y}\int_{-h}^{\zeta}\tau_{xy}\,dz + u_S\left(-\frac{\partial \zeta}{\partial t} - u_S\frac{\partial \zeta}{\partial x} - v_S\frac{\partial \zeta}{\partial y} + w_S\right) \qquad (22)$$
$$-u_B\left(u_B\frac{\partial h}{\partial x} + v_B\frac{\partial h}{\partial y} + w_B\right) + \frac{1}{\rho}\tau_{xx}\Big|_{\zeta}\frac{\partial \zeta}{\partial x} + \frac{1}{\rho}\tau_{xx}\Big|_{-h}\frac{\partial h}{\partial x}$$
$$+\frac{1}{\rho}\tau_{xy}\Big|_{\zeta}\frac{\partial \zeta}{\partial y} + \frac{1}{\rho}\tau_{xy}\Big|_{-h}\frac{\partial h}{\partial y} = 0$$

Substitution of (11) into (22) yields

$$\frac{\partial (HU)}{\partial t} + \frac{\partial}{\partial x}(HUU) + \frac{\partial}{\partial y}(HUV) - fHV + gH\frac{\partial \zeta}{\partial x} - \frac{1}{\rho}\tau_{xz}\Big|_{\zeta}$$
$$+\frac{1}{\rho}\tau_{xz}\Big|_{-h} - \frac{1}{\rho}\frac{\partial}{\partial x}\int_{-h}^{\zeta}\tau_{xx}\,dz - \frac{1}{\rho}\frac{\partial}{\partial y}\int_{-h}^{\zeta}\tau_{xy}\,dz = 0 \qquad (23)$$

The last four terms in this equation are related to the frictional losses and are modeled by empirical correlations. The stress at the surface due to wind friction is often given the form

$$\frac{\tau_{xz}}{\rho}\Big|_{\zeta} = KW^2\cos\psi$$

where K is a dimensionless coefficient that is a function of wind speed, W the wind velocity, and ψ the angle between the wind velocity vector and the x axis. The bottom stress is generally expressed as

$$\frac{\tau_{xz}}{\rho}\Big|_{-h} = gU(U^2 + V^2)^{1/2}/C^2$$

where C is the Chezy coefficient with units (length)½ per time. The last two terms in the equation deal with horizontal transport of momentum and are correlated by

$$(1/H)\int_{-h}^{\zeta}\tau_{xx}\,dz = \epsilon\,\partial U/\partial x \qquad (24a)$$

$$(1/H)\int_{-h}^{\zeta}\tau_{xy}\,dz = \epsilon\,\partial V/\partial y \qquad (24b)$$

where ϵ is a coefficient of eddy viscosity. Substitution of these last four relations into (23) yields

$$\frac{\partial(HU)}{\partial t}+\frac{\partial}{\partial x}(HUU)+\frac{\partial}{\partial y}(HUV)-fHV+gH\frac{\partial\zeta}{\partial x}-KW^2\cos\psi$$
$$+\frac{gU(U^2+V^2)^{1/2}}{C^2}-\frac{1}{\rho}\frac{\partial}{\partial x}\left(\epsilon H\frac{\partial U}{\partial x}\right)-\frac{1}{\rho}\frac{\partial}{\partial y}\left(\epsilon H\frac{\partial U}{\partial y}\right)=0 \qquad (25)$$

If the time derivative and convective terms are expanded by the chain rule, the continuity equation (13) is substituted into (25), and the resulting equation is divided by H, we are left with the somewhat simpler expression

$$\frac{\partial U}{\partial t}+U\frac{\partial U}{\partial x}+V\frac{\partial U}{\partial y}-fV+g\frac{\partial\zeta}{\partial x}-\frac{KW^2}{H}\cos\psi+\frac{gU(U^2+V^2)^{1/2}}{HC^2}=0 \qquad (26)$$

For an analogous development, the y component of the momentum equation is

$$\frac{\partial V}{\partial t}+U\frac{\partial V}{\partial x}+V\frac{\partial V}{\partial y}+fU+g\frac{\partial\zeta}{\partial y}-\frac{KW^2}{H}\sin\psi+\frac{gV(U^2+V^2)^{1/2}}{HC^2}=0 \qquad (27)$$

These last two momentum balance equations form the governing hydrodynamic equations that will be considered in the following finite element models.

III-4-1-2 Weighted residual equations

Using U*, V* and η * as weighting functions, the weighted residual equations are derived according to the conventional procedures of the finite element Galerkin method.

Multiplying both sides of equation (12) by η *, equation (26) by U*, equation (27) by V*, integrating over the whole volume V and Using Green's theorem lead to the following equations.

$$\int_v \eta^*\frac{\partial\eta}{\partial t}dV+\int_v \eta^* u\frac{\partial H}{\partial x}dV+\int_v \eta^* v\frac{\partial H}{\partial y}dV$$
$$+\int_v \eta^* H\frac{\partial u}{\partial x}dV+\int_v \eta^* H\frac{\partial v}{\partial y}dV=0 \qquad (28)$$

$$\int_v u^* \frac{\partial u}{\partial t} dV + \int_v u^* u \frac{\partial u}{\partial x} dV + \int_v u^* v \frac{\partial u}{\partial y} dV$$

$$- f \int_v u^* v dV + g \int_v u^* \frac{\partial u}{\partial x} dV + \frac{g}{HC^2} (u^2 + v^2)^{1/2} \int_v u^* u dV \qquad (29)$$

$$+ \epsilon \int_v \left(\frac{\partial u}{\partial x} \frac{\partial u}{\partial x} + \frac{\partial u}{\partial y} \frac{\partial u}{\partial y} \right) dV$$

$$= \epsilon \int_s \left(u^* \frac{\partial u}{\partial x} n_x + u^* \frac{\partial u}{\partial y} n_y \right) dS$$

$$\int_v v^* \frac{\partial v}{\partial t} dV + \int_v v^* u \frac{\partial v}{\partial x} dV + \int_v v^* v \frac{\partial v}{\partial y} dV$$

$$+ f \int_v v u dV + g \int_v v \frac{\partial \eta}{\partial y} dV + \frac{g}{HC^2} (u^2 + v^2)^{1/2} \int_v v^* v dV \qquad (30)$$

$$+ \epsilon \int_v \left(\frac{\partial v}{\partial x} \frac{\partial v}{\partial x} + \frac{\partial v}{\partial y} \frac{\partial v}{\partial y} \right) dV$$

$$= \epsilon \int_s \left(v^* \frac{\partial v}{\partial x} n_x + v^* \frac{\partial v}{\partial y} n_y \right) dS$$

Where the stress at the surface due to wind is neglected.

III-4-1-3 Finite element equations

It is assumed that the field to be analyzed is divided into small regions called finite elements. Let the interpolating equations for U, V, and H in each finite element be expressed as;

$$\left.\begin{aligned} u \quad (x, y) &= \sum_{\alpha=1}^{3} \Phi_\alpha (x, y) u_\alpha = \Phi_\alpha u_\alpha \\ v \quad (x, y) &= \Sigma \Phi_\alpha (x, y) v_\alpha = \Phi_\alpha v_\alpha \\ \eta \quad (x, y) &= \Sigma \Phi_\alpha (x, y) \eta_\alpha = \Phi_\alpha \eta_\alpha \\ H \quad (x, y) &= \Sigma \Phi_\alpha (x, y) H_\alpha = \Phi_\alpha H_\alpha \end{aligned}\right\} \qquad (31)$$

where Φ_α denotes the interpolation function for U, V, η and H. U_α, V_α, η_α, H_α are the nodal values of U, V, η, H at αth node of each finite element

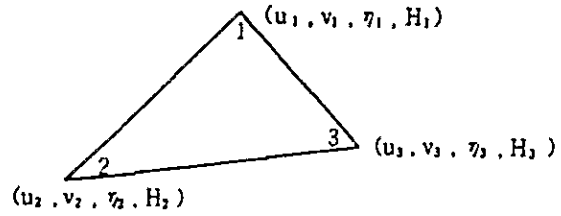

For weighting function U*, V* and η^*, the relation similar to equations (31) are employed in the following forms.

$$\begin{aligned} u^*\ (x,y) &= \Sigma\, \Phi_a\,(x,y)\, u_a^* = \Phi_a u_a^* \\ v^*\ (x,y) &= \Sigma\, \Phi_a\,(x,y)\, v_a^* = \Phi_a v_a^* \\ \eta^*\ (x,y) &= \Sigma\, \Phi_a\,(x,y)\, \eta_a^* = \Phi_a \eta_a^* \end{aligned} \tag{32}$$

In the numerical computation, the same function is used as the interpolation function in equations (31), (32).

Introducing equations (31), (32) into equations (28), (29) and (30) and rearranging the equations lead to the finite element equations in the following form.

$$M_{KL}\,\dot{\eta}_L + K^1_{KLM}\,H_L\,u_M + K^2_{KLM}\,H_L\,v_M + K^1_{KLM}\,u_L\,H_M + K^2_{KLM}\,v_L\,H_M = 0 \tag{33}$$

$$\begin{aligned} &M_{KL}\,\dot{u}_L + K^1_{KLM}\,u_L u_M + K^2_{KLM}\,u_L\,v_M - f M_{KL}\,v_L \\ &\quad + g\,N^1_{KL}\,\eta_L + \frac{g}{H_L C^2}\,(u_L^2 + v_L^2)^{1/2}\,M_{KL}\,u_L + \nu^2 S_{KL}\,u_L = \pi^1_K \end{aligned} \tag{34}$$

$$\begin{aligned} &M_{KL}\dot{v}_L + K^1_{KLM}\,v_L\,u_M + K^2_{KLM}\,v_L v_M + f M_{KL}\,u_L \\ &\quad + g\,N^2_{KL}\,\eta_L + \frac{g}{H_L C^2}\,(u_L^2 + v_L^2)^{1/2}\,M_{KL}\,v_L + \nu^2 S_{KL}\,v_L = \pi^2_K \end{aligned} \tag{35}$$

$$M_{KL} = \int_v \Phi_K \Phi_L dV$$

$$K^1_{KLM} = \int_v \Phi_K \frac{\partial \Phi_L}{\partial x} \Phi_M dV$$

$$K^2_{KLM} = \int_v \Phi_K \frac{\partial \Phi_L}{\partial x} \Phi_M dV$$

$$S_{KLM} = \int_v \left(\frac{\partial \Phi_K}{\partial x} \cdot \frac{\partial \Phi_L}{\partial x} + \frac{\partial \Phi_K}{\partial y} \cdot \frac{\partial \Phi_L}{\partial y} \right) dV$$

$$N^1_{KL} = \int_v \Phi_K \frac{\partial \Phi_L}{\partial x} dV$$

$$N^2_{KL} = \int_v \Phi_K \frac{\partial \Phi}{\partial y} dV$$

III-4-1-4 Numerical integration in time

To solve equatons (33), (34) and (35), numerical integration scheme in time must be introduced. The scheme employed is the two step explicit scheme. The basic idea is the same as that of lax Windroff finite difference method. Consider a function F(t) and its Taylor expansion:

$$F(t + \Delta t) = F(t) + \Delta t \dot{F}(t) + \frac{\Delta t}{2} \ddot{F}(t) \qquad (36)$$

where Δ t is a short time increment. When the values of F(t) and F(t) are computed, the value of F(t + Δt) obtained by using equation (36).

$$F\left(t + \frac{\Delta t}{2}\right) = F(t) + \frac{\Delta t}{2} \dot{F}(t) \qquad (37)$$

$$F(t + \Delta t) = F(t) + \Delta t \dot{F}\left(t + \frac{\Delta t}{2}\right) \qquad (38)$$

In case of the computation by equations (37) and (38), it is not necessary to compute the value of F(t). Applying equations (37) and (38) to equations (33), (34) and (35), the following two step scheme can be obtained:

First step:

$$\overline{M_{KL}}\, u_L\left(t + \frac{\Delta t}{2}\right) = M_{KL}\, u_L(t) + \frac{\Delta t}{2} M_{KL}\, \dot{u}_L(t) \qquad (39)$$

$$\overline{M_{KL}} v_L \left(t+\frac{\Delta t}{2}\right) = M_{KL}\, v_L(t) + \frac{\Delta t}{2} M_{KL}\, \dot{v}_L(t) \tag{40}$$

$$\overline{M_{KL}}\, \eta_L\left(t+\frac{\Delta t}{2}\right) = M_{KL}\, \eta_L(t) + \frac{\Delta t}{2} M_{KL}\, \dot{\eta}_L(t) \tag{41}$$

Second step:

$$\overline{M_{KL}}\, u_L(t+\Delta t) = M_{KL}\, u_L(t) + \Delta t\, M_{KL}\, \dot{u}_L\left(t+\frac{\Delta t}{2}\right) \tag{42}$$

$$\overline{M_{KL}}\, v_L(t+\Delta t) = M_{KL}\, v_L(t) + \Delta t\, M_{KL}\, \dot{v}_L\left(t+\frac{\Delta t}{2}\right) \tag{43}$$

$$\overline{M_{KL}}\, \eta_L(t+\Delta t) = M_{KL}\, \eta_L(t) + \Delta t\, M_{KL}\, \dot{\eta}_L\left(t+\frac{\Delta t}{2}\right) \tag{44}$$

Equations (39) to (44) are pure explicit scheme only if the lumped coefficient system is employed on the left hand side of the equations. Superposed-denotes the lump coefficient matrix.

III-4-2 Dispersion

III-4-2-1 Basic equations

The general equation for dispersion is

$$\frac{\partial C}{\partial t} + \frac{\partial}{\partial x}(uC) + \frac{\partial}{\partial y}(vC) + \frac{\partial'}{\partial z}(wC) = \frac{\partial}{\partial x}\left(K_x \frac{\partial C}{\partial x}\right) + \frac{\partial}{\partial y}\left(K_y \frac{\partial C}{\partial y}\right) + \frac{\partial}{\partial z}\left(K_z \frac{\partial C}{\partial z}\right) \tag{45}$$

where

c : mass concentration

k_x, k_y, k_z: the eddy dispersion coefficient in the x,y, and z directions, respectively

Following the method used for the continuity and momentum equations, equation (45) is integrated over z and Leibnitz' rule applied to yield

$$\begin{aligned}
&\frac{\partial}{\partial t}\int_{-h}^{\eta} C\,dz + \frac{\partial}{\partial x}\int_{-h}^{\eta} (uC)\,dz + \frac{\partial}{\partial y}\int_{-h}^{\eta} (vC)\,dz \\
&\quad - \frac{\partial}{\partial x}\int_{-h}^{\eta}\left(K_x \frac{\partial C}{\partial x}\right)dz - \frac{\partial}{\partial y}\int_{-h}^{\eta}\left(K_y \frac{\partial C}{\partial y}\right)dz \\
&\quad - C|_{z=\eta}\left(\frac{\partial \eta}{\partial t} + u_s \frac{\partial \eta}{\partial x} + v_s \frac{\partial \eta}{\partial y} - w_s\right) - C|_{z=-h}\left(u_s \frac{\partial h}{\partial x} + v_s \frac{\partial h}{\partial y} + w_s\right) \\
&\quad + \left\{\left(K_x \frac{\partial C}{\partial x}\right)|_{z=\eta} \frac{\partial \eta}{\partial x} + \left(K_y \frac{\partial C}{\partial y}\right)|_{z=\eta} \frac{\partial \eta}{\partial y} + \left(K_x \frac{\partial C}{\partial x}\right)|_{z=-h} \frac{\partial h}{\partial x}\right. \\
&\quad \left. + \left(K_y \frac{\partial C}{\partial y}\right)|_{z=-h} \frac{\partial h}{\partial y} - \left(K_z \frac{\partial C}{\partial z}\right)|_{z=\eta} + \left(K_z \frac{\partial C}{\partial z}\right)|_{z=-h}\right\} = 0 \\
&\quad :
\end{aligned} \tag{46}$$

The last group of terms in this series deal with diffusive transport across an interface. For the present discussion, however, they will be neglected. The terms in parentheses premultiplied by $C|_{z=-h}$ and $C|_{z=\eta}$ are zero by boundary conditions (3) and (5). The average mass concentrations C is defined by

$$\bar{C} = \frac{1}{H}\int_{-h}^{\eta} C\,dz \tag{47}$$

Substitution of (47) into (46) yields

$$\begin{aligned}
&\frac{\partial}{\partial t}(H\bar{C}) + \frac{\partial}{\partial x}(HU\bar{C}) + \frac{\partial}{\partial y}(HV\bar{C}) \\
&\qquad = \frac{\partial}{\partial x}\left(HK_x \frac{\partial \bar{C}}{\partial x}\right) + \frac{\partial}{\partial y}\left(HK_y \frac{\partial \bar{C}}{\partial y}\right)
\end{aligned} \tag{48}$$

III-4-2-2 Weighted residual equations

Using C* as weighting function, the weighted residual equation are derived according to the conventional procedures of the finite element Calerkin method.

Multiplying both side of equation (48) by C*, intergrating over the whole volume V and using Greens' theorem, the following Galerkin expression is obtained.

$$\begin{aligned}
&\int_v C^* \frac{\partial}{\partial x}(HU\bar{C})\,dV + \int_v C^* \frac{\partial}{\partial y}(HV\bar{C})\,dV \\
&\quad + \int_v \frac{\partial C^*}{\partial x} \frac{\partial(H\bar{C})}{\partial x}\,dV + \int \frac{\partial C^*}{\partial y} \frac{\partial(H\bar{C})}{\partial y}\,dV \\
&\quad = \int_s C^*\left(\frac{\partial(H\bar{C})}{\partial x}\eta_x + \frac{\partial(H\bar{C})}{\partial y}\eta_y\right)dS
\end{aligned} \tag{49}$$

III-4-2-3 Finite element equations

Let the interpolating function for C and C* in each finite element by expressed as

$$\begin{aligned} \bar{C} &= \sum_{\alpha=1}^{3} \Phi_\alpha \bar{C}_\alpha = \Phi_\alpha C_\alpha \\ C^* &= \Sigma \ \Phi_\alpha C^*_\alpha = \Phi_\alpha C^*_\alpha \end{aligned} \tag{50}$$

Introducing equation (50) into equation (49) and rearranging the equations leads to the finite element equations in the following form.

$$\begin{aligned} & Mi,j\dot{\bar{C}}jK^1_i,jUk\bar{C}j + K^2_i,jVk\bar{C}_J, + R^1_i,j\bar{C}j = \pi_i \\ & Mi,j = H\int\Phi_i\,\Phi_j\,dV \\ & K^1_1,j = H\int_v\Phi_i\,\Phi_{j,x}\,\Phi_k\,dV \\ & K^2_1,j = H\int_v\Phi_i\,\Phi_{J,y}\,\Phi_k\,dV \\ & R^2_1,j = H\,K_x\int_v\Phi_{i,j}\,\Phi_{J,x}dV \\ & R^2_1,j = H\,K_y\int_v\Phi_{1,y}\,\Phi_{j,y}\,dV \\ & \pi_1 \quad = \bar{H}\,K_x\int_s\Phi_i\,\Phi_{J,x}\,dS\bar{C}jnx + \bar{H}\,K_y\int_s\Phi_1\,\Phi_{J,y}\,dS\bar{C}jny \end{aligned} \tag{51}$$

where $\dot{}$ denotes time derivative.

III-4-2-4 Numerical integration in time

Equation (51) can be rewritten as follows:

$$M\dot{\bar{C}} + K\bar{C} = F \tag{52}$$

The scheme employed is Crank-Nicolson scheme, and using this scheme, the following expression is obtained.

$$M\frac{\bar{C}(t+\Delta t)-\bar{C}(t)}{\Delta t} + \frac{1}{2}K\left\{\bar{C}(t)+\bar{C}(t+\Delta t)\right\} = F(t) \tag{53}$$

where Δt is a short time increment.

Application of equation (53), $\bar{C}(t+\Delta t)$ is obtained.

$$\bar{C}(t+\Delta t) = \left\{\frac{1}{\Delta t}M + \frac{1}{2}K\right\}^{-1}\left\{\frac{1}{\Delta t}M - \frac{1}{2}K\right\}\bar{C}(t) + F(t) \tag{54}$$

III-4-3 Termal Diffusion

III-4-3-1 Basic equation

Basic equation for thermal diffusion is expressed as follows:

$$\frac{\partial (UT)}{\partial x} + \frac{\partial (VT)}{\partial y} = \frac{\partial}{\partial x}\left(k_x \frac{\partial T}{\partial x} \right) + \frac{\partial}{\partial y}\left(k_y \frac{\partial T}{\partial y} \right) + \frac{Qo}{\rho Hw C} \qquad (55)$$

where

T : temperature
Q : heat gain or loss for the surface layer of sea basin
Hw : thickness of warm water content
C : specific heat of water
ρ : density of water

The net-exchange rate Q_0 across the sea surface is represented by linear combination.

$$Q_o = Q_s - Q_b + Q_h + Q_c \qquad (56)$$
$$= a + bw$$

where

Qs : absorption of radiation from the sun and the sky
Qb : back radiation from the sea surface
Qh : convention of sensible heat to atmosphere
Qe : condensatin of vapor
a,b : coefficient
W : wind speed

Finite element procedure can be obtained in the same manner with dispersion formuation.

CHAPTER 5 MODEL SETUP AND BOUNDARY SPECIFICATION

III-5-1 Run Case Setup

The run cases are summarized in Table III-5-1 to predict the following factor.

a) The influence on the current and the water quality produced by the topographical change.

b) The influence on the current and the water quality produced by the change of inflow rate and pollutant flux.

In these run cases, two time phases are assumed, one the 1981 as the present stage and the other the 1990 as the future stage.

For Seraya area, in the future stage additional constant current is assumed, such as the direction is contrary to the observed one and the magnitude of velocity is assumed to be same with the observed velocity. Consequently, the additional current direction is from the west to the east which is called the eastward current in this report (the observed constant current is called the westward). Such an additional run case makes it possible to estimate the difference of the water quality produced by the change of current direction.

For Tekong area, in the future stage two run cases are predicted, one is the case when only the coal firing power station is constructed and the other is the case when both the coal firing power station and the integrated steel mill are constructed.

Table III-5-1 Run Case

Analytical item		Present stage (1981)		Future stage (1990)	
		Seraya area	Tekong area	Seraya area	Tekong area
Tidal current		o	o	o	o
Constant current	A	o	o	o	o
	B	-		o	
COD dispersion	A	o	o	o	◎
	B	-		o	
Thermal dispersion	A	o	o	o	o
	B	-		o	

In Seraya area A indicates the current to the west and B indicates the current to the east.
In Tekong area the mark ◎ indicates the two cases, one is only the coal firing power station and the other is both the coal firing power station and the integrated steel mill.

III-5-2 Finite Element Idealization

The analytical areas assumed in Seraya area and Tekong area are illustrated in Fig. III-5-1.

In Seraya area, the analytical area is assumed as 24km wide from the east to the west and 14km long from the south to the north, locating the Seraya island in the center of the analytical area. The boundary line from the south to the north is not parallel to the longitudinal line, so as to make it easy to establish the boundary condition corresponding with the observed constant current which flows along the coastal line.

In Tekong area, the analytical area is assumed as 13km wide from the east to the west and 18km long from the south to the north, locating the Tekong island in the centre of analytical area. For Johore channel, within 1km west area from Ubin island is included in the analytical area.

The both analytical areas are divided into the triangular finite element mesh. According to the analytical formulation used in this report, at every corner point of the triangular, the velocity, the tidal level and the pollutant concentration are defined. The corner point of the triangular element is named as the nodal point, and in finite element idealization, increasing the nodal point (the finite element), the accuracy becomes higher. There is a proportional relation between the number of the used elements and the computing time, accordingly, the finite element idealization is restricted by the computer capacity. As the finite element method allows to use the irregular element, the coastal areas around Seraya island and Tekong island are idealized by small element and around the open boundaries more large-sized elements are used.

The topographical changes between 1981 and 1990 are as follows:

Seraya area —— Sakra island and Bakau island will be connected each other by the reclamation.

Tekong area —— The Fisherman Bank area located in the south of Tekong island will be reclaimed.

These topographical changes are idealized in the finite element mesh. The finite element mesh and the depth distribution of Seraya area and Tekong area are illustrated in Figs. III-5-2, III-5-5 and Figs. III-5-6, III-5-9 respectively. Table III-5-2 shows the preface of finite element idealization on each area.

Adding 2m to Indian Spring Low Water depth which derived from the sea chart, the water depth of each nodal point is defined. 2m is referred from the amplitudes of principal components.

Tabel III-5-2 Preface of finite element idealization

Area	Stage	Nodes	Elements	Maximum length of element side (m)	Minimum length of element side (m)
Seraya area	1981	1355	2387	1414.0	94.3
	1990	1341	2358	1414.0	94.3
Tekong area	1981	1033	1749	753.0	150.0
	1990	1001	1678	753.0	150.0

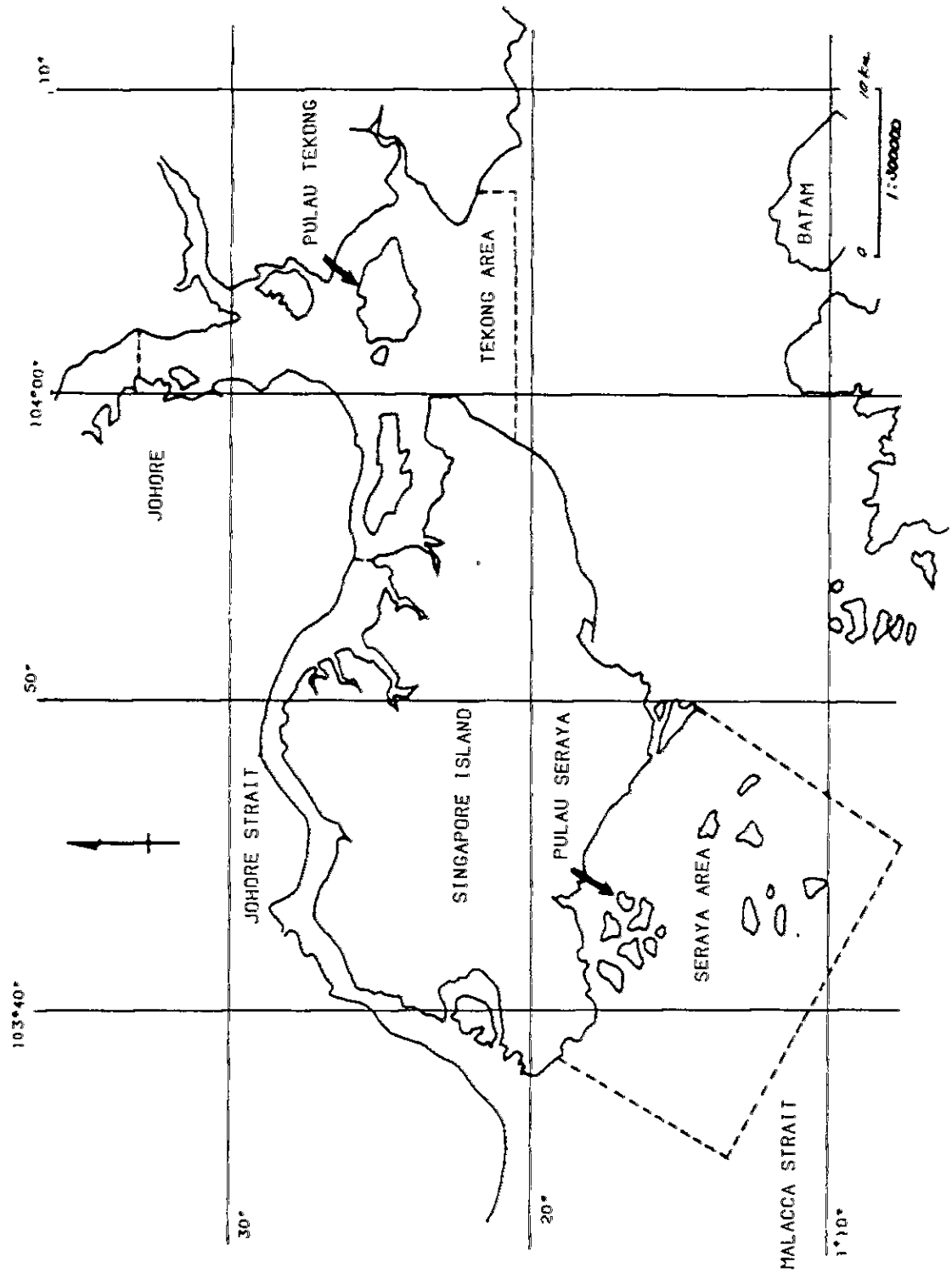

Fig. III-5-1 Analytical area

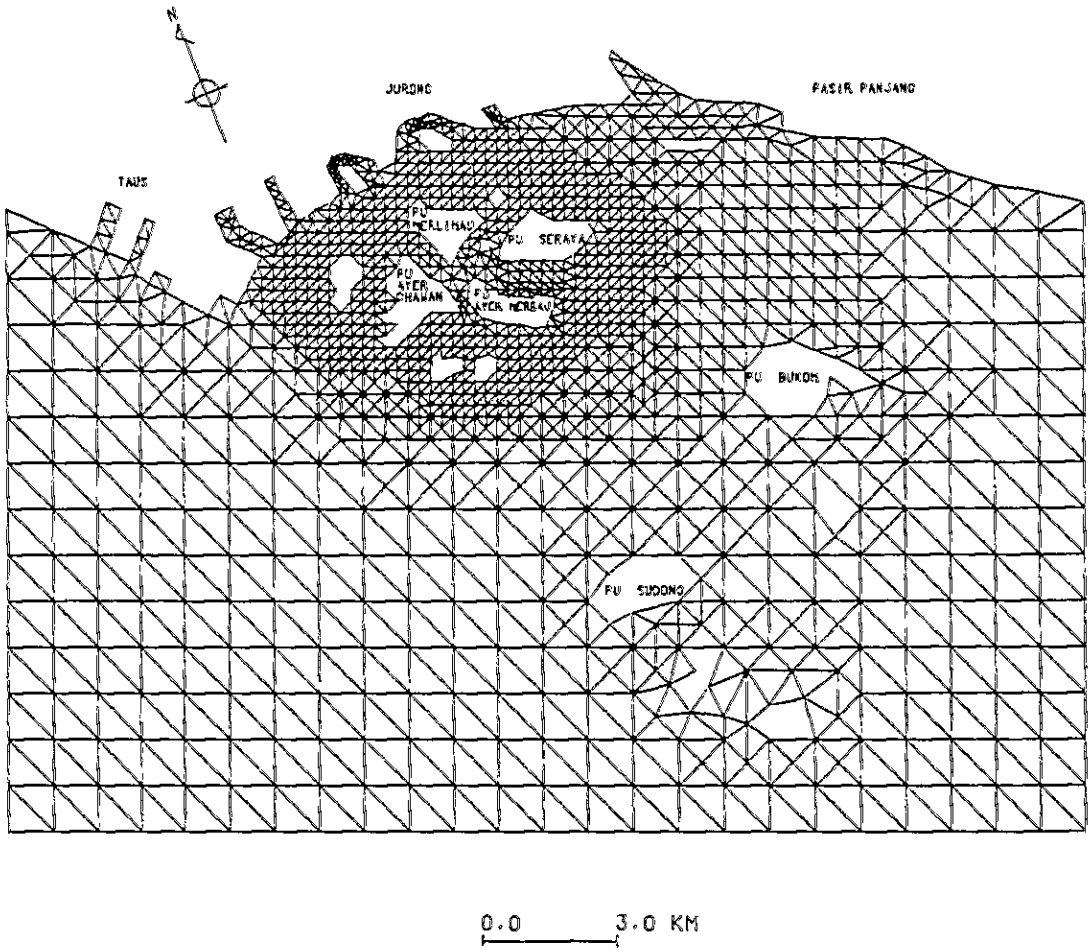

Fig. III-5-2 Finite element mesh in present stage for Seraya Area

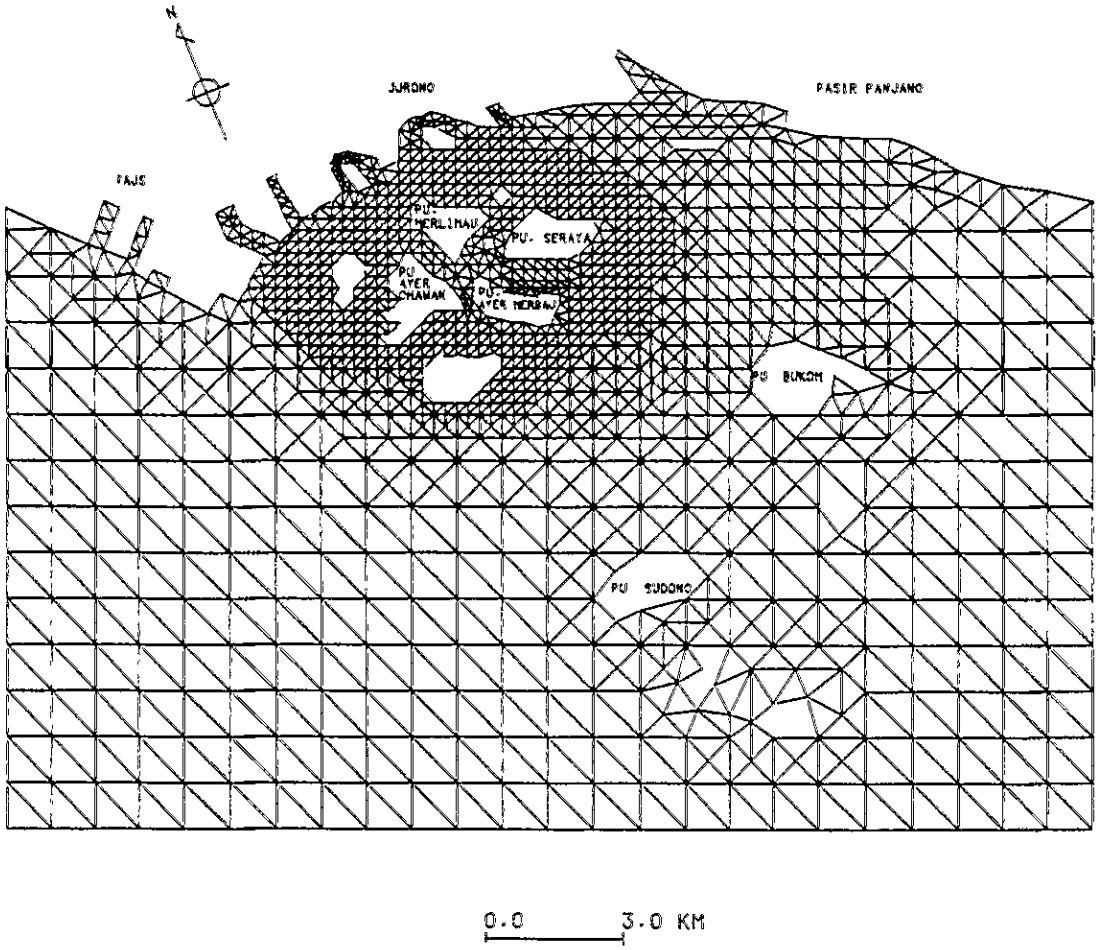

Fig. III-5-3 Finite element mesh in future stage for Seraya Area

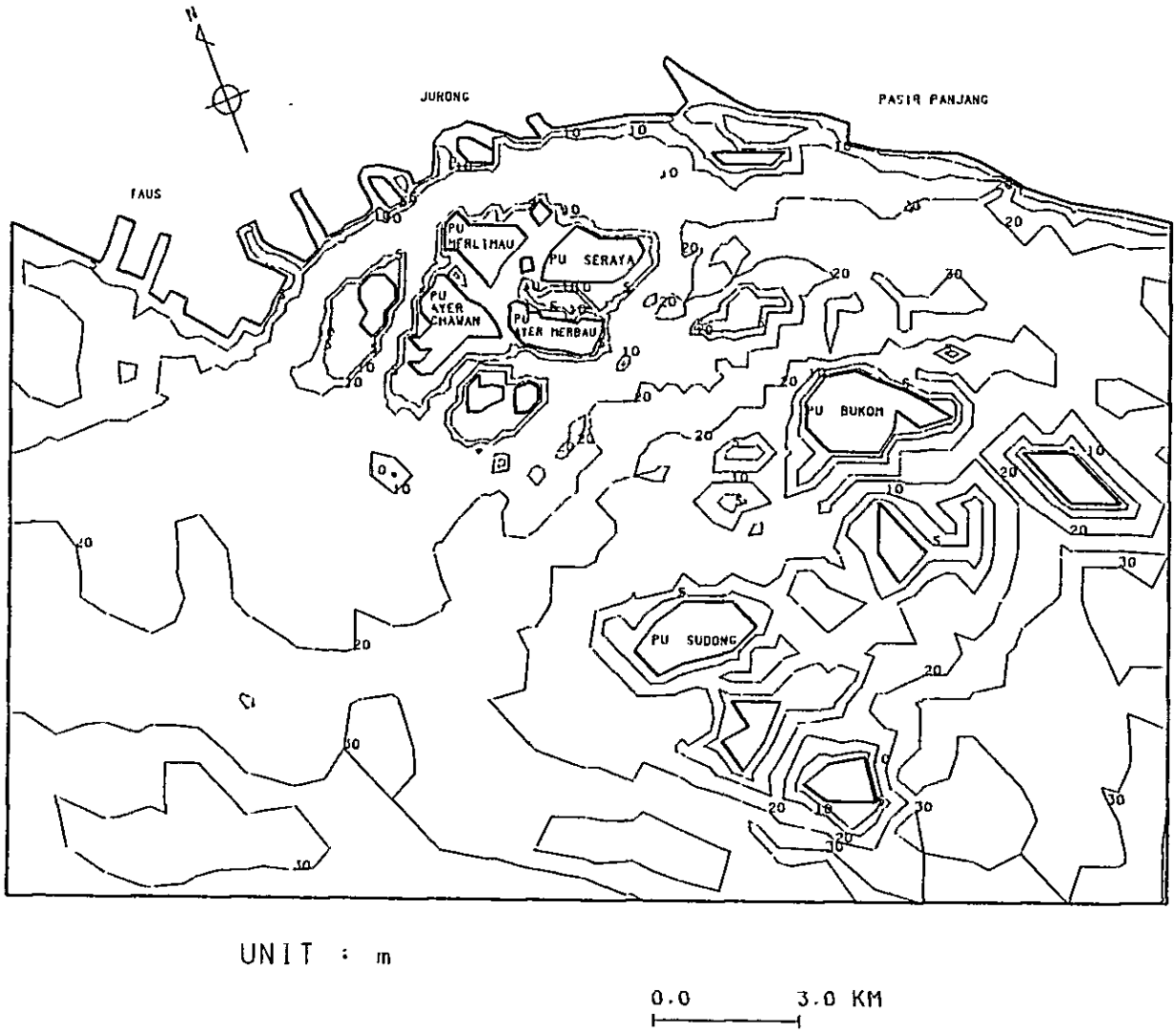

Fig. III-5-4 Depth distribution in present stage for Seraya Area

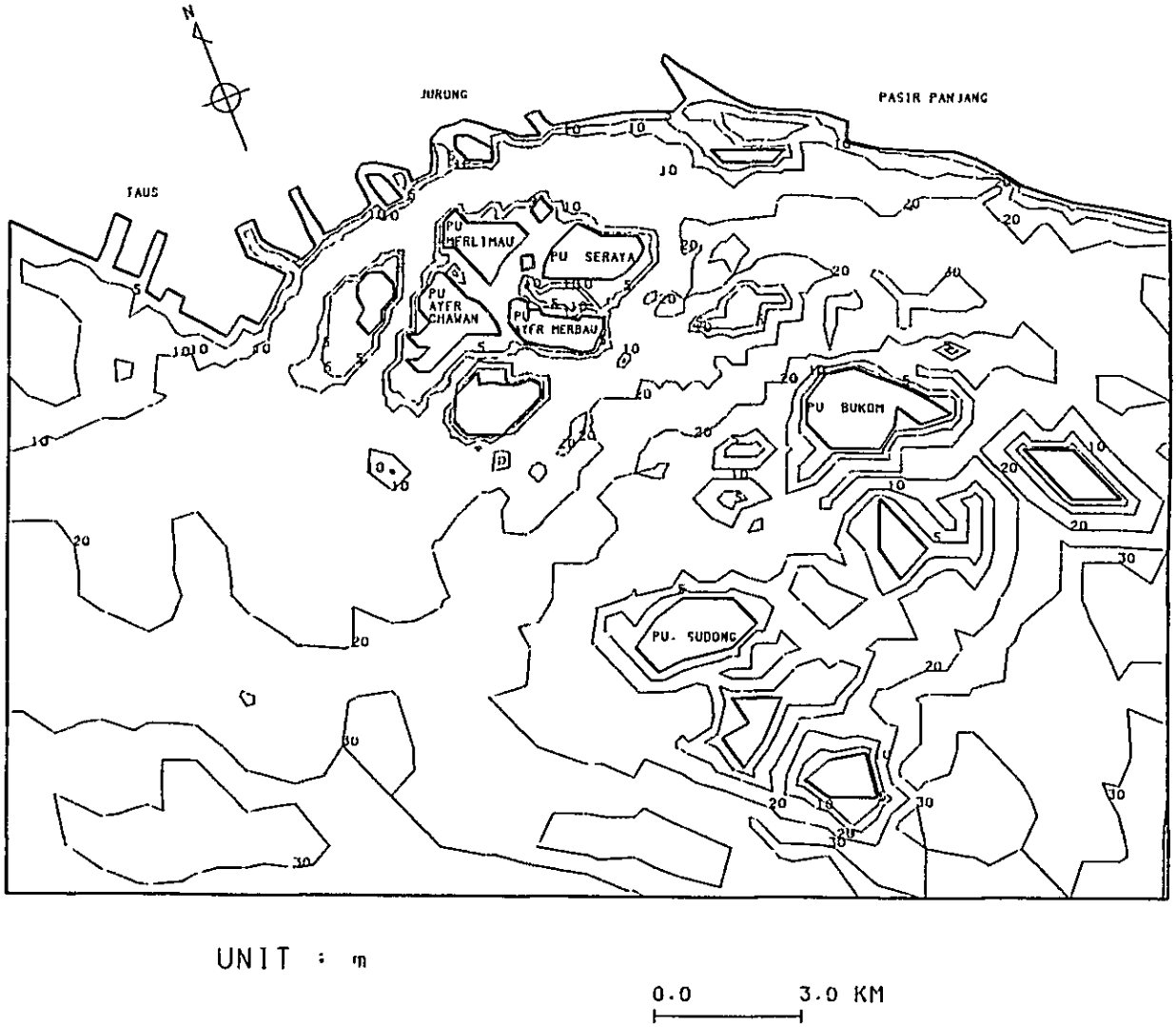

Fig. III-5-5 Depth distribution in future stage for Seraya Area

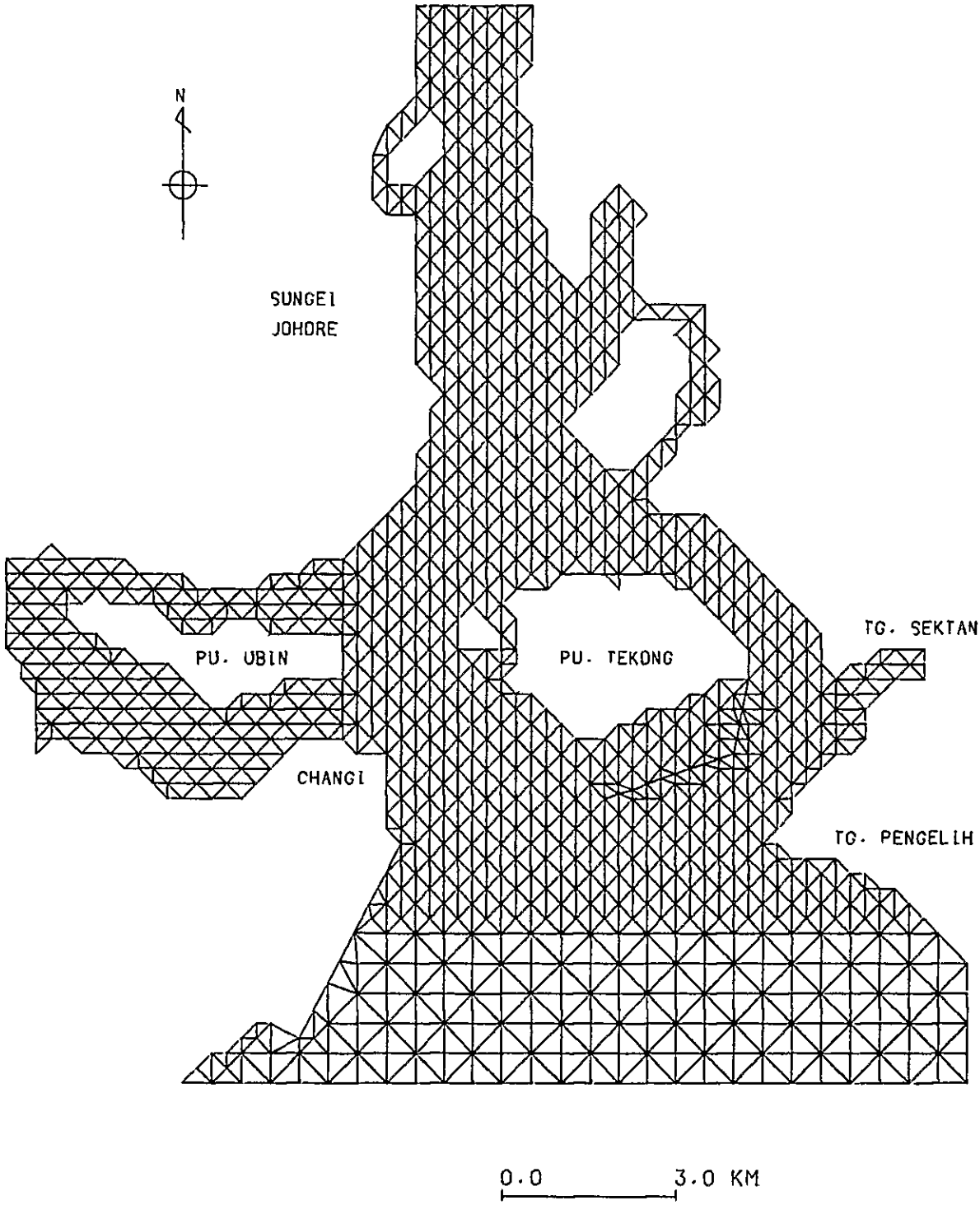

Fig. III-5-6 Finite element mesh in present stage for Tekong Area

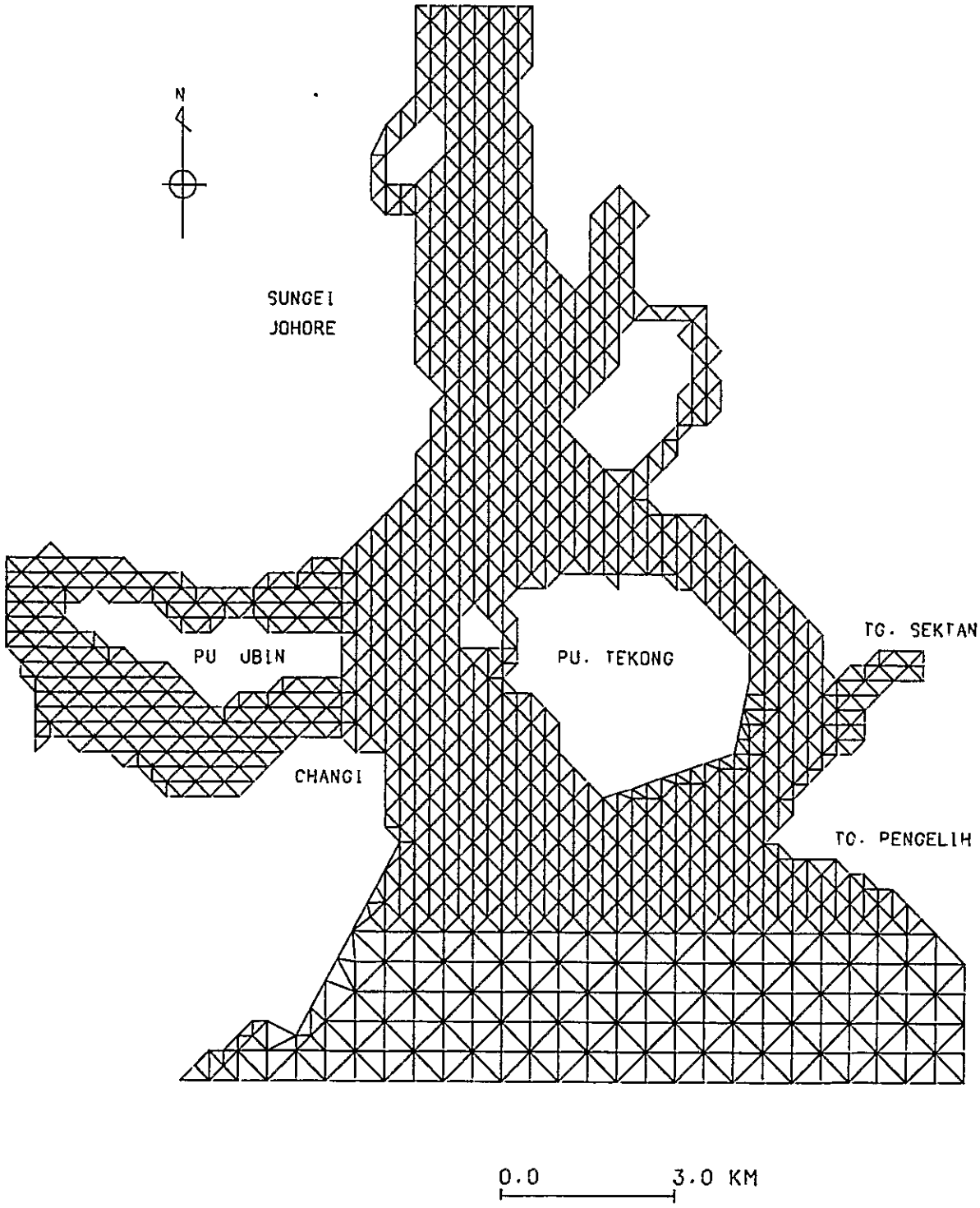

Fig. III-5-7 Finite element mesh in future stage for Tekong Area

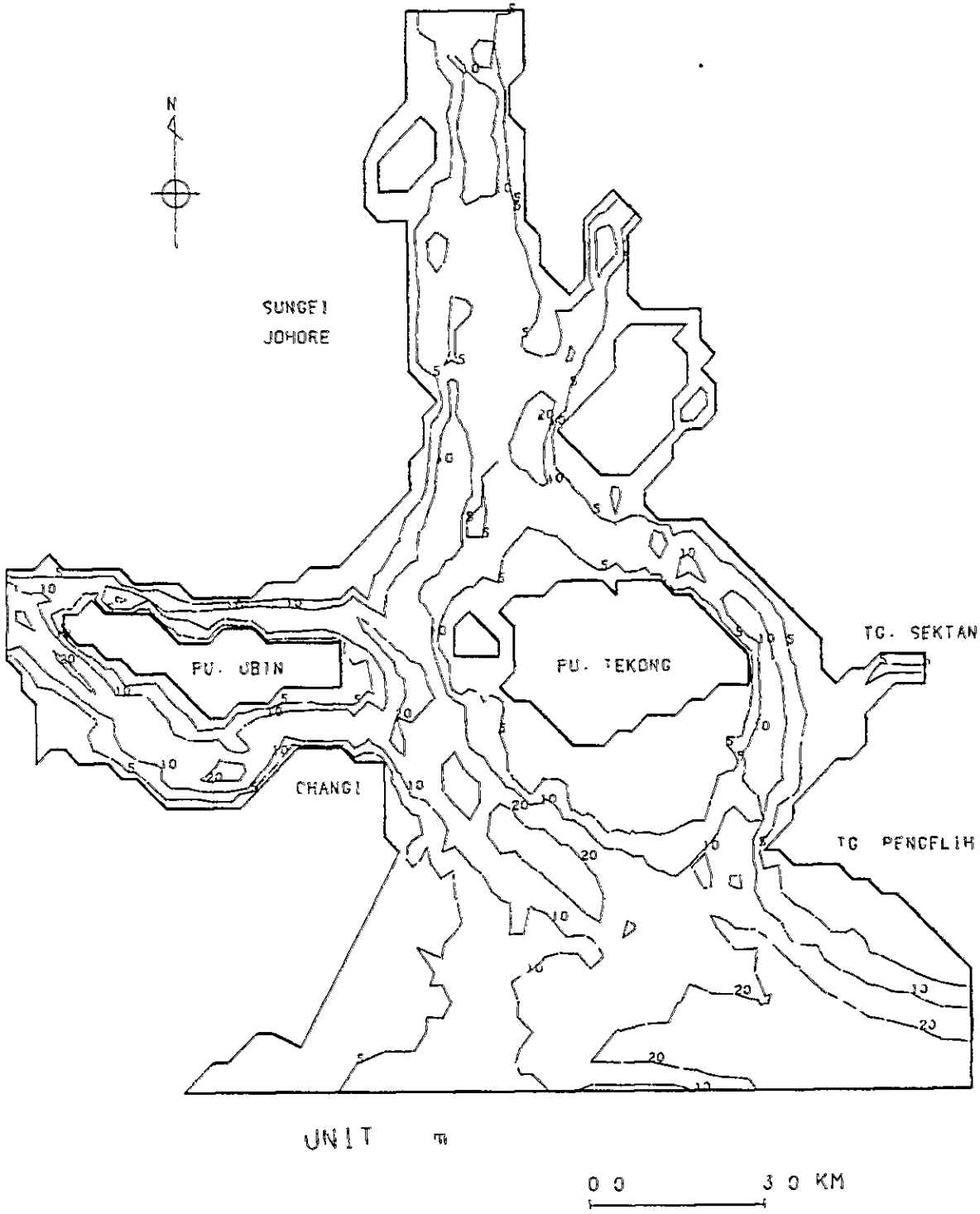

Fig. III-5-8 Depth distribution in present stage for Tekong Area

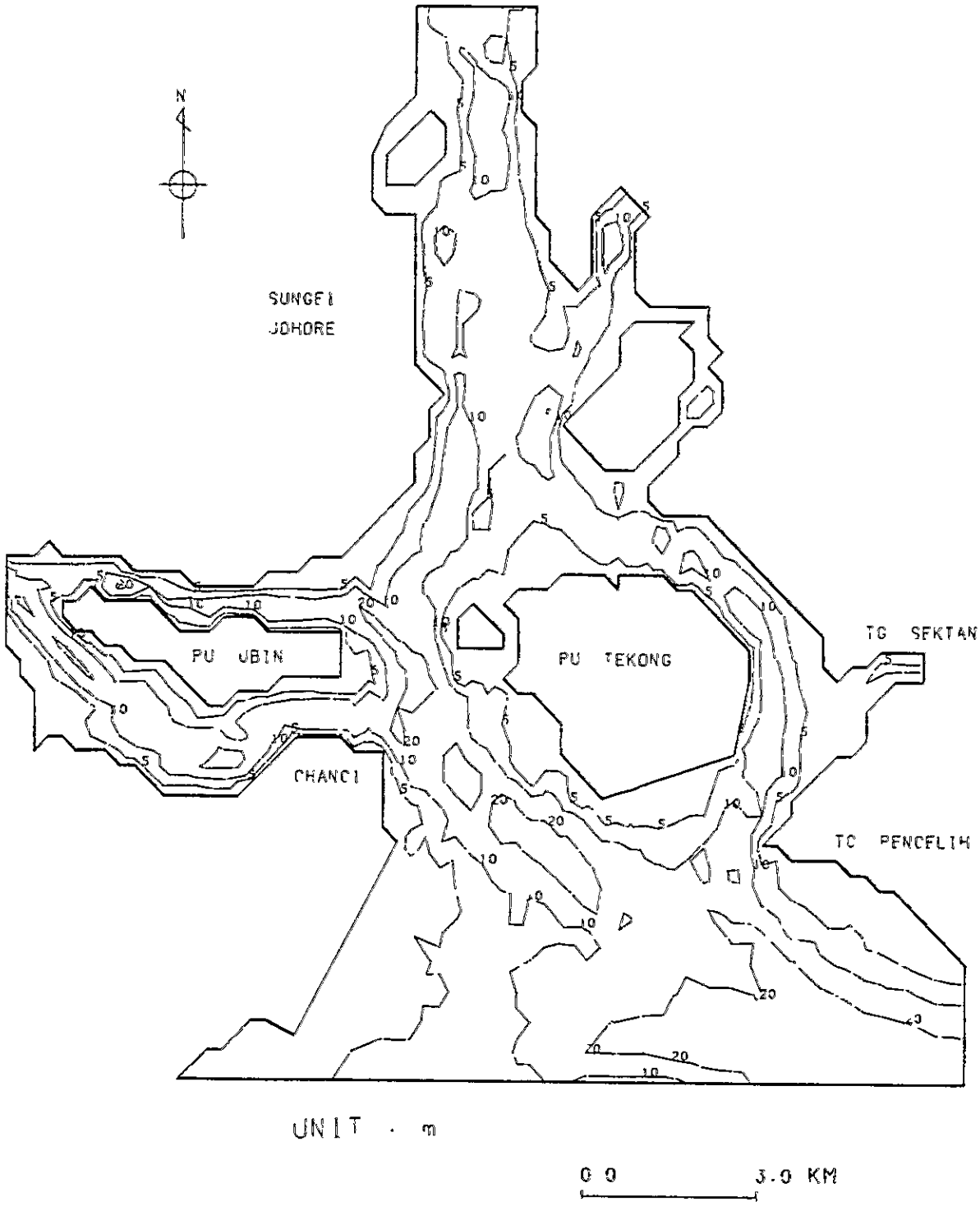

Fig. III-5-9 Depth distribution in future stage for Tekong Area

III-5-3 Boundary Condition

The boundary conditions and the physical constants are summarized in Table III-5-3. About the important conditions, the establishing grounds are specified as follows:

a) The boundary conditions for tidal current

In the both area, on the boundary lines except the coastal lines, the tidal levels and phases are given, and then the tidal currents produced by the surface level change are computed.

In Seraya area, the tidal amplitudes and phases for the boundary conditions are shown in Table III-5-4. These conditions are assumed based on the observed data of K_1 component at Victoria Dock and Jurong Wharf.

In Tekong area, based on the observed data of M_2 component at Slave One, the tidal amplitudes and phases are assumed as shown in Table III-5-5.

After the several trial runs, these conditions are justified as the best agreements are obtained among those trial runs.

In Seraya area, it is assumed that the velocity normal to the southern open boundary line is equal to zero in order to adjust the balance of current around Seraya island. The assumed boundary conditions as the tidal amplitude and phase are slightly larger than observed data and the velocity assumption on the southern boundary line in Seraya area is different from the existing physical process. Such treatments are often made in the numerical simulation and the hydraulic model experiment in order to obtain the best results within the limited analytical area.

b) The boundary conditions for the constant current

Before the explanation of the boundary condition, the computational process on the constant current is described.

The constant current is produced by the ocean current, the river inflow, the wind drift current and the tidal residual current, and its time scale is longer than the tidal periods. In the current predictional model, such long time scale currents are incorporated as the constant current.

The computational results of tidal current show not only the oscillating velocity distributions but also the constant current obtained by averaging the velocities for one tidal period. This constant current is named as the tidal residual current.

Once the velocity comes into existence by the topographic effect, the nonlineality of current cascades up the velocity and the residual current is produced in this process.

The constant current for the current prediction model consists of the residual current and the steady state current produced by any other physical processes.

In the numerical simulation, the constant current is obtained by superposing the residual current with the computed result as the steady state current.

The computation on the steady state current is carried out separately from the tidal current computation, and it is assumed that any other physical processes except the residual current are included in that numerical result.

Accordingly, the boundary condition on the computation of steady state current must be obtained after the computation of tidal current.

As the boundary condition of the steady state current, the velocity distribution is assumed at the each nodal point on the open boundary. The river inflow rate and the rates of intake and outlet produced by industries are defined at the appropriate nodal points.

In Seraya area, the velocity distribution on the open boundary is shown in Fig. III-5-10 to compute the steady state westward current. Integrating the velocity, the total inflow rate amounts to about 30,000 m^3/sec. On the run case of the steady state eastward current established in the future stage, the boundary velocities are illustrated in Fig. III-5-11 and the total inflow rate is equal to the former case.

It is assumed that the velocity normal to the southern open boundary line is equal to zero from the same view point with the computation of tidal current.

In Tekong area, the velocity distribution on the open boundary is shown in Fig. III-5-12. Integrating the velocity, the total inflow rate amounts to about 8,000 m^3/sec.

As the inflow rate at Johore river is unknown, it is evaluated as follows. The flow pattern obtained from the residual current presents the inflow motion at the mouth of Johore river. It can be assumed that when the numerical results show good agreement with the observed constant current, the inflow rate from the Johore river is justified.

In this manner, the numerical result indicates the current produced by superposing the residual current with the steady state current.

Henceforce, the concept on the constant current is defined as the current produced by composing the residual current obtained from the tidal current computation and the current obtained from the steady state current computation.

c) Bottom frictional coefficient

In the numerical formulation, the bottom shear stresses are usually given by quadratic formula as following relationship:

$$F = K \cdot \rho |u| \cdot u$$

where F is the bottom shear stress k the bottom frictinal coefficient, ρ the density of water and u the averaged current velocity.

The attempt to evaluate the bottom frictional coefficient had been done by Unoki (1963) and Hino (1964).

Unoki has estimated the bottom frictional coefficient in Tokyo bay as $k = 2.6 \times 10^{-3}$. This value is often applied in numerical simulation as the standard of the bottom frictional coefficient at the coastal sea bottom.

d) Diffusion coefficient

The way to evaluate the diffusion coefficient exactly have not been established yet and in this time the feasible method to estimate the diffusion coefficient in coastal sea are as follows:

1 estimation by tracer such as salinity distribution
2 estimation by observed velocity fluctuations

From the observation at 1981, the both type data are available.

According to the observed salinity distributions, the vertical and horizontal differences indicate only 1 or 2 % in each area, and it shows the homogeneous water quality. The slight salinity difference means that the fresh water inflow rate is small or the large diffusive power produces the rapid mixing process. So it is difficult to estimate the diffusion coefficient by observed salinity distribution. According to the observed velocity fluctuations, the diffusion coefficient is estimated by G. I. Taylor's theorem as follows:

$$Kx = \overline{U_v'^2} \int_0^\infty R_{LU}(t)\,dt$$

$$Ky = \overline{V_v^2} \int_0^\infty R_{LV}(t)\,dt$$

where R_{LU} and R_{LV} are Lagrangian auto-correlation coefficient for x and y direction respectively, $\overline{U_v'^2}$, $\overline{V_v^2}$ are the squareded mean Lagrangian velocity fluctuations.

Since the current meter is fixed in the sea, the observed data is Eulerian velocity. Generally, the current observation in Lagrangian system is difficult and the correlation between Eulerian system and Lagrangian system is not cleared.

But assuming the similarity of the auto-correlation coefficient between the Eulerian system and Lagrangian system in microscale turbulence, the following transformation equation can be obtained (Hay Pasquill, 1959);

$$R_L(\eta) = R_E(t) \qquad \eta = \beta_t$$

where β indicates the non-dimensional parameter depend on the turbulence-scale.

The value of has the wide range from 1.0 to 8.5 and its average is 4.0 by Hay et al's observation. β is scattered in the wide range like their observation.

But sometimes we assume that the Eulerian correlation to be equal to the Lagrangian correlation. Accordingly β is assumed to be equal to 1.0, then the diffusion coefficient can be estimated.

Table III-5-6 shows the diffusion coefficient in both areas estimating from the current observation result in 1981. For reference, the estimation from the observation in 1979 is also shown.

On this table, the order of diffusion coefficient shows to be about 10^6 in both areas.

The predominant components are from east to west in Seraya area and from south to north in Tekong area, respectively but the differences compared with another component are not so large in both areas.

Referencing these data, the diffusion coefficients assumed in the dispersion computation are shown in Table III-5-6.

Table III-5-6 Diffusion coefficient estimated by observed velocity fluctuations
(unit : cm^2/sec)

SERAYA area						TEKONG area			
Year	1979			1981			1981		
Point	Direction component	Diffusion *1 coefficient	Point	Direction component	Diffusion *1 coefficient	Point	Direction component	Diffusion *2 coefficient
ST.1	N–S	4.54×10^5	SC 1	N–S	5.19×10^6	TC.1	N–S	5.59×10^6
	E–W	1.39×10^6		E–W	3.32×10^6		E–W	2.59×10^5
ST 2	N–S	7.88×10^5	SC.2	N–S	3.10×10^4	TC.2	N–S	3.83×10^6
	E–W	1.89×10^6		E–W	2.29×10^6		E–W	2.03×10^6
ST 3	N–S	5.84×10^5	SC.3	N–S	3.82×10^5	TC.3	N–S	9.71×10^6
	E–W	4.21×10^6		E–W	4.32×10^6		E–W	5.23×10^6
ST 4	N–S	1.15×10^6	SC.4	N–S	8.84×10^5	TC 4	N–S	7.59×10^6
	E–W	3.91×10^5		E–W	4.99×10^6		E–W	1.32×10^6
ST.5	N–S	1.19×10^6	SC.5	N–S	3.26×10^5	–	N–S	–
	E–W	5.53×10^6		E–W	1.97×10^6		E–W	–
–	N–S	–	SC.6	N–S	1.08×10^7	–	N–S	–
	E–W	–		E–W	9.39×10^6		E–W	–
Mean	N–S	8.33×10^5	Mean	N–S	2.94×10^6	Mean	N–S	6.68×10^6
	E–W	1.85×10^6		E–W	4.38×10^6		E–W	9.15×10^5

*1 Omit the period more than 24 hours in SERAYA area.
*2 Omit the period more than 12 hours in TEKONG area

e) Concentration on open boundary (COD)

The concentration on the open boundary is assumed as the background concentration of the analytical area.

In order to assume the concentration on open boundary, the water quality observation is carried out.

The concentration on open boundary is estimated with reference to the current condition of the time when the water quality had observed and the observed concentration distribution.

In Seraya area, on the west boundary line the concentration is assumed as 0.1 ppm which is equal to the lowest value in the observed data. Those stations are located in the west from the Seraya island, and on the east boundary line the concentration distribution is assumed from 0.1 ppm to 1.0 ppm.

In Tekong area, from the observed data the concentration is lower in the south of Tekong island and higher in the north of Tekong island. Consequently, on the southern open boundary line, the concentration is assumed as 0.75 ppm and the northern open boundary line where corresponds to the Johore river mouth, is assumed as 2.75 ppm.

After the many trial runs, these boundary values are assumed since the best agreements are obtained among those trial runs.

Table III-5-3 Boundary conditions and physical constants

Item	SERAYA area	TEKONG area	
	Preface	Preface	Remarks
TIDAL CURRENT			
· Tidal current	· Amplitude and phase lag (Table 3-5-4)	· Amplitude and phase lag (Table 3-5-5)	
· Constant current	· Velocity (Fig. 3-5-10, Fig 3-5-11)	· Velocity (Fig 3-5-12)	
· Shore line	· Un = 0 Unnormal direction velocity to shore line	· Un = 0	
· Inflow rates	· Table 3-5-7, Fig 3-5-13	· Table 3-5-8, Fig 3-5-13	
· Coriob's parameter	· $\phi = 1\,1°$, $f = 2\omega \sin\phi$ $\omega = 0\,729 \times 10^{-4}$ rod/sec, ϕ· Latitude	· $\phi = 1.25°$	
· Coefficient of eddy viscocity	· 10^6 cm²/sec	· 10^6 cm²/sec	
· Bottom frictional coefficient	· $2\,6 \times 10^{-2}$, 0 0	· $2\,6 \times 10^{-2}$	
· Time interval	· 12 sec	· 15 sec	
COD DISPERSION			
· Lods	· Table 3-5-7, Fig. 3-5-13	· Table 3-5-8, Fig 3-5-13	
· Diffusion coefficient	· 3×10^6 cm²/sec	· 1×10^6 cm²/sec	
· Open boundary concentration	· 0.1 ~ 1 0 ppm	· 0.75 ~ 2.75 ppm	
THERMAL DISPERSION			
· Temperature difference	· Table 3-5-7, Fig 3-5-13	· Table 3-5-8, Fig. 3-5-13	
· Mean air temperature · Mean wind velocity · Mean water temperature	· 26 6°C · 2 04 m/sec Table 3-5-9 · 28.4°C	· 26.5°C · 2 20 m/sec Table 3-5-9 · 28.4°C	Mean of the observation data
· Thickness of warm water content	· Equale to water depth	· Equale to water depth	
· Diffusion coefficient	· 3×10^6 cm²/sec	· 1×10^6 cm²/sec	

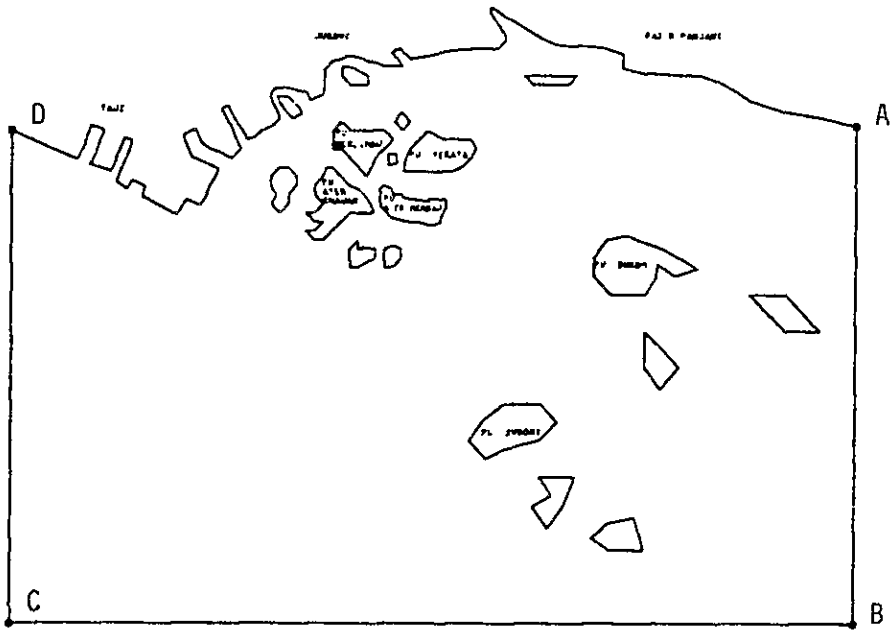

Table III-5-4 Tidal amplitudes and phases for boundary condition in Seraya Area

Point	Amplitudes (cm)	Phase (^{o})	Remarks
A	29.0	180	
B	29.0	165	
C	29.0	265	
D	29.0	280	

interpolated among each point

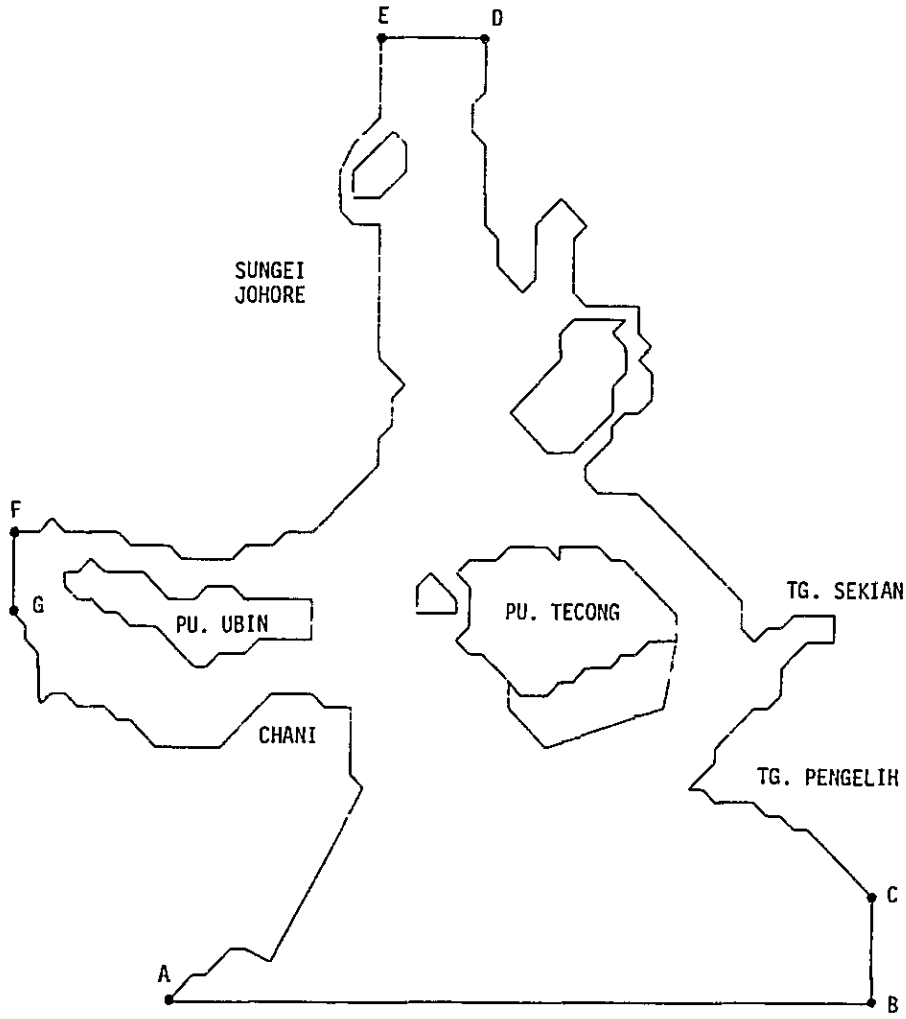

Table III-5-5 Tidal amplitudes and phases for boundary condition in Tekong Area

Point	Amplitudes (cm)	Phase (°)	Remarks
A	75.0	0.0	
B	75.0	0.0	
C	75.0	0.0	
D	80.0	50.0	
E	80.0	50.0	
F	80.0	75.0	
G	80.0	75.0	

interpolated among each point

Fig. III-5-10 Velocity distribution on the open boundary (westward current)

Fig. III-5-11 Velocity distirbution on the open boundary (eastward current)

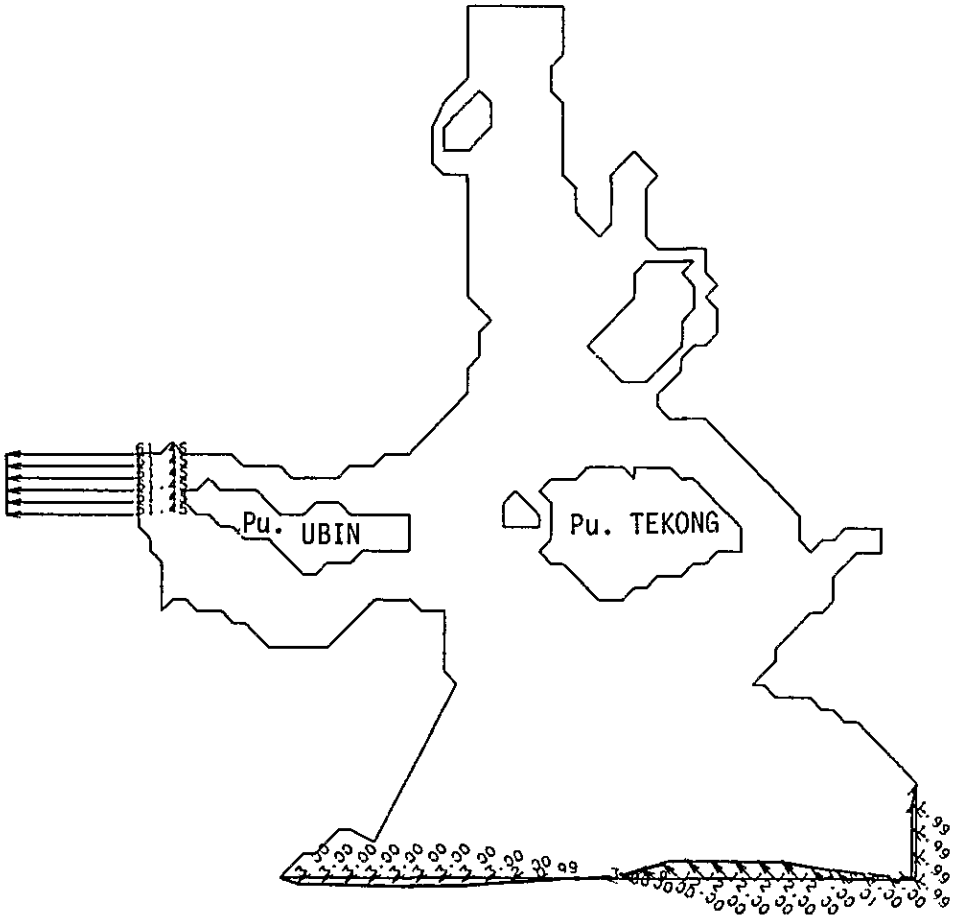

Fig. III-5-12 Velocity distribution on the open boundary in Tekong Area

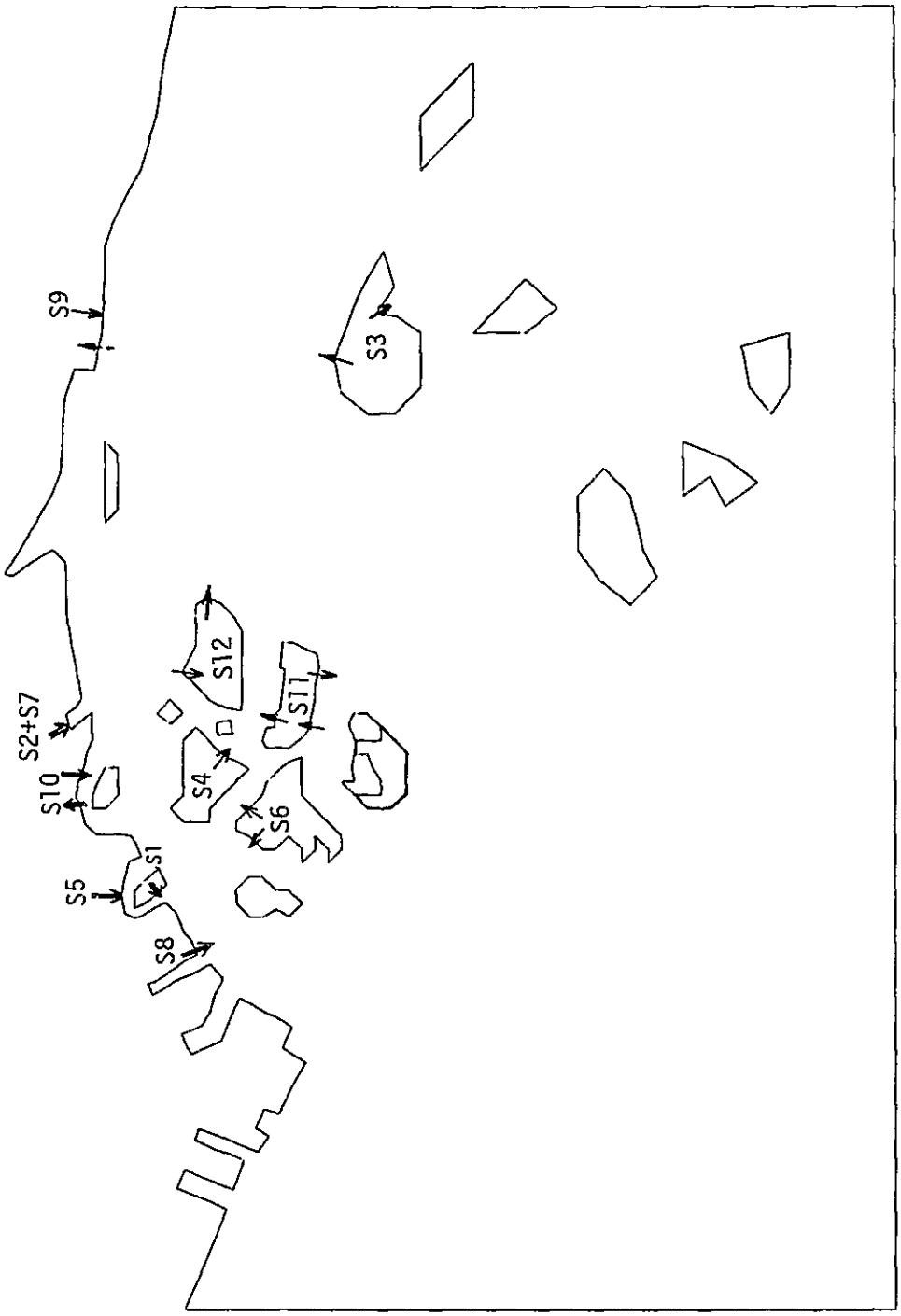

Fig. III-5-13 Location of inflow and outlet points

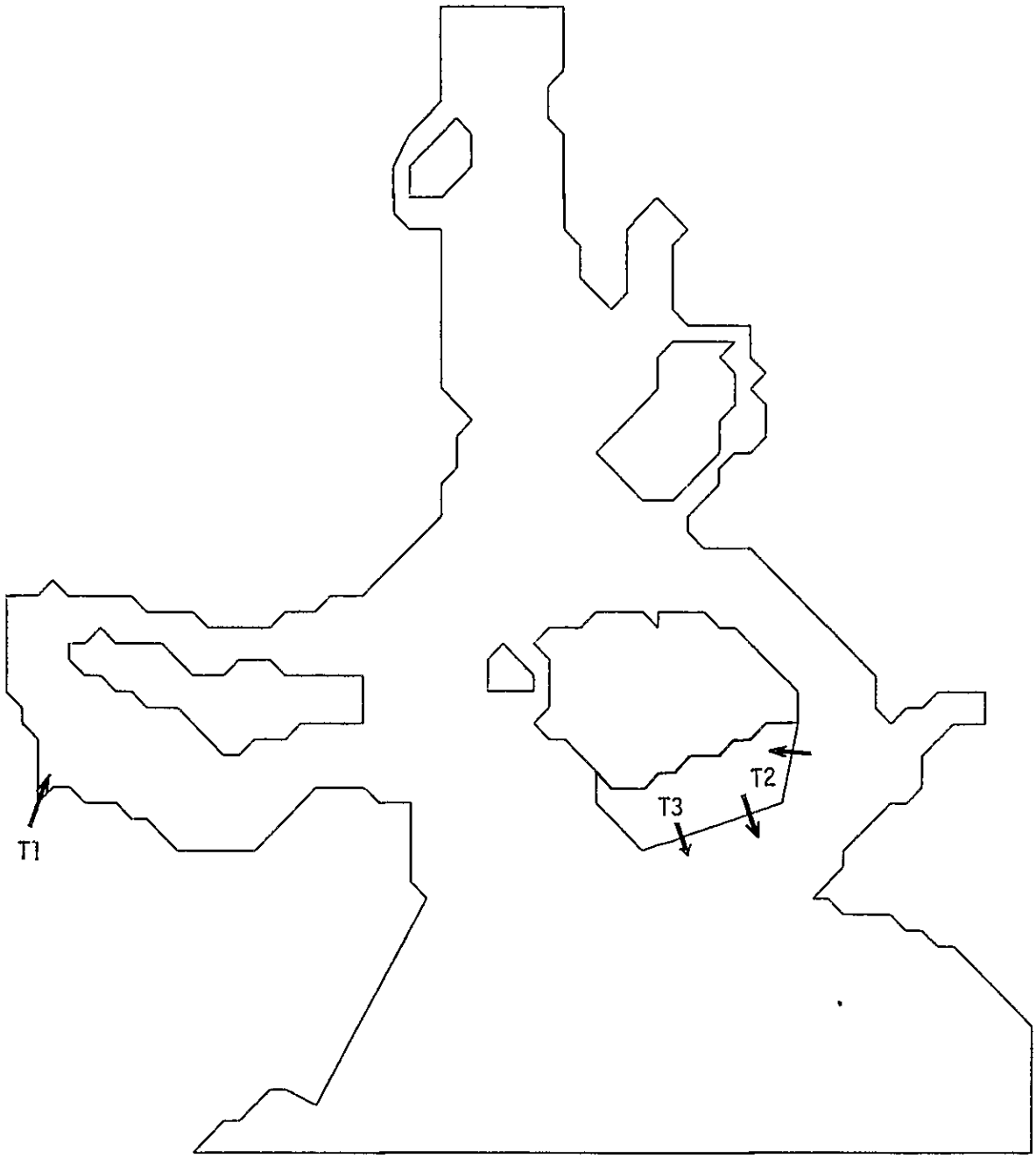

Fig. III-5-14 Location of inflow and outlet points

Table III-5-7 Data on emission source in Seraya Area

Point	Name	1981 Temp.* (°C)	1981 Inflow rates (m^3/day)	1981 COD loads (kg/day)	1990 Temp.* (°C)	1990 Inflow rates (m^3/day)	1990 COD loads (kg/day)	Remarks
S 1	Jurong Shipyard Ltd.	1.5	12,050	16.10	1.5	18,457	24.66	
S 2	Sugar Industry of Singapore Ltd.	5.0	43,230	273.37	5.0	107,689	680.98	
S 3	Shell Eastern pte. Ltd.	10.0	672,455	2,243.64 7,843.64	10.0	1,040,293	3,482.19 12,145.44	Maximum value is adopted.
S 4	Singapore Refining Co. pte. Ltd.	15.0	175,080	17,038.20	15.0	270,850	26,358.24	
S 5	Mobil Oil Singapore pte. Ltd.	-	3,700	129.50	-	5,724	200.34	
S 6	Esso Singapore pte. Ltd.	2.0	359,250	-	2.0	555,763	-	
S 7	Ulu Pandan Singapore Treatment	-	136,000	3,626.67	-	272,000	7,253.33	
S 8	Jurong Swage Treatment	-	-	-	---	240,000	6,400.00	
S 9	Pasir Panjang Power Station	5.6	1,441,440	-	5.6	1,441,440	-	
S10	Jurong Stage Power Station	5.6	2,882,880	-	5.6	2,882,880	-	
S11	Petrochemical Corp. of Singapore	-	-	-	14.0	1,443,120	104.00	
S12	P. Seraya Power Station	-	-	-	8.3	2,641,500	75.00	
	Total	-	5,726,085	23,327.48 28,927.48	-	10,917,716	44,578.74 53,241.99	

* Temp. : Temperature difference across condensers

Table III-5-8 Data on emission source in Tekong Area

Point	Name	1981 Temp.* (°C)	1981 Inflow rates (m^3/day)	1981 COD loads (kg/day)	1990 Temp.* (°C)	1990 Inflow rates (m^3/day)	1990 COD loads (kg/day)	Remarks
T1	Kim Chuam Sewage Treatment	-	218,000	4,360.00	-	255,000	6,800.00	
T2	P. Tekong Power Station	-	-	-	8.3	2,401,500	75.00	
T3	Integrated Steel Mill	-	-	-	-	9,300	65.10	
	Total	-	218,000	4,360.00	-	2,665,800	6,940.10	

* Temp. : Temperature difference across condensers

Table III-5-9 Air temperature and wind velocity (mean)

Point	Item		JAN.	FEB.	MAR.	APR.	MAY.	JUN.	JUL.	AUG.	SEP	OCT.	NOV.	DEC.	ANV.	Mean Value of March	Remarks
JTC *1 Jurong Flatted Factory Bldg.	Wind Velocity Appearance Frequency (%)	(kt) 0	6.0	12.6	12.2	17.9	20.0	15.3	12.8	15.5	18.9	22.9	19.6	12.3	15.6	4.08kt	Value of weighted average, obtained multiplying medium value of respective rank with appearance frequency
		1–3	19.7	20.8	33.3	42.0	36.6	30.0	21.1	22.4	29.7	33.2	34.1	22.6	29.2		
		4–6	44.9	41.9	39.2	28.8	27.1	31.3	32.7	28.9	29.3	26.0	32.6	38.7	33.3		
		7–10	25.1	22.9	13.6	10.5	15.0	21.3	30.5	29.2	19.9	15.7	12.2	23.2	19.7	2.04 m/sec	
		11–16	4.3	1.8	1.7	0.8	1.1	1.9	2.9	3.9	2.0	2.1	1.5	3.1	2.2		
		17–21	–	–	–	–	0.2	0.2	–	0.1	0.2	0.1	–	0.1	–		
		22–27	–	–	–	–	–	–	–	–	–	–	–	–	–		
*2 Changi Air Base	Mean Wind Velocity of Respective Directions (kt)	N	(53) 6.7	(51) 6.5	(27) 5.1	(14) 4.9	(5) 3.9	(5) 4.3	(6) 4.2	(1) 4.0	(1) 3.4	(9) 3.4	(27) 3.5	(48) 4.6	(21) 4.5	4.40kt	Value in bracket is appearance frequency Value of weighted average, obtained multiplying mean velocity of respective directions with appearance frequency
		NE	(13) 8.6	(35) 9.3	(28) 6.7	(13) 6.2	(7) 4.2	(4) 3.7	(4) 4.5	(1) 2.6	(2) 4.3	(5) 4.9	(17) 7.3	(43) 9.3	(14) 6.0		
		E	(1) 6.0	(1) 8.3	(5) 7.1	(10) 6.9	(6) 5.6	(4) 4.3	(6) 6.0	(1) 5.0	(1) 3.8	(2) 5.6	(4) 5.1	(1) 7.7	(3) 5.9		
		SE	(1) 7.0	(–) 7.5	(1) 6.5	(6) 7.0	(9) 6.1	(9) 6.7	(9) 7.5	(17) 8.1	(7) 7.1	(5) 6.5	(3) 6.2	(–) 6.3	(5) 6.9		
		S	(–) –	(1) 5.7	(1) 5.2	(6) 6.1	(15) 7.0	(20) 6.1	(27) 7.9	(35) 7.2	(27) 6.7	(16) 6.6	(3) 6.8	(1) 7.2	(13) 6.0		
		SW	(–) 6.0	(–) –	(–) 10.0	(5) 4.0	(8) 5.4	(11) 5.8	(9) 7.1	(14) 5.8	(23) 7.1	(12) 6.2	(2) 5.3	(1) 5.8	(7) 5.7		
		W	(3) 4.0	(–) –	(5) 3.8	(12) 3.6	(9) 3.6	(13) 5.4	(9) 4.9	(11) 5.5	(9) 5.1	(12) 5.2	(7) 5.2	(–) 4.3	(7) 4.2		
		NW	(23) 3.0	(10) 2.2	(16) 2.4	(13) 2.6	(13) 2.9	(8) 4.7	(10) 3.8	(3) 3.2	(11) 6.0	(14) 4.2	(13) 3.8	(3) 4.5	(12) 3.6		
		Calm	(6) –	(2) –	(17) –	(21) –	(28) –	(27) –	(20) –	(17) –	(29) –	(25) –	(19) –	(3) –	(18) –		
	Mean Temperature (°C)		26.2	27.1	27.4	27.7	28.0	27.9	27.4	28.0	27.4	27.3	26.2	26.3	27.2	27.4	24Hr Mean
Singapore total area	Mean Temperature (°C)		25.5	26.1	26.5	26.9	27.3	27.1	27.1	26.9	26.8	26.6	26.1	25.6	26.6	26.5	24Hr Mean

Note: *1 PERIOD 1978 — 1 year
*2 PERIOD 1975–1979 — 5 years
*3 PERIOD 1929–1941, 1948–1979 — 45 years

(METEOROLOGICAL SERVICE SINGAPORE)

CHAPTER 6 NUMERICAL RESULTS

III-6-1 Results in Seraya Area

III-6-1-1 Currents

--- The verification

After the computation of the present stage, the numerical result is compared with the current pattern which is established by observation, and the verification of simulation model is performed. The tidal current is computed for three tidal periods (72 hours) and the constant current is computed for 1000 time steps (3.3 hours) to obtain the sufficiently stable results.

The following verification is carried out.

As for the tidal current, the comparisons of current ellipse between observed one and computed one are performed at the observation stations. The comparison items are the length of major axis which correspond to the maximum velocity, the direction of major axis which correspond to the current direction of the maximum velocity, and the ellipse configuration which shows the current characteristic.

As for the constant current, the computed velocity vectors are compared with the observed constant current vector.

The Table III-6-1 shows the comparison of the current ellipse about the length and direction of major axis. In Figs. III-6-1 and III-6-2, the observed and the computed current ellipses are illustrated.

And in Table III-6-2, the constant current vectors are summarized. From these tables and figures, the numerical result is verified as follows:

1 Comparing the numerical result with observed data in 1981 about the current ellipse, the differences are shown approximately from -6 cm/sec to 3 cm/sec on the length of major axis.

Relatively large differences are shown at the st.1 as 3 cm/sec and the st. 3 as -6 cm/sec, and these stations are locating in the north and the south from Seraya island. But the ratios of maximum velocities between computed results and observed data are as follows; at st. scl as 0.8951, st. sc2 as 0.9925, st.sc3 as 1.1720, st. sc4 as 0.9815, st sc5 as 0.9490, st. sc6 as 1.0046 and the average is 0.9991. These ratios indicate the good agreement between the computed results and the observed data.

As for the directions of major axis which indicate the current directions of maximum velocities, the differences between the computed results and observed data are shown approximately from -23° to 14°, so that the computed current directions have good agreements with observed data. The computed current ellipses have the flat shapes similar observed data and the obvious oscillatng currents on straight line are simulated.

2 Comparing the computed result with observed data in 1979 additionally, as follows:

The computed length of the major axis is from 0.3 to 24 cm/sec longer than observed one at every observation station. At the stations locating between the islands, the ratios of maximum velocities between computed results and the observed data have the following differences. The ratios are at st.1 as 0.1826, at st.3 as 0.9636, at st.4 as 0.2197, at st.5 as 0.6252 and the averaged ratio is 0.5320. These ratios do not indicate the good agreements. The gradients of major axis have such large differences as from -132° to 3° between the computed results and the observed data.

3 As for the tidal current of K1 component, the following reason is considered for the bad agreements between the computed results and observed data performed in 1979.

In the tidal current computation of K1 component, it is the most important object that the computed result should have the good agreement compared with the observed data performed in 1981. Since the directions of major axis have some differences in the narrow channels around the islands, the finite element mesh cannot explain the complicated topography sufficiently around the islands.

4 About the constant current, the computed velocity vector is compared with the observed data obtained in 1981.

The differences of current velocities are from -5.5 to 2.6 cm/sec. The ratios of velocities between computed one and observed one are at st.sc1 as 0.8491, at st.sc5 as 1.0883, at st.sc3 as 1.3035, at st.sc4 as 1.2823, at st.sc5 as 1.1886, at st.sc6 as 1.2384 and the average is 1.1584. These ratios indicate that the computed velocity is a little bit larger than the observed one.

In the current directions, the differences between the observed and computed current are shown from 5 to 30°. These comparisons show the good agreement with each other.

From these view points, the computed results can successfully explain the observed physical processes about the tidal current and constant current. These verified numerical results are illustrated in Fig. III-6-3 as constant current and in Fig. III-6-4 as the every 2 hours current patterns in which the constant current and the tidal current are superposed each other.

Table III-6-1 Comparison between the observed and the computed tidal ellipses

Point		Maximum velocity (cm/s) a OBS.	b CALC.	c = a - b Difference	d = b/a ratio	Direction (°) e OBS.	f CALC.	g = e - f Difference
1981	SC 1	30.40	27.21	3.19	0.8951	130	116	14
	SC 2	41.13	40.82	0.31	0.9925	86	99	-13
	SC 3	37.27	43.68	-6.41	1.1720	74	62	12
	SC 4	22.17	21.76	0.41	0.9815	86	90	-4
	SC 5	23.94	22.72	1.22	0.9490	72	95	-23
	SC 6	48.10	48.32	-0.22	1.0046	45	45	0
1979	ST 1	29.79	5.44	24.35	0.1826	119	125	-6
	ST 2	39.98	23.84	16.14	0.5963	123	124	-1
	ST 3	7.97	7.68	0.29	0.9636	7	139	-132
	ST 4	15.36	4.48	10.88	0.2917	151	56	95
	ST 5	52.72	32.96	19.76	0.6252	63	60	3

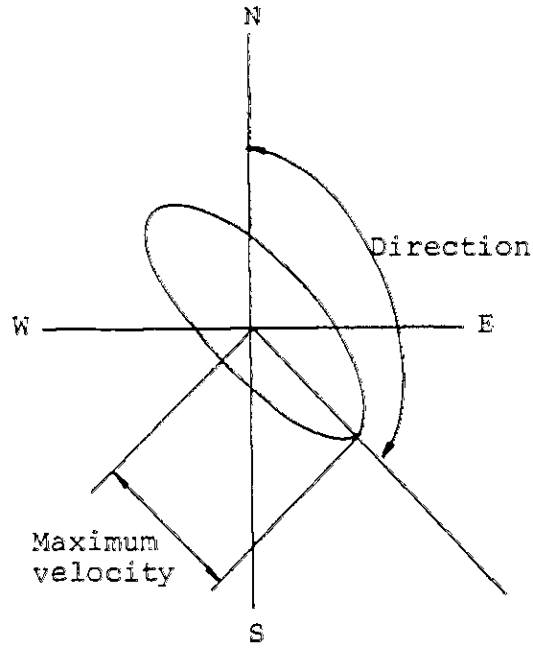

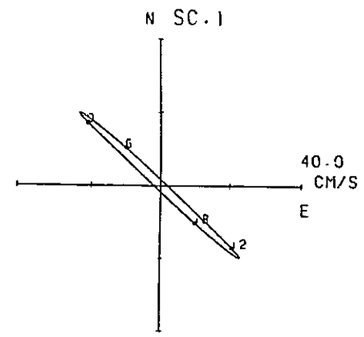

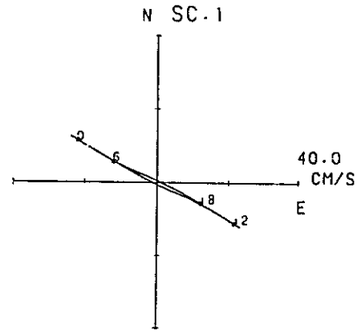

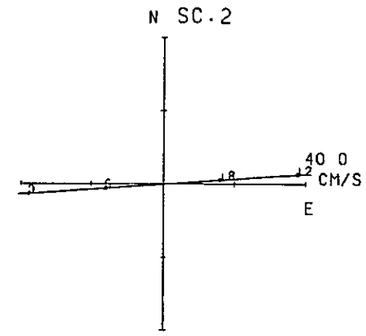

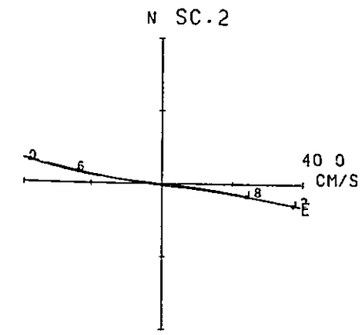

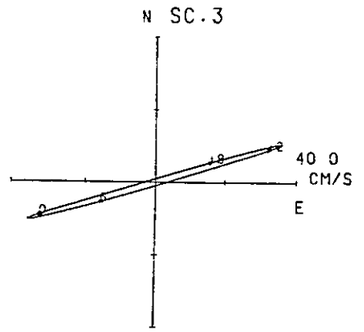

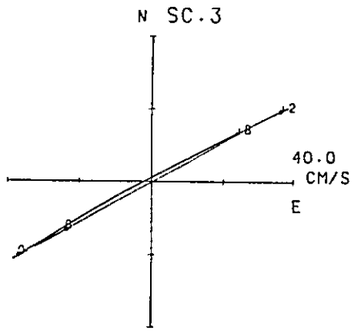

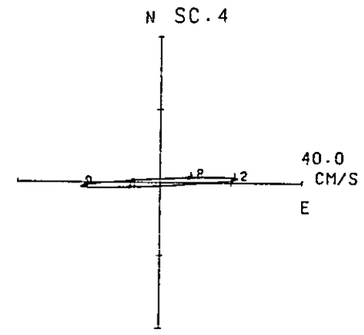

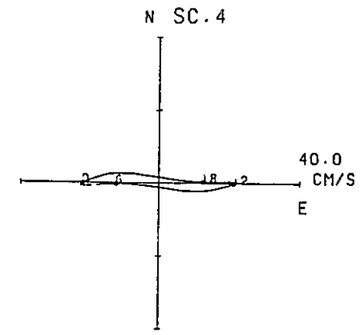

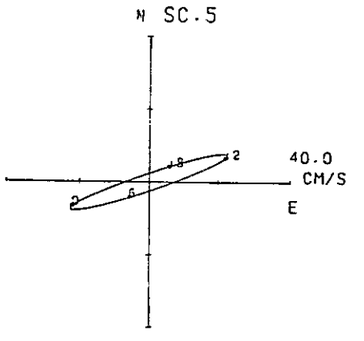

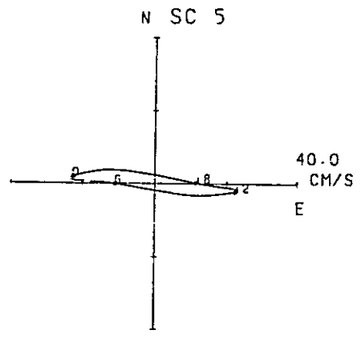

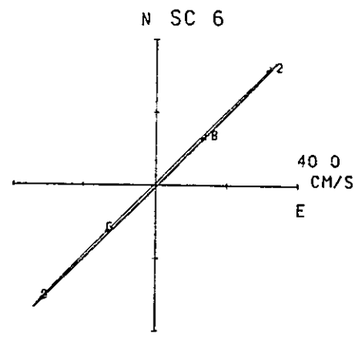

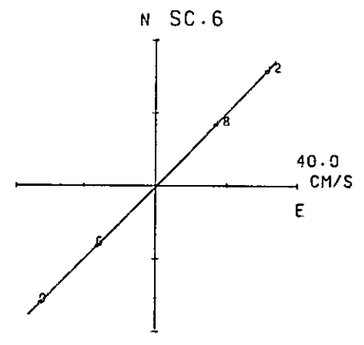

Fig. III-6-1 Observed (1981) and computed current ellipses

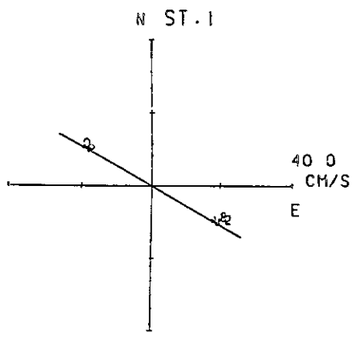

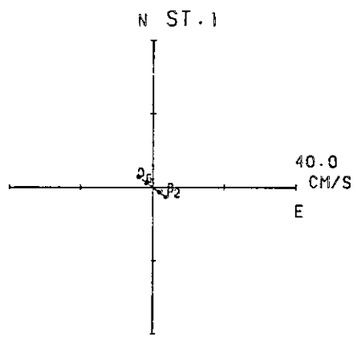

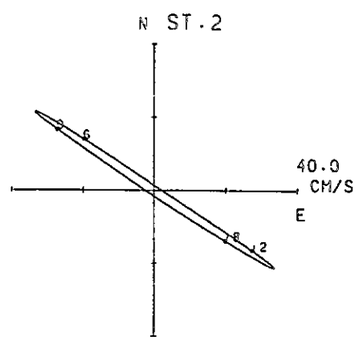

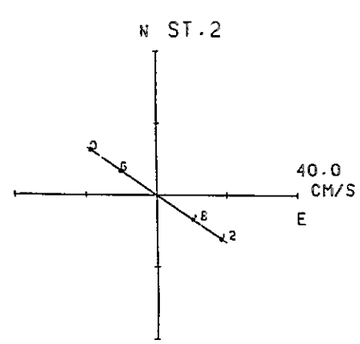

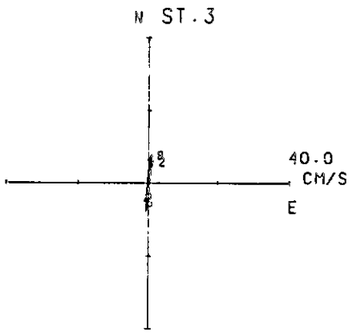

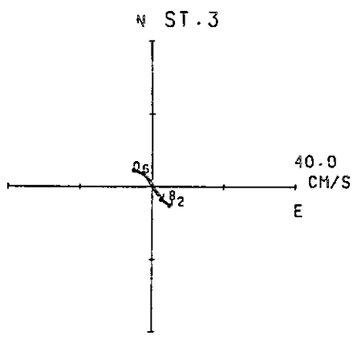

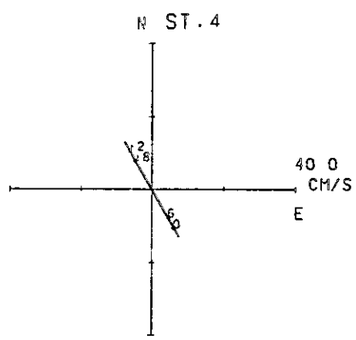

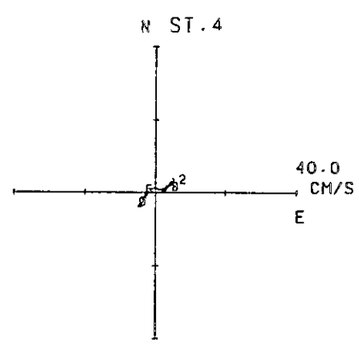

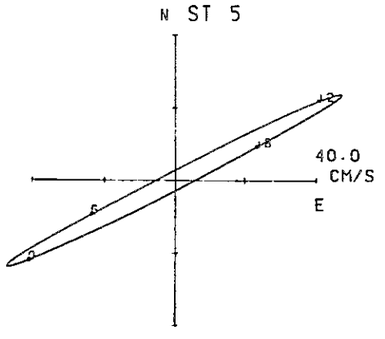

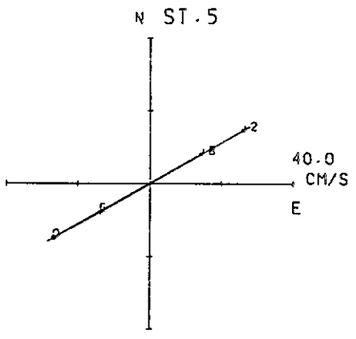

Fig. III-6-2 Observed (1979) and computed current ellipses

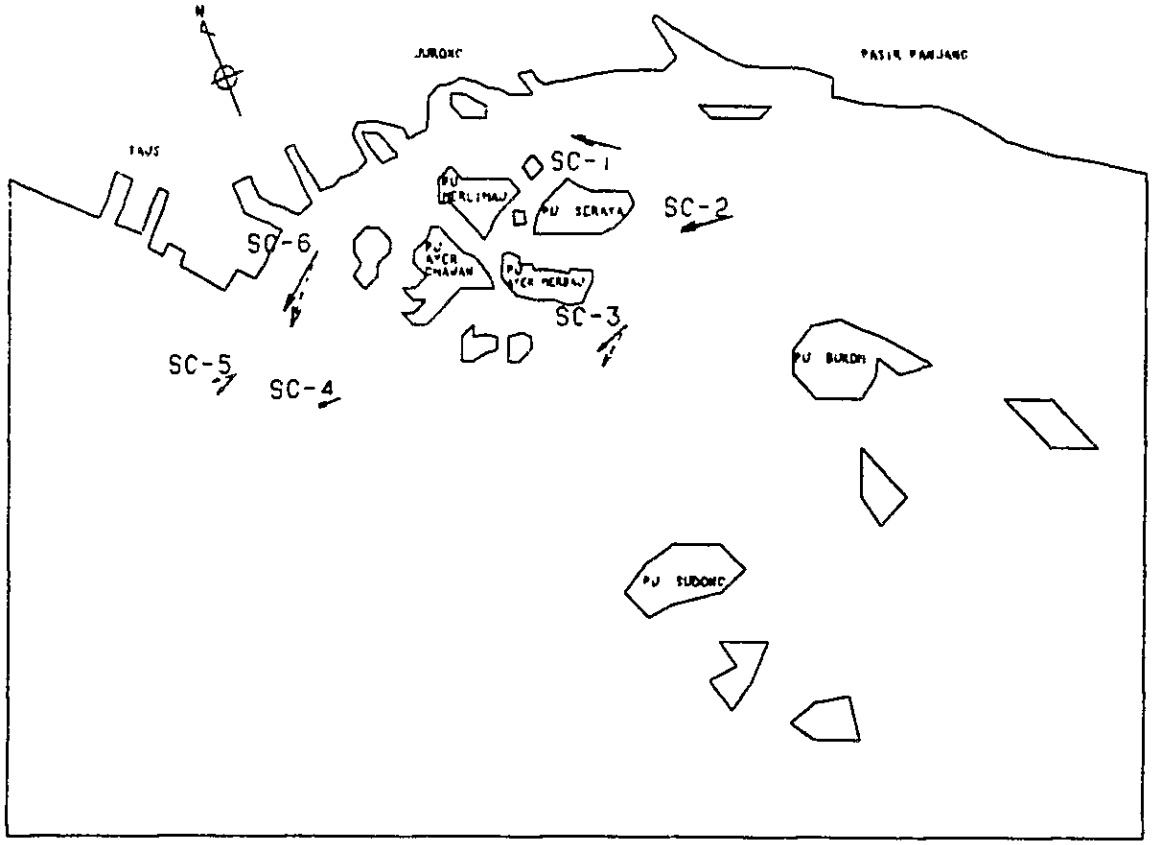

25.0 cm/s

——— OBSERVATION (1981)

- - - - CALCULATION

0.0 3.0 km

Table III-6-2 Comparison of the constant current vector

POINT	OBSERVATION		CALCULATION		DIFFERENCE		
	a VELOCITY (cm/s)	b DIRECTION (°)	c VELOCITY (cm/s)	d DIRECTION (°)	e=a-c VELOCITY (cm/s)	f=b-d DIRECTION (°)	g=c/a VELOCITY RATIO
SC-1	17 44	327 60	14 80	299 27	2 63	28 34	0 849
SC-2	19 48	297 22	21.20	280 15	-1 72	17 06	1 0883
SC-3	13 46	270 67	17 55	239 00	-4.09	31 67	1 3035
SC-4	7 96	287 49	10 20	277 28	-2 25	10 21	1 2823
SC-5	9 77	267 79	11 62	276 93	-1 84	9 13	1 1886
SC-6	23 22	253 06	28 76	225 96	-5 54	27 10	1.2384
					N DIRECTION S		

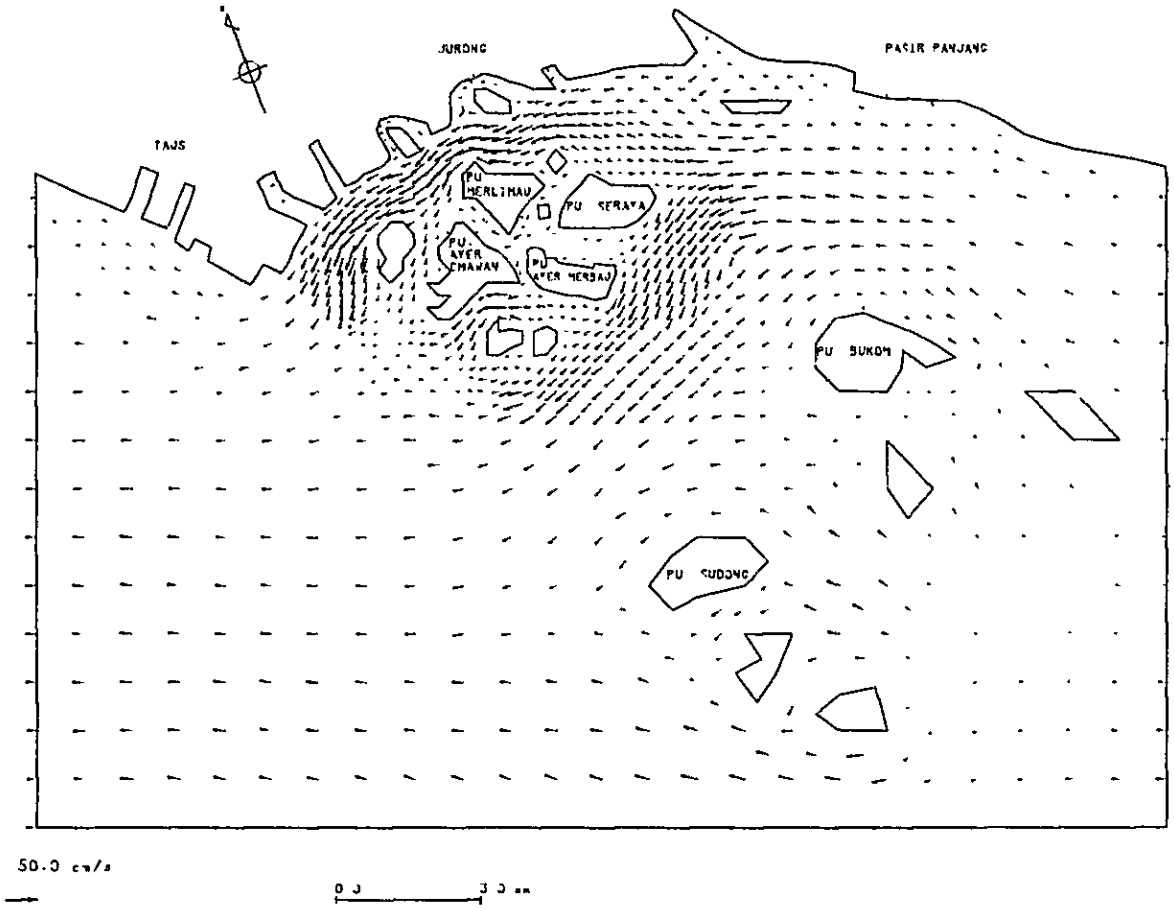

Fig. III-6-3 Constant current in present stage

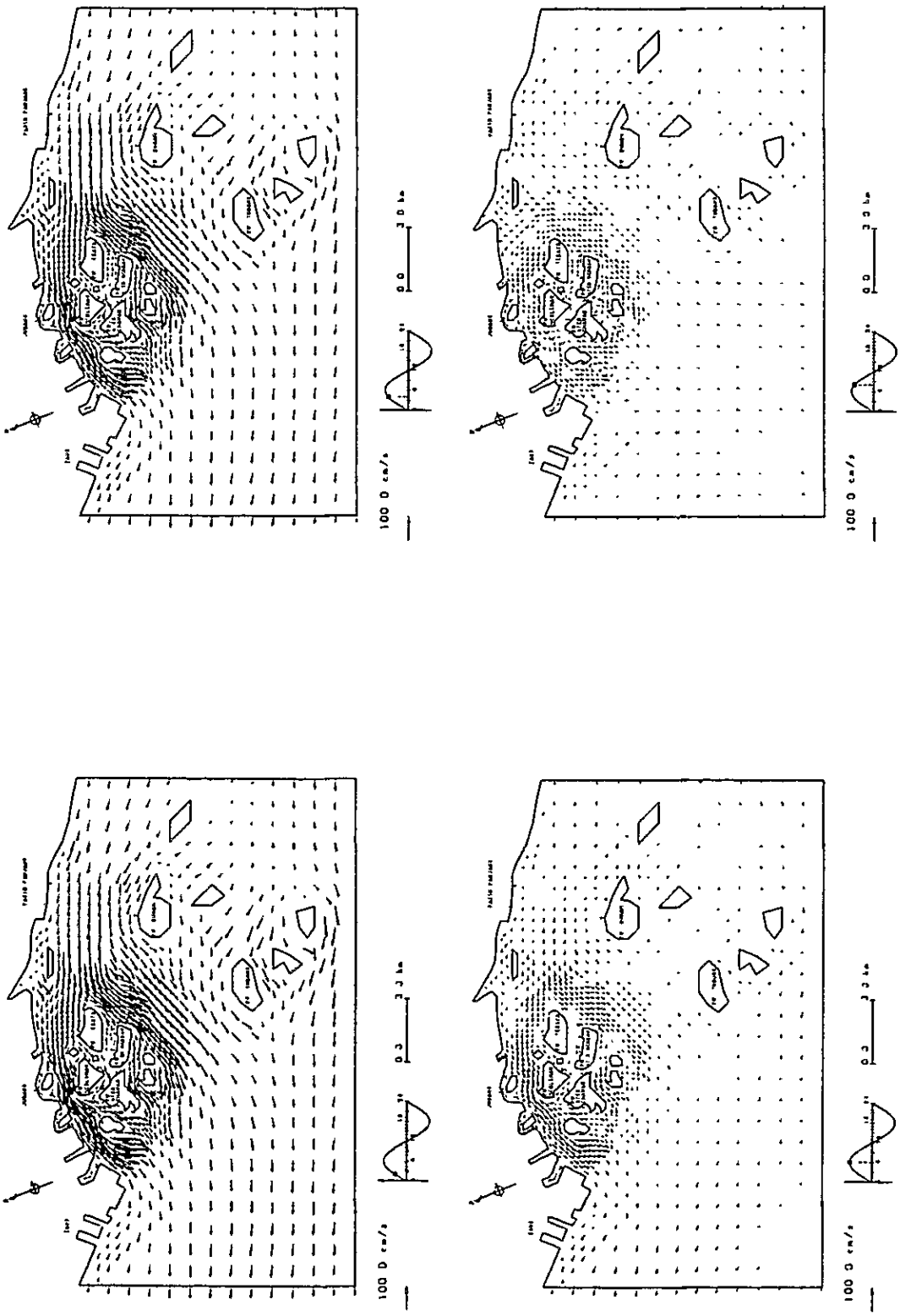

Fig. III-6-4-(1) Current patterns in present stage

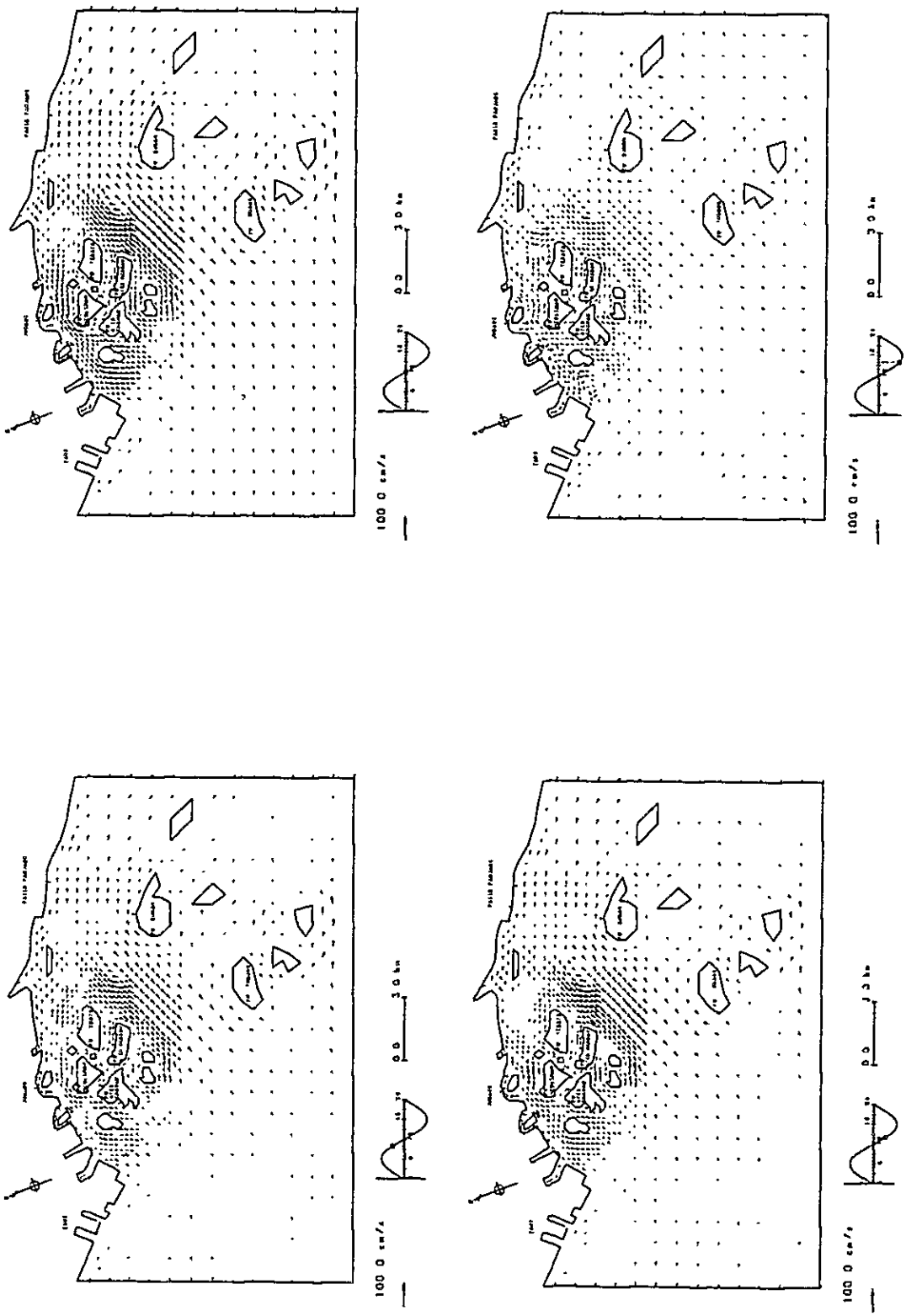

Fig. III-6-4-(2) Current patterns in present stage

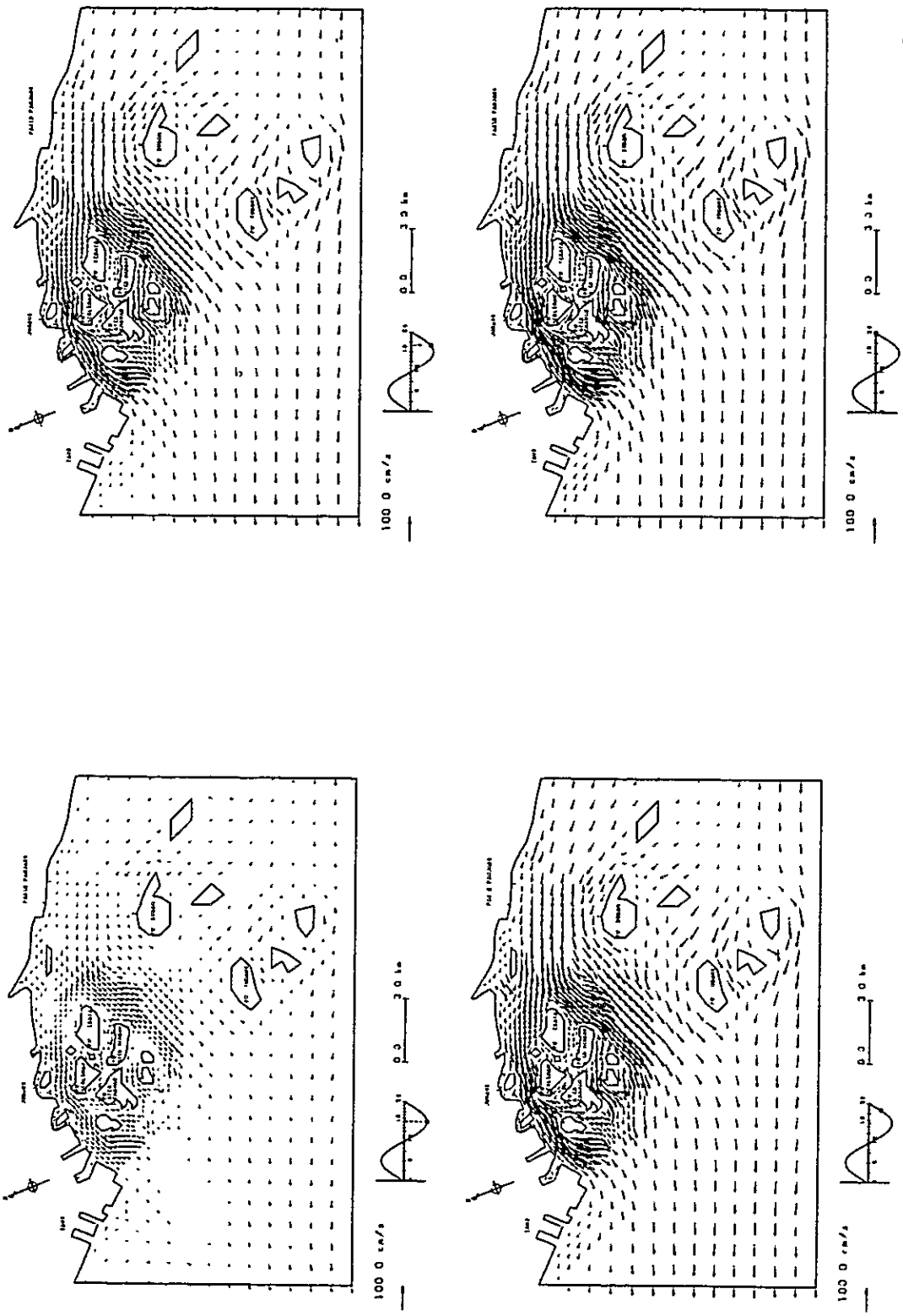

Fig. III-6-4-(3) Current patterns in present stage

— Current in the future stage

When the current computation of the future stage is carried out, the following assumptions are introduced:

The boundary conditions on the open boundary and physical constants are same with the present stage.

The local topography and the discharge rates are changed according to the future development plan.

Fig. III-6-5 and Fig. III-6-6 show the constant current in future stage. Fig. III-6-7 and Fig. III-6-8 show every 2 hours current pattern in which the constant current and the tidal current are superposed each other.

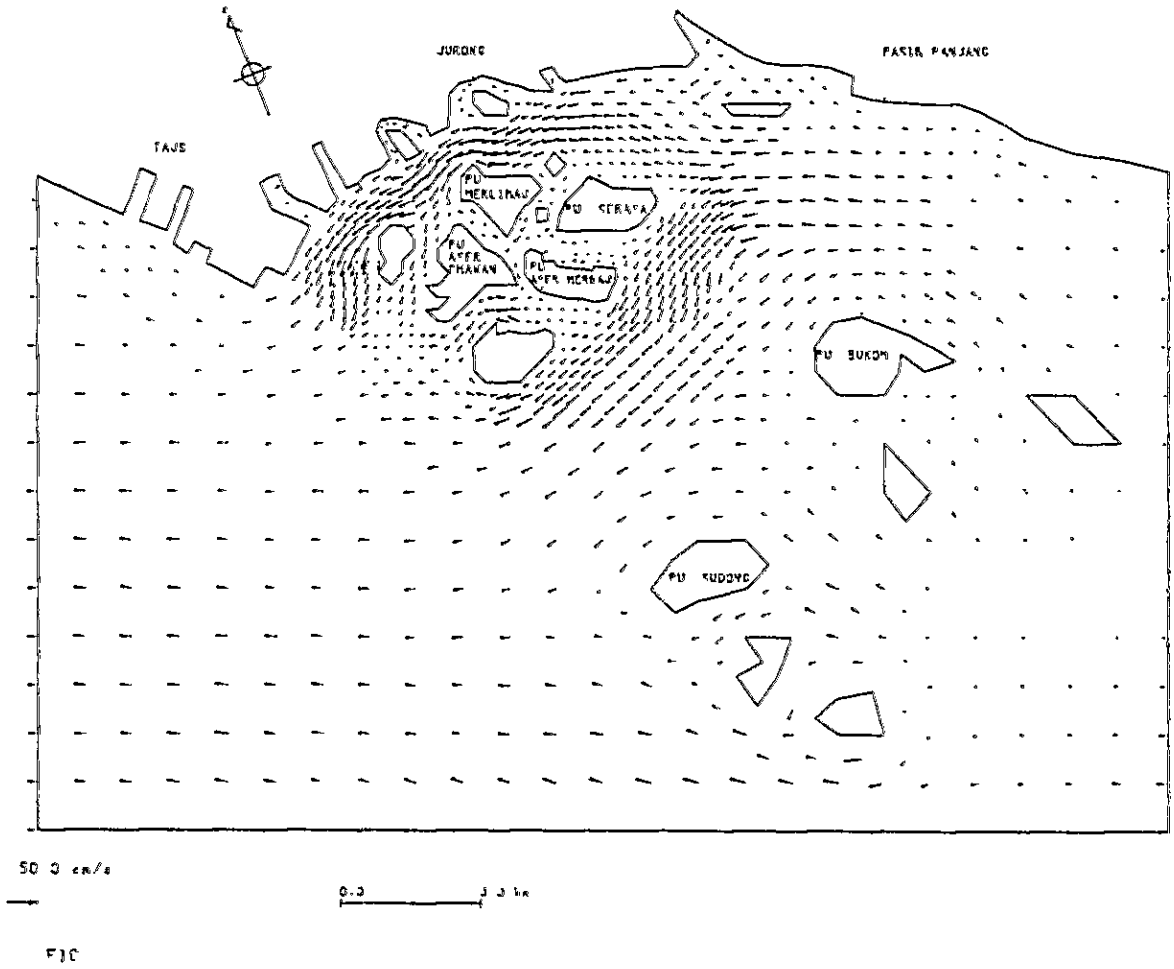

Fig. III-6-5 Constant current in future stage (westward current)

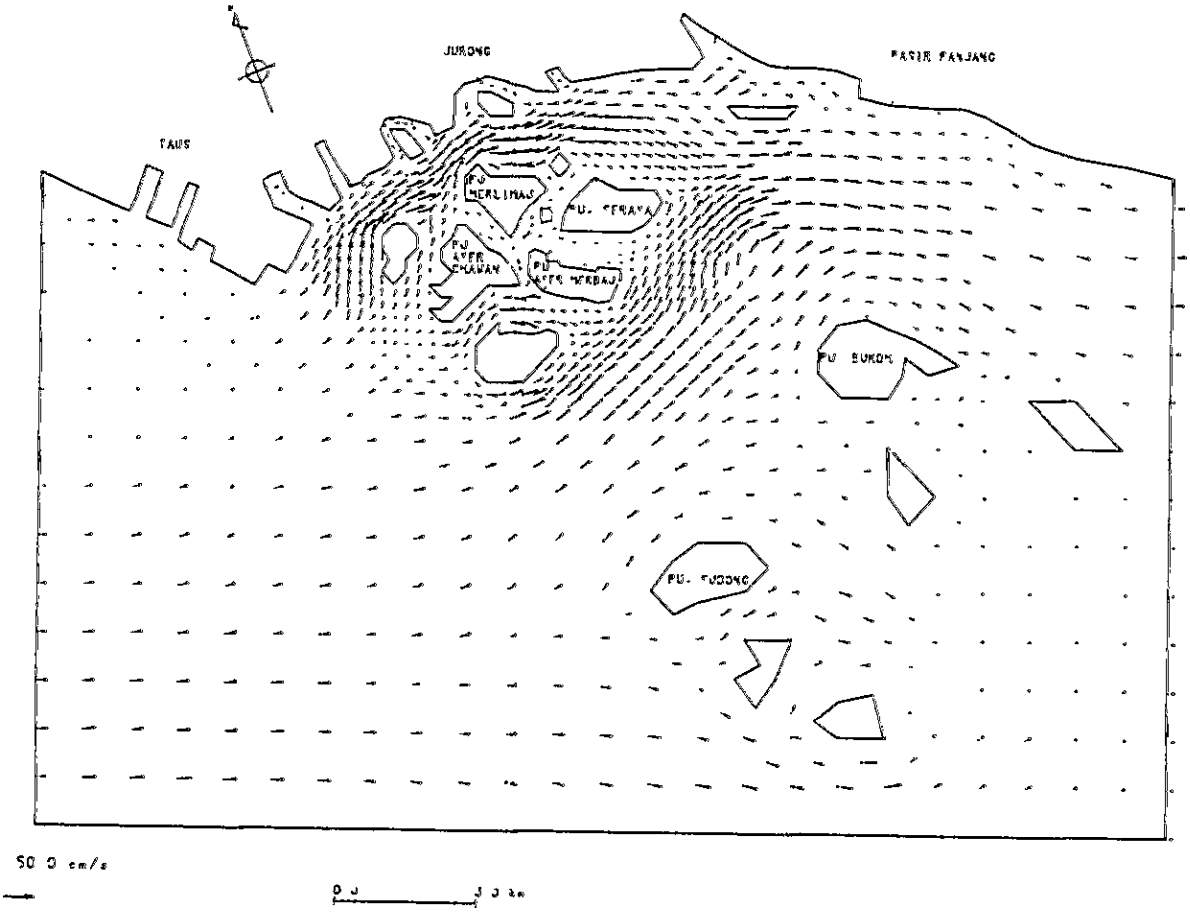

Fig. III-6-6 Constant current in future stage (eastward current)

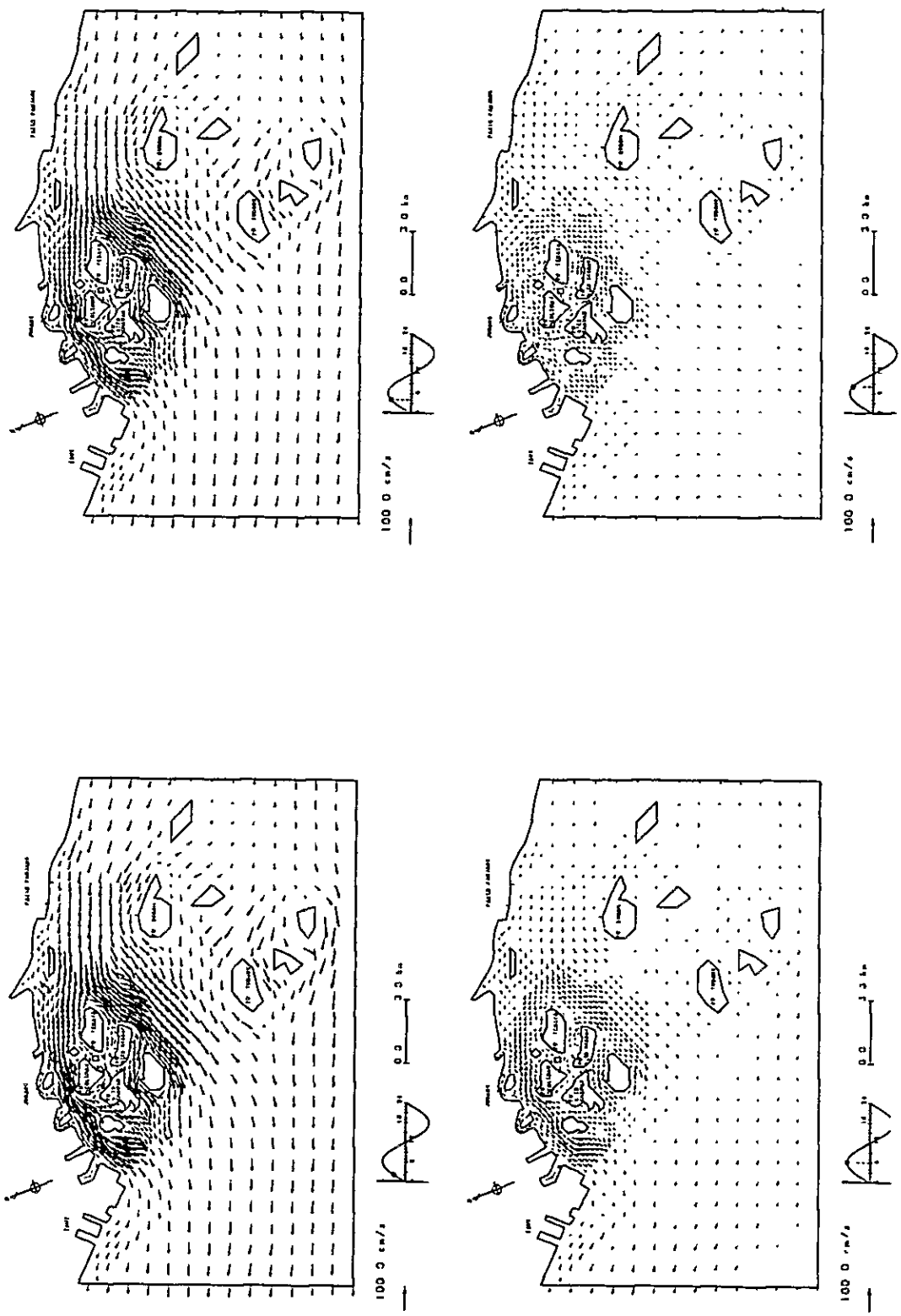

Fig. III-6-7-(1) Westward current patterns in future stage

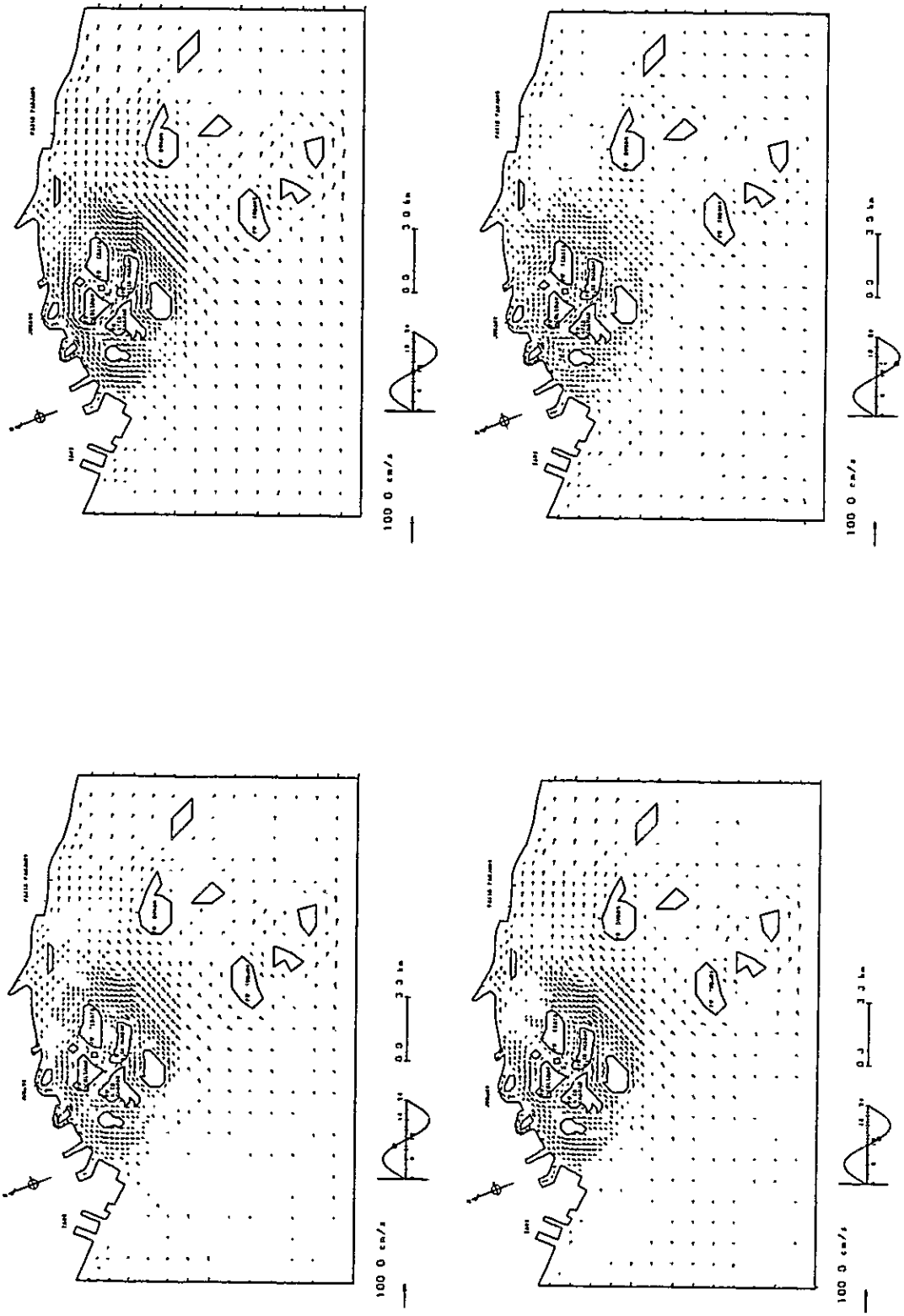

Fig. III-6-7-(2) Westward current patterns in future stage

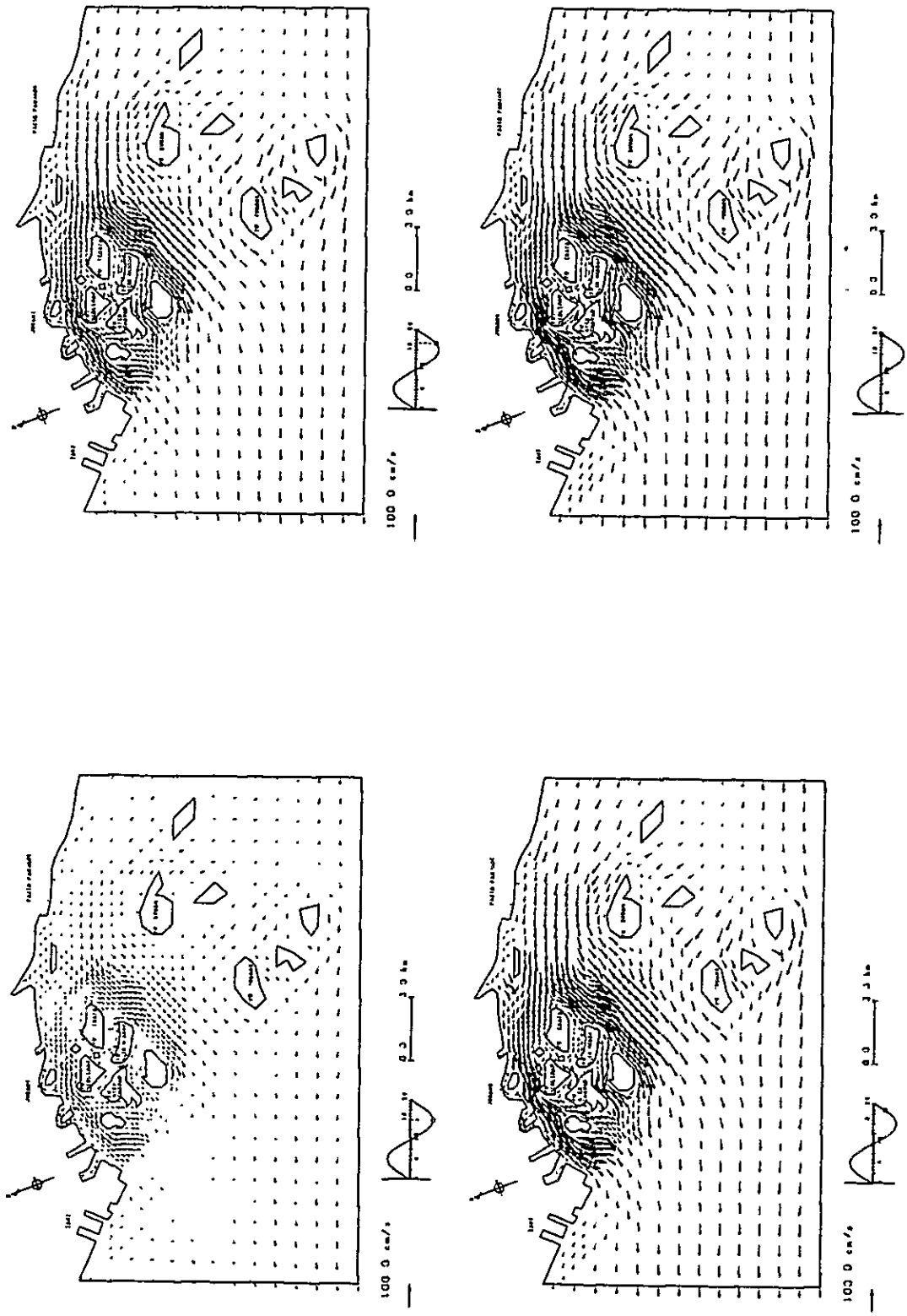

Fig. III-6-7-(3) Westward current patterns in future stage

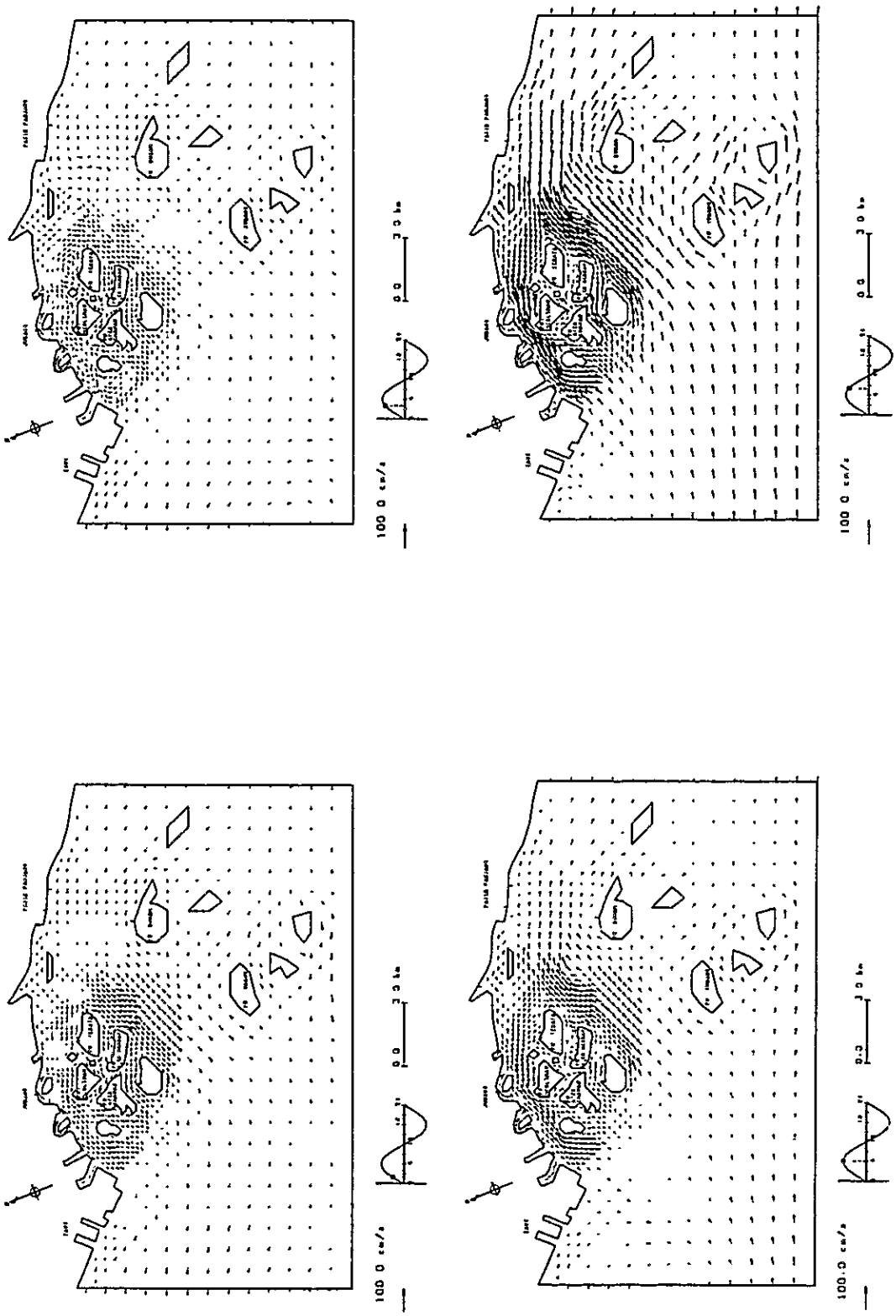

Fig. III-6-8-(1) Eastward current pattern in future stage

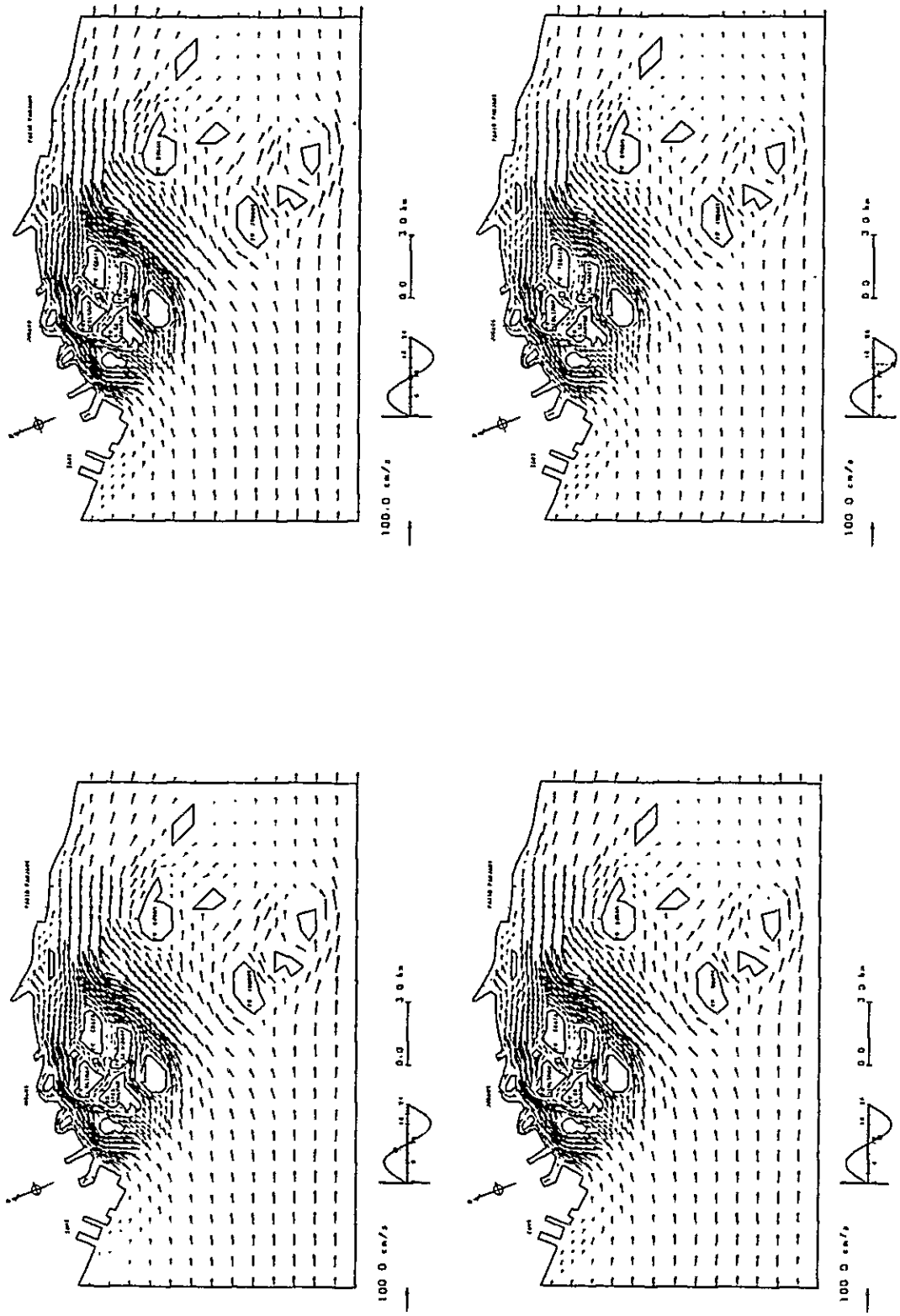

Fig. III-6-8-(2) Eastward current pattern in future stage

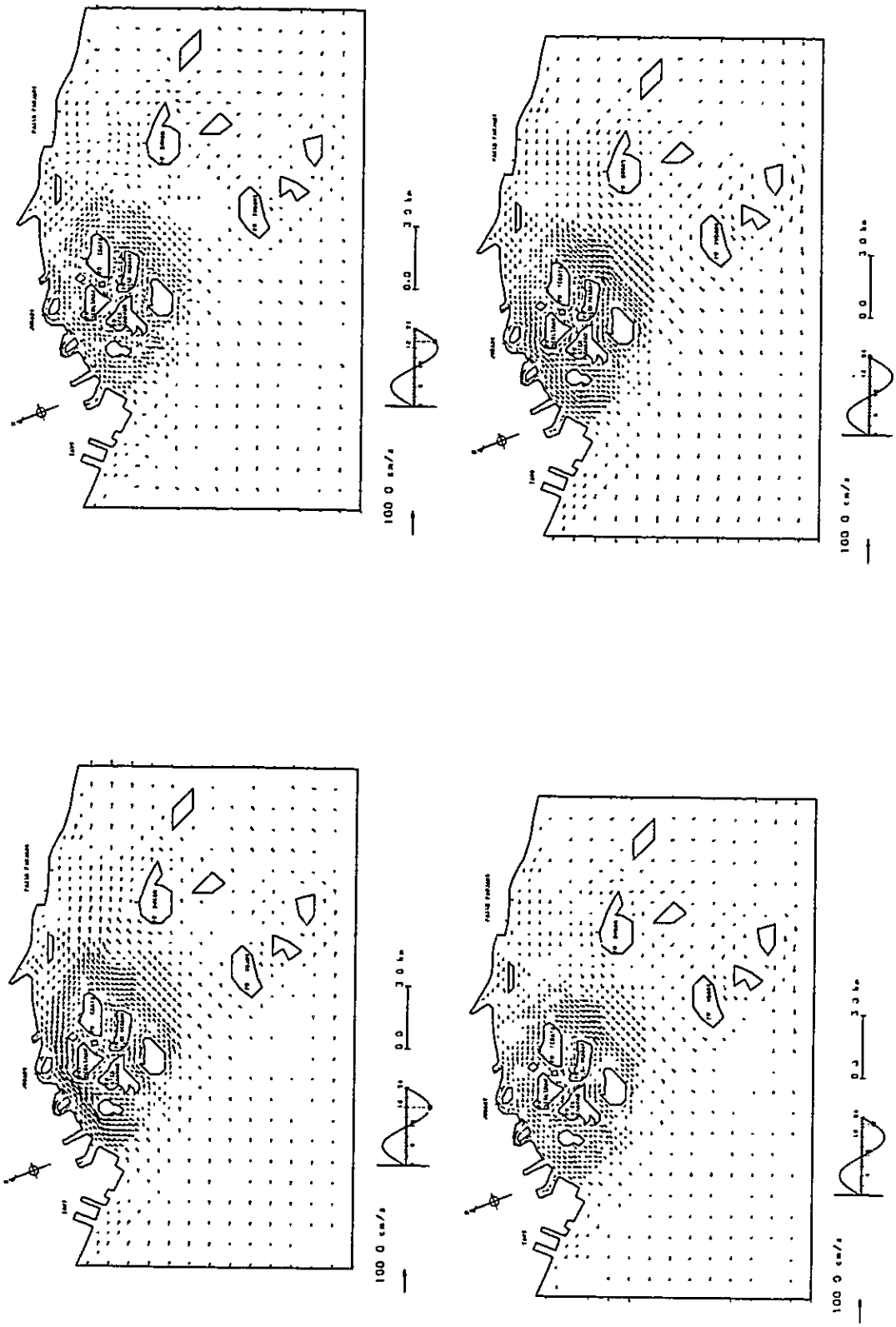

Fig. III-6-8-(3) Eastward current pattern in future stage

— The change of current

The comparison of the numerical results between the present stage and the future stage is performed, concerning with the current in which the westward constant current and tidal current are superposed each other.

Fig. III-6-9 shows the changes of velocity and current directon of every 2 hours at the representative points.

Fig. III-6-10 shows the distribution of velocity change at ebb tide and flood tide.

From these figures, the change of current in the future stage can be summarized as follows (the comment about the tidal time is equal to that of Jurong Wharf):

1 At high water, small magnitude westward current pattern remains. The difference of velocity is less than 1 cm/sec between the present and the future. The difference of current direction only can be found out about 2^{o} changes at point H near Sakra island and Bakau island.

2 After 3 hours from the high water, the tidal current cancel with the constant current, and the current flows from the west to the east with the comparatively small velocity. The difference of velocity between the present and the future is more than 1 cm/sec at point H and F around Sakra island and Bakau island. Fig. III-6-10 shows that, comparing the future stage's result with the present stage, in the area between Sakra or the Bakau island and Chawar or Merbau island (3 km x 1 km) the velocity is increasing within about 6 cm/sec, and, in the south to Sakra island and Bakau island the velocity is decreasing within about 4 cm/sec. The maximum difference of current direction is equal to 2^{o} in the south to Bakau island.

3 At the low water, the current directions are generally equal to the west. At every comparison point, the change of velocity is less than 1 cm/sec. The change of current direction is shown at point H and G west to Sakra and Bakau isalnd as 2^{o}.

4 After 3 hours from the low water, as the constant current and tidal current have the same directions, the maximum velocity is coming out and the strongest current to the west is shown. At the point H, the difference of velocity gets to 4 cm/sec. In Fig. III-6-10 it is shown that in the area between Sakra or Bakau island and Chawar or Merbau island (2 km x 1 km) the velocity is increasing up to 6 cm/sec.

From these points, the change of current is shown only around Sakra and Bakau islands where the topography is changed.

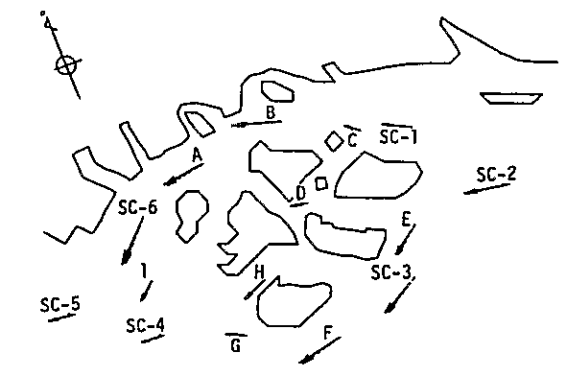

POINT	PRESENT STAGE a VELOCITY (cm/s)	PRESENT STAGE b DIRECTION (°)	FUTURE STAGE c VELOCITY (cm/s)	FUTURE STAGE d DIRECTION (°)	DIFFERENCE a-c VELOCITY (cm/s)	DIFFERENCE b-d DIRECTION (°)	g=c/a VELOCITY RATIO
SC-1	25 07	297 48	25 08	297 48	-0 00	0 00	1.0002
SC-2	38 78	279 32	38 78	279 32	-0 00	0 00	1 0001
SC-3	42 16	240 41	42 19	240 56	-0 03	0 16	1 0008
SC-4	21 38	269 27	21 32	269 26	0 06	0 01	0 9970
SC-5	22 69	274 13	22 66	274 15	0.03	0 01	0 9986
SC-6	46 60	225 80	46 62	225 80	0 02	0 00	1 0004
A	41 55	261 47	41 57	261 47	-0 02	0 00	1 0004
B	41 54	285 91	41 55	285 91	-0 01	0 00	1 0002
C	17 86	308 15	17 86	308 15	-0 00	0 00	1 0002
D	20 13	282 76	20 06	282 79	0 06	0 03	0 9968
E	32 04	235 75	32.06	235 75	-0 01	0 00	1 0004
F	42 68	256 60	41 77	255 48	0 91	1 12	0 9787
G	18 89	292 94	18 00	293 32	0 88	0 37	0 9532
H	27 85	247 15	31 74	249 02	-3 89	1 87	1 1395
I	25 58	227.90	25 60	227.62	-0 03	0 28	1.0011

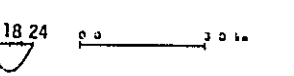

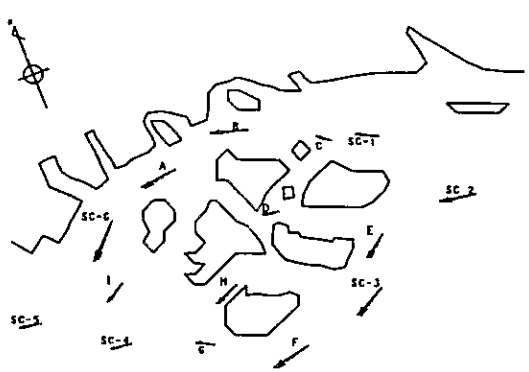

POINT	PRESENT STAGE a VELOCITY (cm/s)	PRESENT STAGE b DIRECTION (°)	FUTURE STAGE c VELOCITY (cm/s)	FUTURE STAGE d DIRECTION (°)	DIFFERENCE a-c VELOCITY (cm/s)	DIFFERENCE b-d DIRECTION (°)	g=c/a VELOCITY RATIO
SC-1	15 81	295 97	15 82	295 99	-0 01	0 01	1 0006
SC-2	28 07	278 00	28 07	278 00	0 01	0 00	0 9998
SC-3	31 15	240 90	31 17	241 08	-0 02	0 19	1.0005
SC-4	16 52	275 32	16 41	275 39	0 11	0.08	0 9935
SC-5	17.40	279 67	17 35	279 71	0 05	0 05	0 9973
SC-6	28 75	225 44	28 77	225 44	-0 02	0 00	1 0007
A	25 53	261 52	25 55	261 52	-0 02	0 00	1 0009
B	25 78	286 30	25 80	286 30	-0 02	0 00	1.0008
C	11 14	307 82	11 15	307 83	-0 01	0 01	1.0007
D	13 42	283 03	13 38	283 08	0 04	0 05	0 9970
E	23 13	235 79	23 13	235 80	-0 00	0 01	1 0001
F	31 90	257 10	31.14	255 80	0 76	1 31	0 9762
G	15 60	297 04	14.88	298 15	0 72	1.11	0 9536
H	19 08	246 94	21 81	248 96	-2 73	2 02	1 1433
I	16 99	242 86	16 97	242.16	0 02	0 70	0 9988

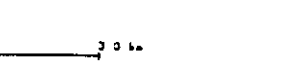

Fig. III-6-9-(1) Change of velocity and current direction

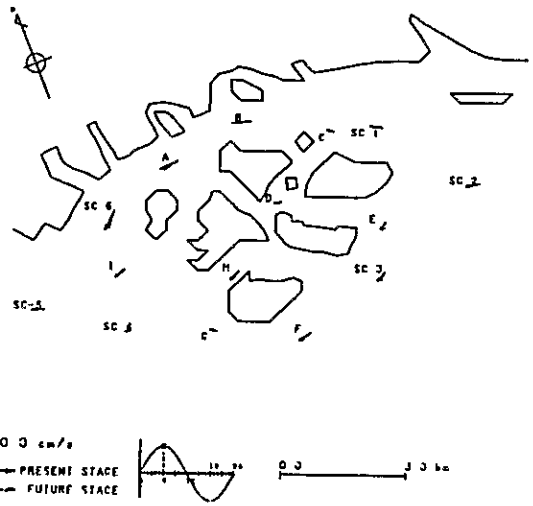

POINT	PRESENT STAGE		FUTURE STAGE		DIFFERENCE		c/a VELOCITY RATIO
	a VELOCITY (cm/s)	b DIRECTION (°)	c VELOCITY (cm/s)	d DIRECTION (°)	c-a VELOCITY (cm/s)	f-b-d DIRECTION (°)	
SC-1	0.99	326 63	0.99	326 59	-0 00	0 04	1 0046
SC-2	2 09	86 64	2 09	86 63	-0 00	0 01	1 0011
SC-3	3 05	53 09	3 08	54 13	-0 03	1.04	1 0093
SC-4	2.40	313 19	2 41	313 63	0.01	0 44	1.0023
SC-5	4 60	306 29	4.61	306 26	-0 00	0 02	1 0005
SC-6	2 42	226 02	2 42	226 00	-0 01	0 03	1 0023
A	1 80	261 69	1 81	261 63	0 00	0 06	1 0025
B	1 78	286 37	1 79	286 37	-0 01	0.00	1 0043
C	1 00	306 82	1 00	306 84	-0.00	0 01	1 0042
D	2 07	284.08	2 08	284 07	-0 01	0.00	1 0060
E	1 68	42 67	1 69	42 92	-0 01	0.25	1 0084
F	3 15	77.34	3 12	75.71	0 02	1 62	0 9921
G	1.11	339 66	1 15	341 03	-0 04	1 37	1 0397
H	1.67	246.55	1 81	248 75	-0 14	2 20	1.0827
I	4 75	306 28	4.73	306 24	0 01	0.04	0 9975

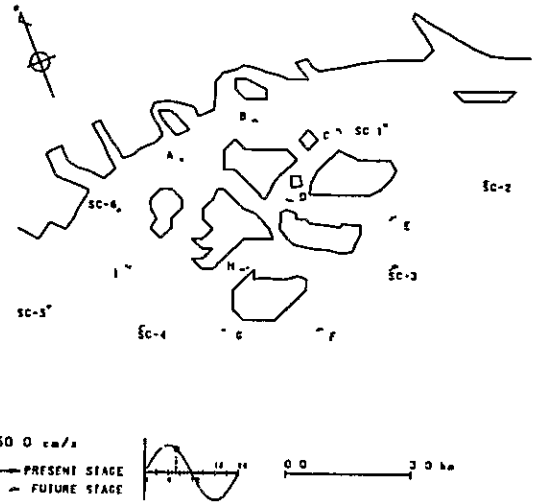

POINT	PRESENT STAGE		FUTURE STAGE		DIFFERENCE		c/a VELOCITY RATIO
	a VELOCITY (cm/s)	b DIRECTION (°)	c VELOCITY (cm/s)	d DIRECTION (°)	c-a VELOCITY (cm/s)	f-b-d DIRECTION (°)	
SC-1	13 05	114.78	13 05	114 80	-0.01	0.02	1 0005
SC 2	24 18	97 07	24 18	97.08	0 00	0 00	0 9999
SC-3	27 37	61.90	27 40	62 23	-0 04	0 33	1.0014
SC-4	12.48	89 73	12.38	89.81	0 10	0 08	0 9921
SC-5	11 34	90 18	11.30	90 21	0 04	0 03	0 9962
SC-6	22.67	44.55	22 68	44.55	-0 02	0 00	1 0007
A	20 70	82.29	20 72	82 29	-0 02	0 00	1 0009
B	21.45	107.35	21 47	107.35	-0 02	0 00	1 0008
C	8.59	127 13	8 60	127.14	-0.01	0 01	1 0006
D	9 42	102.26	9 38	102 35	0 04	0 08	0 9955
E	19 16	54.32	19 16	54.33	-0 00	0.02	1 0001
F	27.99	77 63	27 20	75 91	0 79	1.72	0 9718
G	12 78	115 87	12.11	116.93	0 67	1 06	0 9474
H	14.99	66 25	17 43	68 50	-2.44	2.26	1 1631
I	13 79	48 96	13 80	48 18	-0 02	0 77	1 0013

Fig. III-6-9-(2) Change of velocity and current direction

POINT	PRESENT STAGE		FUTURE STAGE		DIFFERENCE		
	VELOCITY (cm/s)	DIRECTION (°)	VELOCITY (cm/s)	DIRECTION (°)	VELOCITY (cm/s)	DIRECTION (°)	VELOCITY RATIO
SC-1	22.47	116.78	22.48	116.80	-0.01	0.01	1.0003
SC-2	35.64	98.16	35.64	98.16	0.00	0.00	1.0000
SC-3	39.31	62.57	39.36	62.85	-0.05	0.28	1.0013
SC-4	19.64	89.60	19.74	89.66	0.10	0.05	0.9949
SC-5	19.88	93.55	19.84	93.58	0.04	0.02	0.9980
SC-6	40.22	44.48	40.24	44.48	-0.02	0.00	1.0006
A	36.33	82.58	36.35	82.59	0.02	0.01	1.0007
B	37.87	107.58	37.88	107.58	-0.02	0.00	1.0004
C	15.27	126.99	15.28	127.00	-0.01	0.01	1.0003
D	17.70	101.83	17.63	101.89	0.07	0.06	0.9959
E	27.83	54.73	27.81	54.74	-0.00	0.00	1.0000
F	39.59	77.20	38.54	75.59	1.05	1.62	0.9735
G	19.42	114.42	17.52	115.27	0.90	0.85	0.9512
H	25.31	66.13	29.26	68.38	-3.71	2.25	1.1463
I	23.43	90.58	23.45	90.14	-0.02	0.44	1.0009

POINT	PRESENT STAGE		FUTURE STAGE		DIFFERENCE		
	VELOCITY (cm/s)	DIRECTION (°)	VELOCITY (cm/s)	DIRECTION (°)	VELOCITY (cm/s)	DIRECTION (°)	VELOCITY RATIO
SC-1	26.48	117.16	26.49	117.16	-0.01	0.01	1.0002
SC-2	40.03	98.57	40.03	98.57	-0.00	0.00	1.0000
SC-3	43.75	62.71	43.81	62.96	-0.06	0.25	1.0013
SC-4	22.41	89.61	22.31	89.63	0.10	0.02	0.9956
SC-5	23.47	94.45	23.43	94.47	0.04	0.02	0.9984
SC-6	47.52	44.43	47.53	44.43	0.02	0.00	1.0005
A	42.64	82.68	42.67	82.68	-0.02	0.01	1.0006
B	44.60	107.64	44.61	107.64	-0.01	0.00	1.0003
C	18.05	127.08	18.06	127.08	-0.00	0.01	1.0002
D	21.48	101.57	21.39	101.63	0.08	0.06	0.9961
E	31.41	54.85	31.11	54.85	-0.00	0.00	1.0000
F	43.73	76.97	42.62	75.41	1.11	1.55	0.9746
G	20.38	113.91	19.47	114.67	0.91	0.76	0.9544
H	29.81	66.02	31.95	68.26	-4.13	2.24	1.1387
I	27.21	51.02	27.23	50.66	-0.02	0.36	1.0008

Fig. III-6-9-(3) Change of velocity and current direction

POINT	PRESENT STAGE VELOCITY (cm/s)	PRESENT STAGE DIRECTION (°)	FUTURE STAGE VELOCITY (cm/s)	FUTURE STAGE DIRECTION (°)	DIFFERENCE VELOCITY (cm/s)	DIFFERENCE DIRECTION (°)	VELOCITY RATIO
SC-1	24.13	117.12	24.14	117.13	0.01	0.01	1.0003
SC-2	37.66	98.53	37.66	98.53	-0.00	0.00	1.0000
SC-3	41.49	62.48	41.54	62.73	0.05	0.25	1.0013
SC-4	21.28	91.14	21.18	91.20	-0.10	0.06	0.9955
SC-5	22.50	96.17	22.46	96.20	-0.04	0.02	0.9983
SC-6	43.39	44.45	43.41	44.45	0.02	0.00	1.0004
A	38.67	82.58	38.59	82.79	-0.07	0.21	0.9982
B	40.41	107.46	40.42	107.57	0.01	0.11	1.0004
C	16.51	127.36	16.52	127.37	0.00	0.01	1.0003
D	20.39	101.58	20.01	101.64	-0.38	0.06	0.9963
E	29.44	54.84	29.45	54.85	0.00	0.00	1.0001
F	41.22	76.87	40.20	75.36	-1.02	-1.52	0.9751
G	19.43	114.88	19.58	115.67	0.15	0.80	0.9362
H	27.66	65.95	31.40	68.17	3.75	2.22	1.1360
I	24.94	53.76	24.93	53.86	-0.01	0.09	1.0004

POINT	PRESENT STAGE VELOCITY (cm/s)	PRESENT STAGE DIRECTION (°)	FUTURE STAGE VELOCITY (cm/s)	FUTURE STAGE DIRECTION (°)	DIFFERENCE VELOCITY (cm/s)	DIFFERENCE DIRECTION (°)	VELOCITY RATIO
SC-1	15.49	115.95	15.40	115.97	-0.01	0.01	1.0005
SC-2	27.37	97.87	27.37	97.87	0.00	0.00	1.0000
SC-3	30.43	62.07	30.47	62.34	0.04	0.27	1.0013
SC-4	16.24	96.12	16.14	96.25	-0.10	0.13	0.9936
SC-5	17.18	100.63	17.14	100.68	-0.04	0.05	0.9975
SC-6	27.72	44.52	27.73	44.52	0.01	0.00	1.0005
A	24.38	82.24	24.40	82.24	0.02	0.00	1.0007
B	23.34	107.30	23.36	107.30	0.02	0.00	1.0007
C	10.59	127.82	10.60	127.83	0.01	0.01	1.0006
D	13.48	102.04	13.44	102.10	-0.04	0.05	0.9969
E	21.63	54.99	21.64	55.00	0.00	0.01	1.0002
F	30.74	77.12	29.96	73.57	-0.78	-1.55	0.9744
G	15.50	118.41	14.88	119.54	-0.62	1.12	0.9600
H	18.88	65.41	21.45	67.62	2.58	2.21	1.1365
I	16.83	65.57	16.80	64.91	-0.03	-0.66	0.9980

Fig. III-6-9-(4) Change of velocity and current direction

POINT	PRESENT STAGE		FUTURE STAGE		DIFFERENCE		VELOCITY RATIO
	VELOCITY (cm/s)	DIRECTION (°)	VELOCITY (cm/s)	DIRECTION (°)	VELOCITY (cm/s)	DIRECTION (°)	
SC-1	1.03	143.53	1.04	143.53	0.00	0.00	1.0048
SC-2	1.68	267.07	1.68	267.37	-0.00	0.31	1.0028
SC-3	2.49	229.44	2.61	230.44	-0.02	0.99	1.0095
SC-4	2.02	129.12	2.62	129.74	0.01	0.63	0.9975
SC-5	4.72	124.91	4.72	124.96	0.00	0.04	0.9992
SC-6	2.59	45.90	2.60	45.98	-0.01	0.02	1.0021
A	1.02	81.09	1.02	81.63	-0.01	0.06	1.0026
B	1.91	106.44	1.92	106.44	-0.01	0.00	1.0045
C	1.04	127.54	1.34	127.55	0.00	0.01	1.0043
D	2.20	103.73	2.22	103.74	-0.01	0.01	1.0058
E	1.62	222.16	1.63	222.36	0.01	0.20	1.0092
F	2.52	256.87	2.52	255.72	-0.00	1.15	1.0010
G	1.42	150.15	1.41	152.53	0.01	2.38	0.9963
H	1.93	65.95	2.11	68.17	-0.18	2.22	1.0935
I	5.10	126.57	5.05	126.42	0.04	0.15	0.9913

POINT	PRESENT STAGE		FUTURE STAGE		DIFFERENCE		VELOCITY RATIO
	VELOCITY (cm/s)	DIRECTION (°)	VELOCITY (cm/s)	DIRECTION (°)	VELOCITY (cm/s)	DIRECTION (°)	
SC-1	13.48	295.75	13.48	295.75	-0.00	0.00	1.0002
SC-2	24.07	278.31	24.07	278.31	-0.00	0.00	1.0001
SC-3	27.18	239.98	27.21	239.98	-0.03	0.21	1.0011
SC-4	11.81	267.64	11.76	267.64	0.04	0.03	0.9962
SC-5	10.84	268.23	10.82	268.23	0.02	0.00	0.9979
SC-6	24.02	225.32	24.03	225.32	-0.01	0.00	1.0003
A	21.69	261.75	21.69	261.75	-0.01	0.00	1.0004
B	22.01	286.39	22.01	286.39	0.00	0.00	1.0002
C	9.08	308.50	9.09	308.50	0.00	0.01	1.0002
D	9.46	281.89	9.42	281.94	0.04	0.05	0.9953
E	20.21	234.66	20.22	234.67	-0.01	0.00	1.0006
F	27.51	256.89	26.88	255.70	0.63	1.19	0.9772
G	11.54	294.66	11.02	295.13	0.53	0.47	0.9543
H	14.45	246.53	16.07	248.46	2.21	1.93	1.1531
I	14.30	218.64	14.33	218.31	-0.03	0.33	1.0020

Fig. III-6-9-(5) Change of velocity and current direction

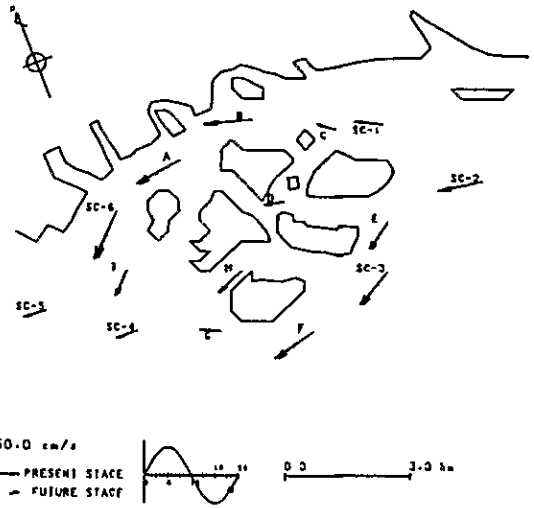

POINT	PRESENT STAGE		FUTURE STAGE		DIFFERENCE		a/c VELOCITY RATIO
	a VELOCITY (cm/s)	b DIRECTION (°)	c VELOCITY (cm/s)	d DIRECTION (°)	a-c VELOCITY (cm/s)	f=b-d DIRECTION (°)	
SC-1	23.40	297.60	23.40	297.60	-0.00	0.00	1.0000
SC-2	36.00	279.47	36.01	279.47	-0.01	0.00	1.0002
SC-3	39.45	240.08	39.49	240.24	-0.04	0.16	1.0010
SC-4	18.98	267.14	18.94	267.10	0.04	0.04	0.9981
SC-5	19.48	271.07	19.46	271.07	0.02	0.00	0.9990
SC-6	43.54	225.73	43.55	225.73	-0.01	0.00	1.0003
A	38.87	261.60	38.88	261.61	-0.01	0.00	1.0002
B	38.92	285.97	38.92	285.97	-0.00	0.00	1.0000
C	16.46	308.51	16.46	308.51	0.00	0.00	1.0000
D	17.82	282.27	17.75	282.30	0.07	0.33	0.9963
E	29.89	235.32	29.91	235.32	-0.02	0.00	1.0006
F	39.76	256.46	38.93	255.40	0.83	1.06	0.9792
G	16.82	292.58	16.08	292.69	0.74	0.11	0.9560
H	25.07	246.90	28.59	248.73	3.52	1.83	1.1406
I	24.09	221.21	24.12	221.04	-0.03	0.16	1.0011

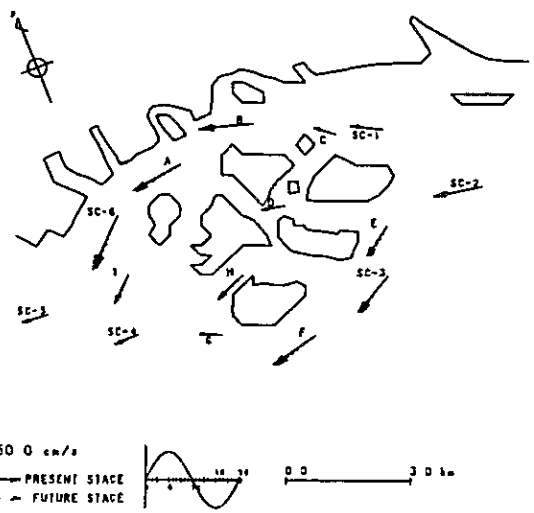

POINT	PRESENT STAGE		FUTURE STAGE		DIFFERENCE		a/c VELOCITY RATIO
	a VELOCITY (cm/s)	b DIRECTION (°)	c VELOCITY (cm/s)	d DIRECTION (°)	a-c VELOCITY (cm/s)	f=b-d DIRECTION (°)	
SC-1	27.49	297.96	27.49	297.95	-0.00	0.00	1.0001
SC-2	40.88	279.73	40.89	279.73	-0.01	0.00	1.0002
SC-3	44.29	240.25	44.33	240.40	-0.04	0.15	1.0009
SC-4	22.10	267.21	22.06	267.18	0.04	0.03	0.9981
SC-5	23.40	271.92	23.38	271.92	0.02	0.00	0.9990
SC-6	51.63	225.88	51.64	225.88	-0.01	0.00	1.0003
A	46.01	261.49	46.02	261.50	-0.01	0.00	1.0003
B	45.85	285.80	45.85	285.80	-0.00	0.00	1.0001
C	19.61	308.37	19.61	308.38	-0.00	0.00	1.0000
D	21.97	282.56	21.51	282.59	0.07	0.02	0.9968
E	33.76	235.65	33.78	235.65	-0.02	0.00	1.0006
F	44.69	256.41	43.77	255.36	0.91	1.05	0.9795
G	19.12	291.83	18.26	291.91	0.86	0.08	0.9549
H	29.69	247.11	33.78	248.92	-4.09	1.82	1.1377
I	27.94	223.20	27.97	223.04	-0.03	0.17	1.0010

Fig. III-6-9-(6) Change of velocity and current direction

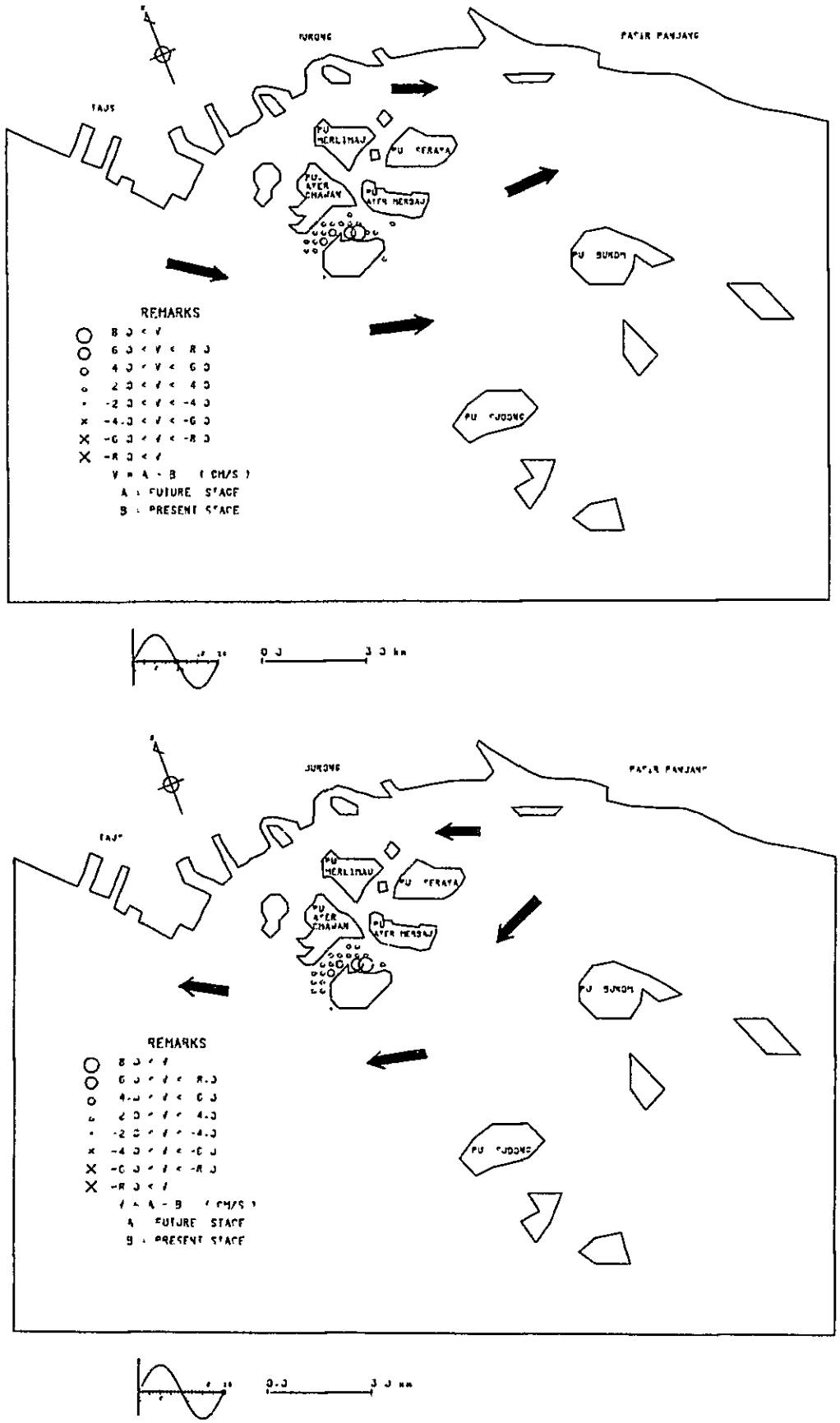

Fig. III-6-10 Distributions of velocity change

III-6-1-2 COD dispersion

— The verification

After the computation of the present stage, the numerical results are compared with the observed COD concentrations, and then the verification of simulation model is carried out.

In Seraya area, since the water quality was observed at eastward current, the unsteady computation is perfomed to predict the water quality corresponding to the current. The computed results at eastward current corresponding to the observation time are utilized for comparison.

Fig. III-6-11 shows the computed distribution of COD concentration and the comparison between the observed data and the computed result is shown in Fig. III-6-12 and Table III-6-3. Further, Fig. III-6-13 shows the COD concentrations at typical sections. Summarizing the verification from these numerical result as follows:

1 The computed distribution of COD concentration shows that in the west to Seraya and Bakau islands the concentration is low, and that in the east to these islands it is high. These characteristics are same with observed one.

2 When the computed result is compared with the observed data at the stations amount to 21 points (S1 to S49), the maximum difference is equal to 1.9 ppm. Averaging the data at these stations, the observed concentration is equal to 0.65 ppm and the computed one is equal to 0.61 ppm, which means only the slight difference is shown.

3 The following correlation obtained between observed data and the computed results are given as follows:

Correlation coefficient 0.83

Linear regression $y = 1.059x + 0.004$

where y is observed value and x computed value

Excluding the station S1 and S2 locating at the mouth of Pandan river.

Correlation coefficient 0.97

Linear regression $y = 1.084x - 0.148$

From these considerations it is found that the computed result has good agreement with observed data.

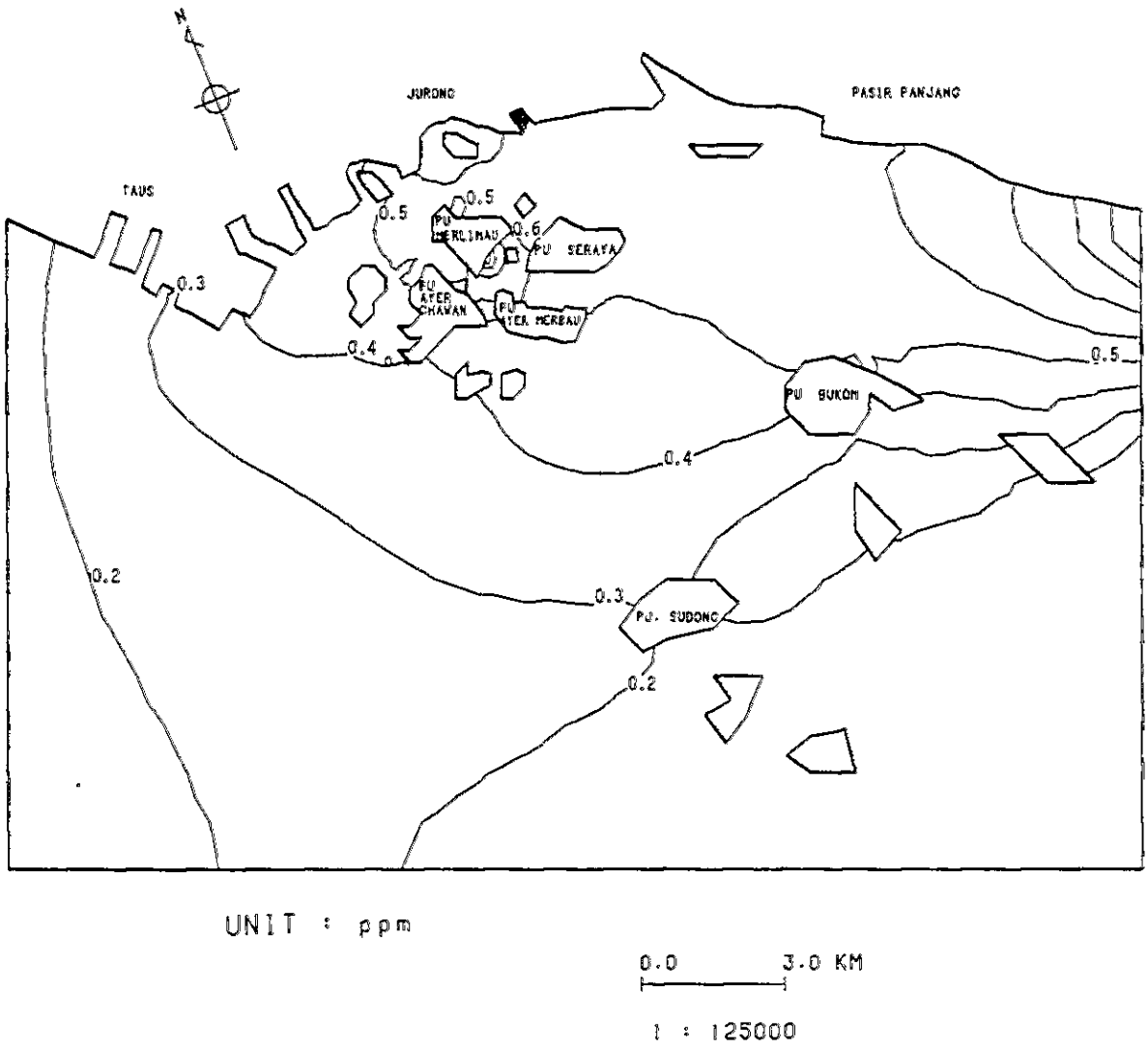

Fig. III-6-11 Computed distribution of COD in present stage (low water)

Table III-6-3 Comparison between observed and computed

(UNIT : PPM)

POINT	OBS	CALC.
S 1	1.30	0.51
S 3	2.40	0.52
S 5	0.70	0.53
S 6	0.70	0.51
S 12	0.70	0.51
S 13	0.30	0.51
S 16	3.90	3.74
S 21	0.10	0.45
S 24	0.40	0.50
S 25	0.40	0.63
S 28	0.20	0.51
S 29	0.10	0.43
S 30	0.60	0.39
S 31	0.50	0.50
S 36	0.10	0.38
S 38	0.20	0.33
S 39	0.10	0.48
S 45	0.60	0.38
S 47	0.10	0.33
S 48	0.10	0.31
S 49	0.10	0.31
MEAN	0.65	0.66

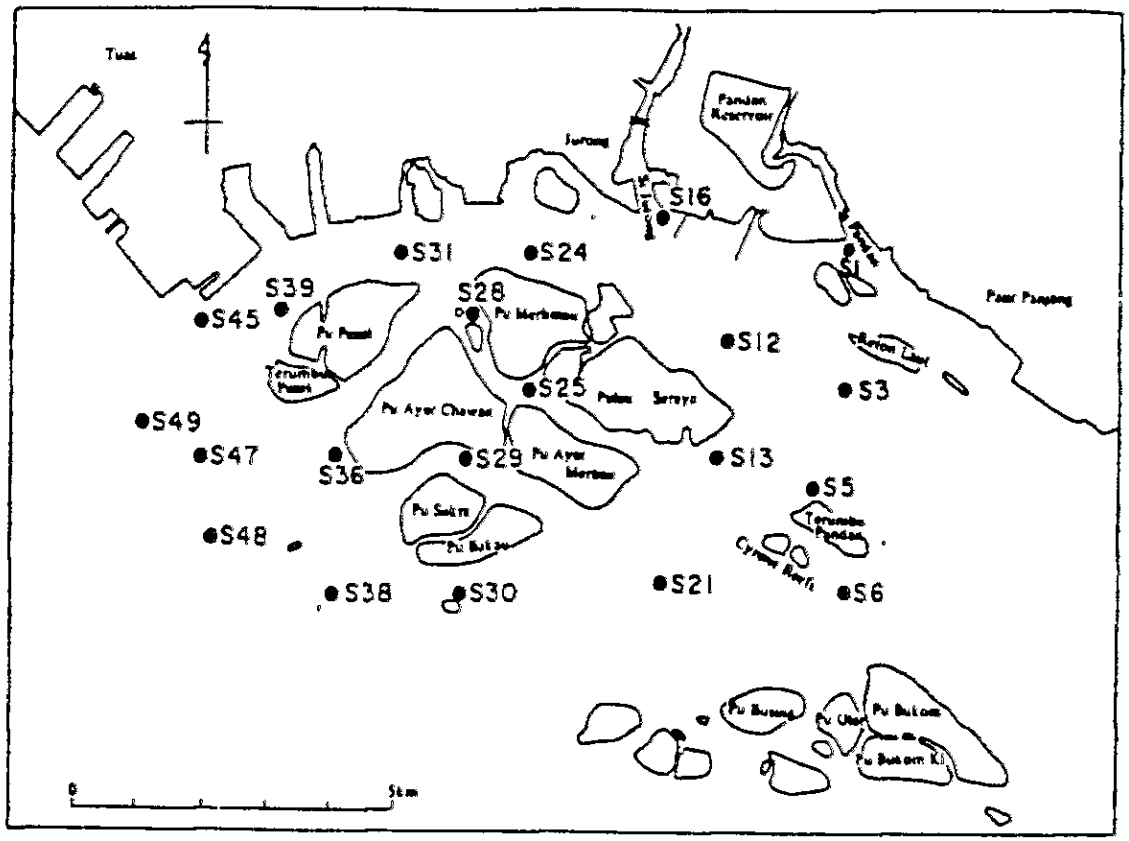

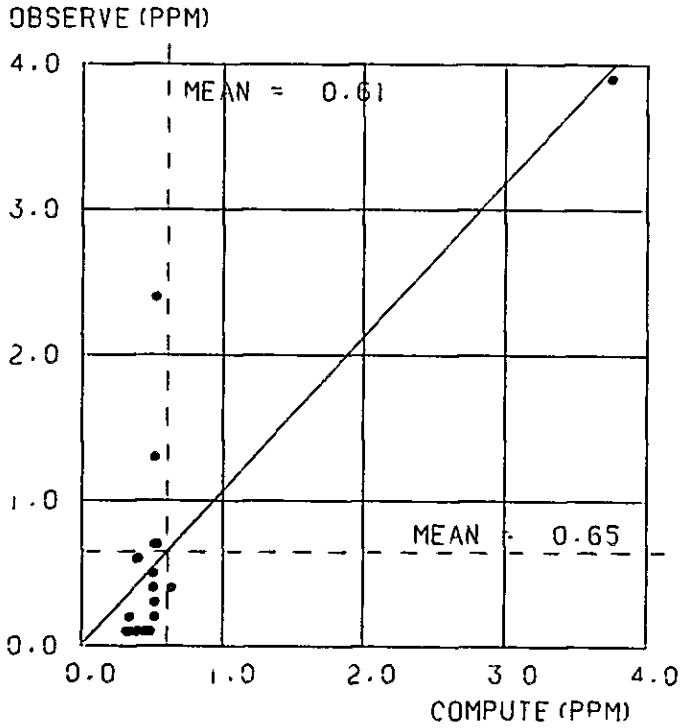

$Y = 1.06X + 0.004$ $R = 0.83$

Fig. III-6-12 Corelation between observed and computed

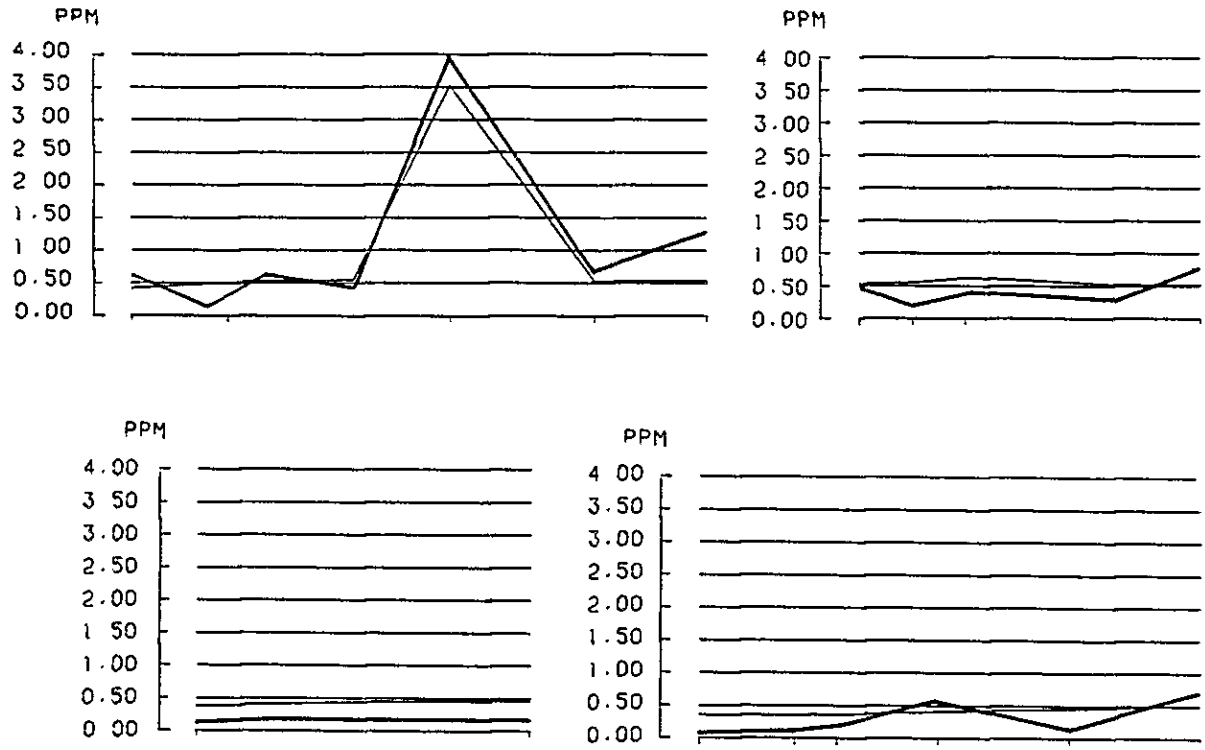

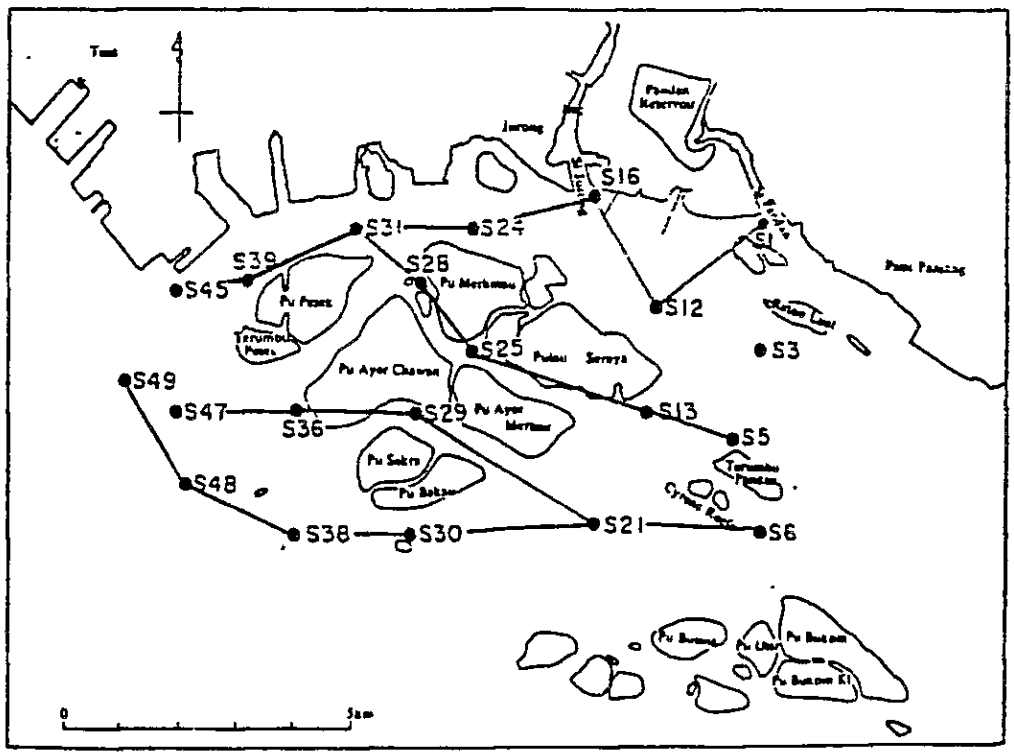

Fig. III-6-13 COD concentrations at typical sections

The unsteady computation applied in the verification is carried out to compute the COD concentration corresponding to the certain temporal tidal stage. Apart from such computation, the steady state computation is performed to compute the averaged COD concentration.

Averaging the numerical results computed by the unsteady state model for one tidal cycle, the variation of water quality produced by oscillating current is excluded and the averaged water quality is obtained. This averaged water quality has the same meaning with the numerical results computed by the steady state model. Table III-6-5 shows the numerical results computed by the steady state model and the averaged water quality for a tidal cycle. The both concentrations have slight differences. Fig. III-6-14 shows the distribution of COD concentration at the present stage computed by the steady state model.

Table III-6-5 Steady state results and averaged water quality for tidal cycle

(UNIT : PPM)

POINT	UN-STEADY	STEADY	DIFFERENCE
A	0.529	0.562	-0.033
B	0.642	0.648	-0.006
C	0.503	0.545	-0.042
D	0.504	0.536	-0.032
E	0.444	0.496	-0.052
F	0.398	0.460	-0.062
G	0.343	0.408	-0.065
H	0.331	0.407	-0.076
I	0.402	0.485	-0.083
J	0.470	0.539	-0.069

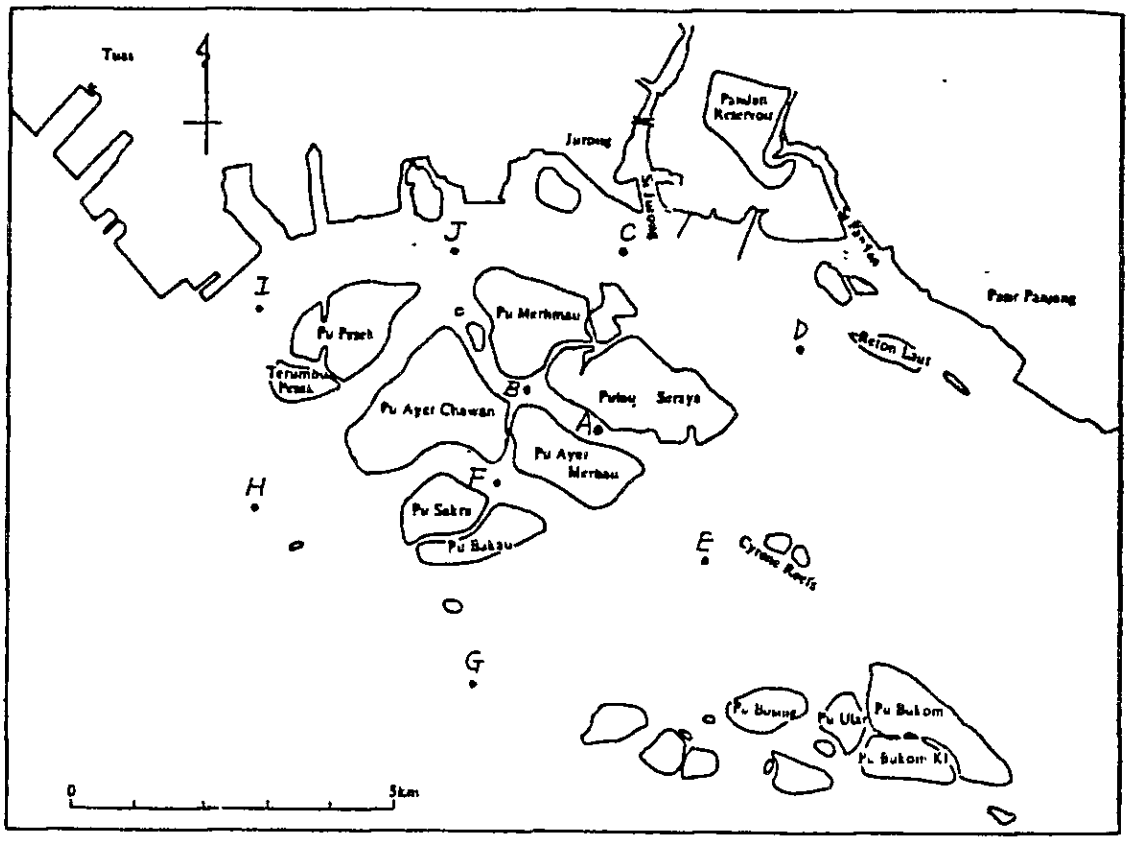

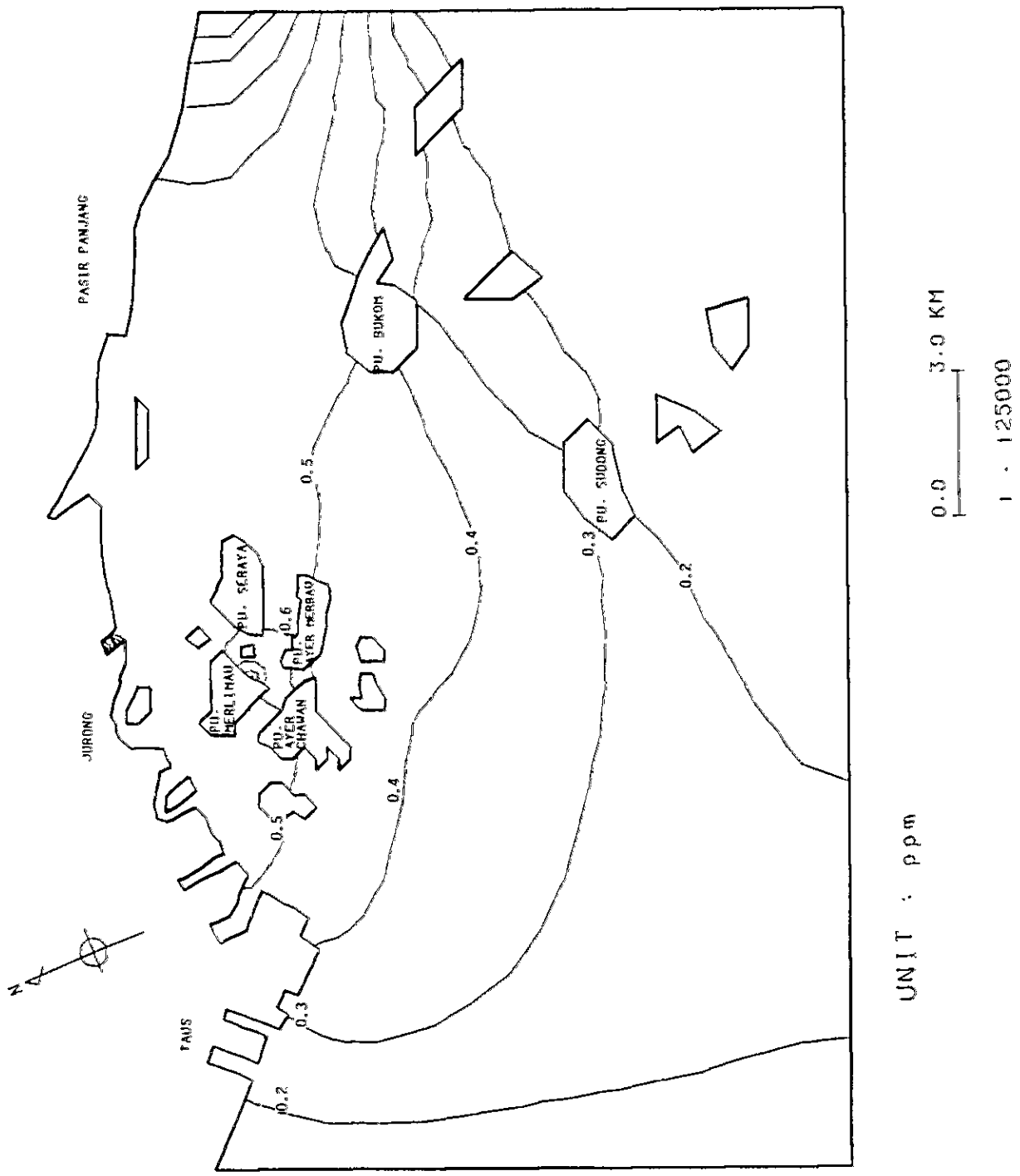

Fig. III-6-14 Steady state results of COD distribution

— The water quality in the future stage

Inputting the data on topography and pollutant flux of future stage, the computation is performed in the same manner with that of present stage.

Figs. III-6-15 and III-6-16 show the horizontal distribution of COD concentrations, Table III-6-16 shows the concentrations at the representative points, and Fig. III-6-17 shows the COD concentrations on the typical sections. From these figures and table, the water quality in the future stage is summarized as follows:

1 Comparing the water quality produced by westward current between the present and future stage, the change of COD concentration beyond 1 ppm is shown only at S1 locating in the mouth of Pandan river.

Averaging the concentrations at the stations amount to 21 points (S1 - S49), it is equal to 0.62 ppm in the present stage and 0.77 ppm in the future stage. This concentration increment (0.15 ppm) is produced by the increase of pollutant flux.

2 In the future stage when the water quality produced by the westward current is compared with the one by eastward current, the latter is lower than the former except the mouth of Pardan river, because the inflow from the west boundary purifies the water quality for the latter case.

Averaging the computed results at the 21 observation stations (S1 - S49), it is equal to 0.50 ppm, and 0.27 ppm less than the averaged concentration produced by the westward current. Additionally it is 0.12 ppm less than the averaged concentration of present stage produced by the westward current.

These considerations show that the water quality of the future stage is 3.0 ppm higher than that of the present stage in the maximum value at the mouth of Pandan river but the averaged concentration is only about 0.5 ppm higher than that of the present stage.

In Seraya area the pollutant flux induced from the east side boundary (the side of Singapore port) has more influence on the water quality than the pollutant fluxes assumed on the shore line.

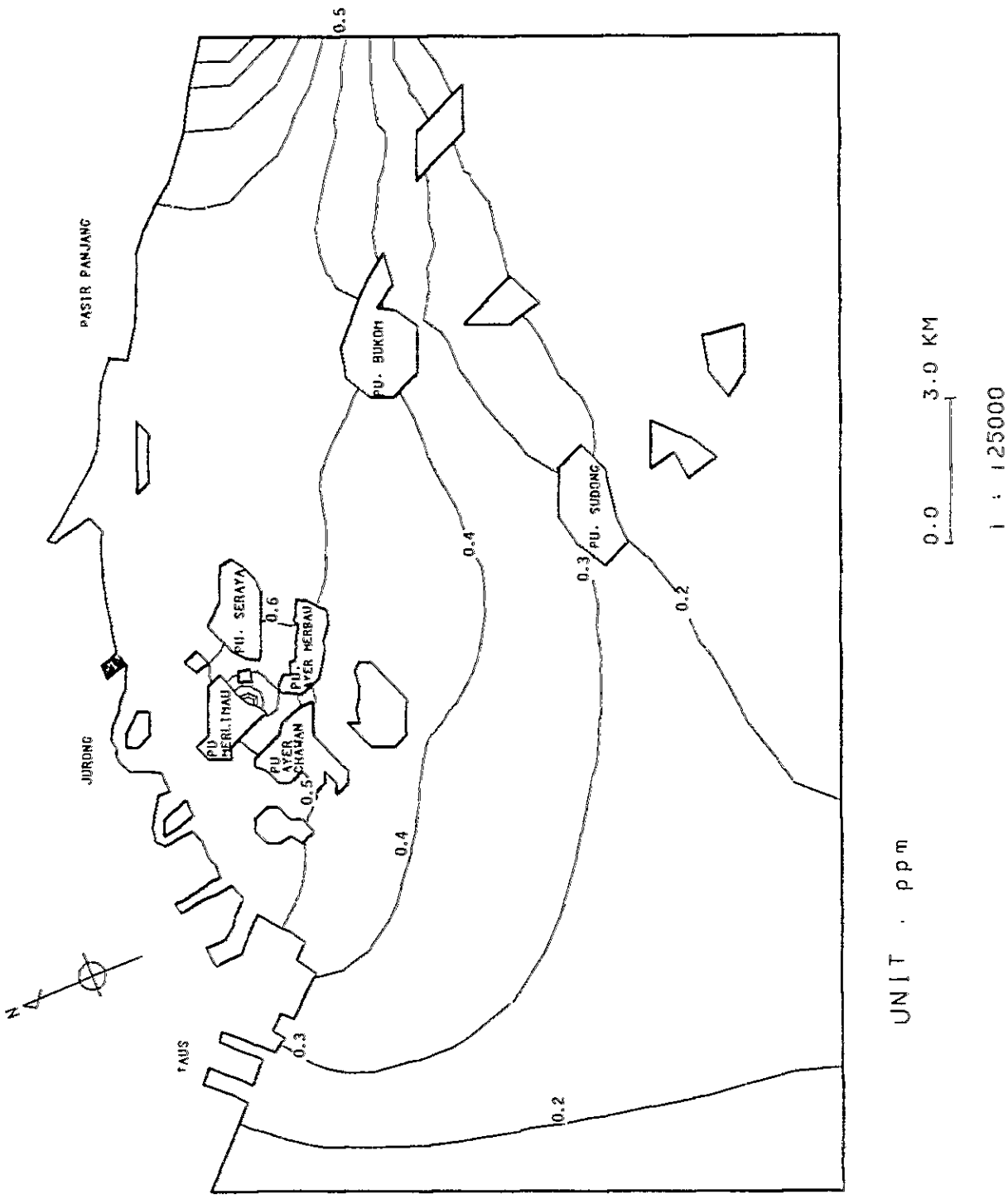

Fig. III-6-15 COD distribution by westward current in future stage

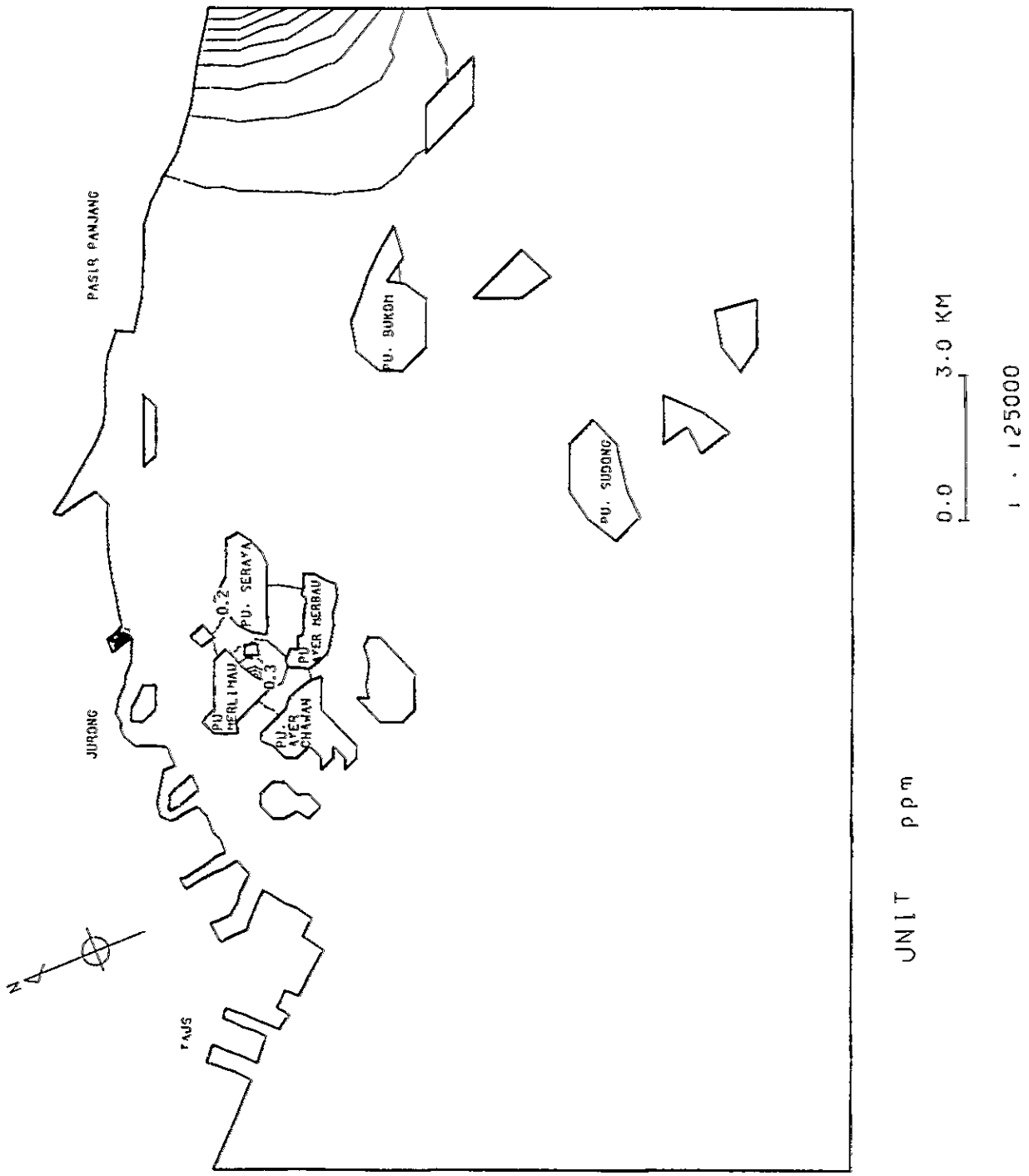

Fig. III-6-16 COD distribution by eastward current in future stage

Table III-6-6 COD consentrations at the representative points

(UNIT : PPM)

POINT	PRESENT STAGE	FUTURE STAGE	
		E-W	W-E
S 1	0.540	0.544	0.157
S 3	0.535	0.539	0.146
S 5	0.524	0.527	0.135
S 6	0.508	0.512	0.130
S 12	0.532	0.536	0.148
S 13	0.520	0.524	0.134
S 16	3.518	6.383	7.830
S 21	0.461	0.466	0.112
S 24	0.543	0.565	0.144
S 25	0.623	0.687	0.277
S 28	0.549	0.581	0.146
S 29	0.450	0.462	0.115
S 30	0.409	0.413	0.104
S 31	0.529	0.562	0.129
S 36	0.416	0.428	0.105
S 38	0.366	0.371	0.102
S 39	0.512	0.546	0.119
S 45	0.415	0.430	0.103
S 47	0.374	0.383	0.102
S 48	0.357	0.363	0.102
S 49	0.357	0.366	0.101
A	0.550	0.551	0.155
B	0.524	0.527	0.155
C	0.291	0.294	0.151
D	0.140	0.141	0.113
E	0.542	0.554	0.169
F	0.409	0.413	0.105
G	0.286	0.289	0.102
H	0.273	0.276	0.100
I	0.252	0.256	0.100

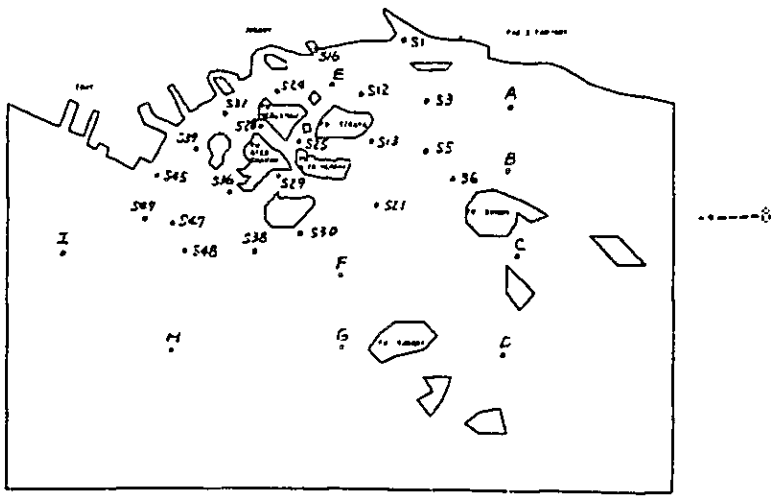

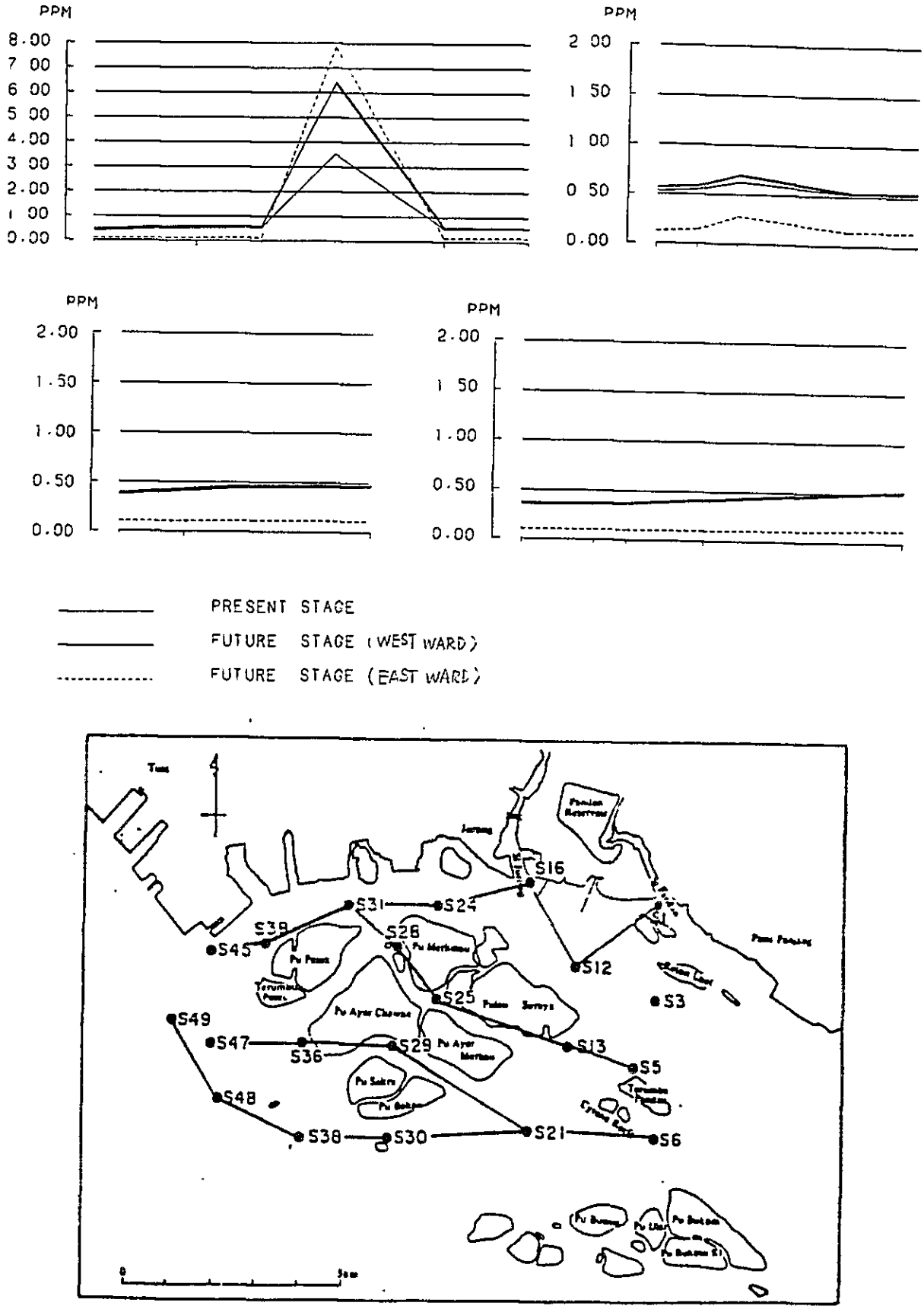

Fig. III-6-17 COD concentrations at the typical sections